UNIVERSITÀ DEGLI STUDI DI PADOVA

DIPARTIMENTO DI SCIENZE CHIMICHE

CORSO DI LAUREA MAGISTRALE IN
SCIENZA DEI MATERIALI

TESI DI LAUREA MAGISTRALE

Thermochemical catalysis for CO_2 splitting: supports for Ni,Mg-ferrites

RELATORE: Prof.ssa Antonella Glisenti

CONTRORELATORE: Prof. Miriam Mba Blazquez

LAUREANDO: Simone Costa

ANNO ACCADEMICO 2021/2022

Index:

1. INTRODUCTION

1.1. Global warming and pollution:

One of the main problems nowadays is represented by global warming, which leads to an increase in the temperature of the planet with disastrous consequences especially for animals and plants. In fact, the melting of glaciers is leading to the extinction of the species that occupy them, such as penguins, polar bears, etc.

To prevent this climate change from becoming irreversible (it is estimated that an increase of 2 °C is enough to make the situation unchangeable[1]) the whole world, and especially the European Union, is trying to decrease the concentration of CO_2 in the atmosphere and limit its emissions because it is the main responsible for this climate change. This greenhouse gas is produced almost everywhere, for example from animals' respiration (which transform, through cellular respiration, oxygen and glucose into carbon dioxide and energy), the cement production process, the internal combustion engine present in vehicles, etc.

Although this gas seems to be little present in the atmosphere (figure 1[2]) compared to oxygen and nitrogen, its concentration is sufficient to cause serious damage to the environment, and moreover its presence in the atmosphere has increased, as can be seen in figure 2[3], starting from 1750 (year of the first industrial revolution) until about 2016, the year of the graph. To date, the concentration of carbon dioxide is even higher.

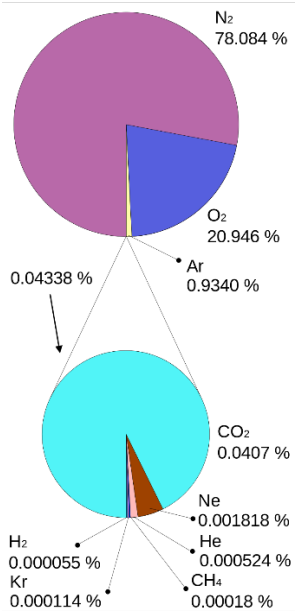

Figure 1. Concentration of CO_2 in the atmosphere of our planet.

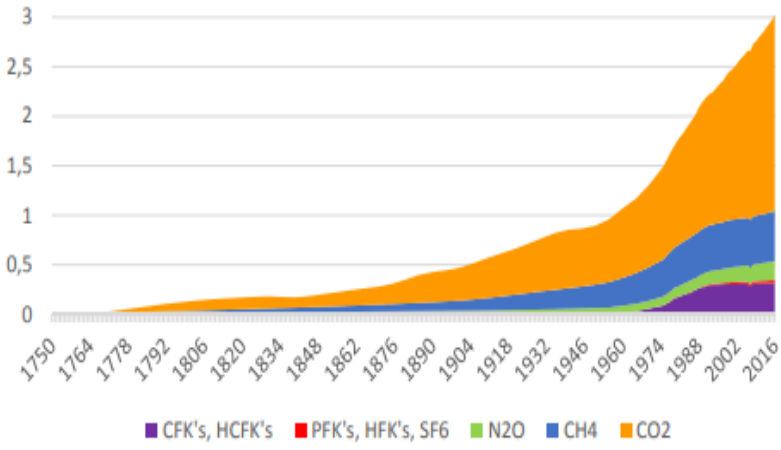

Figure 2. Trend of the concentration of various gases, including CO_2, on planet Earth, from 1750 until 2016. Note the increase in greenhouse gases over the years.

There can be several methods to reduce the presence of this gas in the atmosphere: reforest the planet (plants are able, through chlorophyll photosynthesis, to transform carbon dioxide and water into oxygen and sugar by absorbing a photon), capture and store carbon dioxide and finally transform it into more industrially attractive substances such as carbon monoxide, methane, methanol, etc.

The capture and storage of this gas may be the easiest method to reduce its presence in the atmosphere, however it is a short-term process since sooner or later the CO_2 warehouses will vanish (you can't fill the planet with these), so the transformation of this gas into substances easier to use seems to be the best way.

In addition, the formation of carbon monoxide turns out to be very useful to solve another modern problem: the decrease in oil resources and the consequent increase in the cost of fuels.

1.2. Fischer-Tropsch process:

Carbon monoxide, in fact, can be used coupled with hydrogen in Fischer-Tropsch processes to produce synthetic fuels. The process is not yet fully understood since there are multiple active reaction mechanisms[4].

The main reactions are those of hydrogenation and polymerization of carbon monoxide, however there are two other reactions which are the conversion of the water gas shift and the secondary conversion of the primary products of the Fischer-Tropsch process.

The reaction process is shown in figure 3[4].

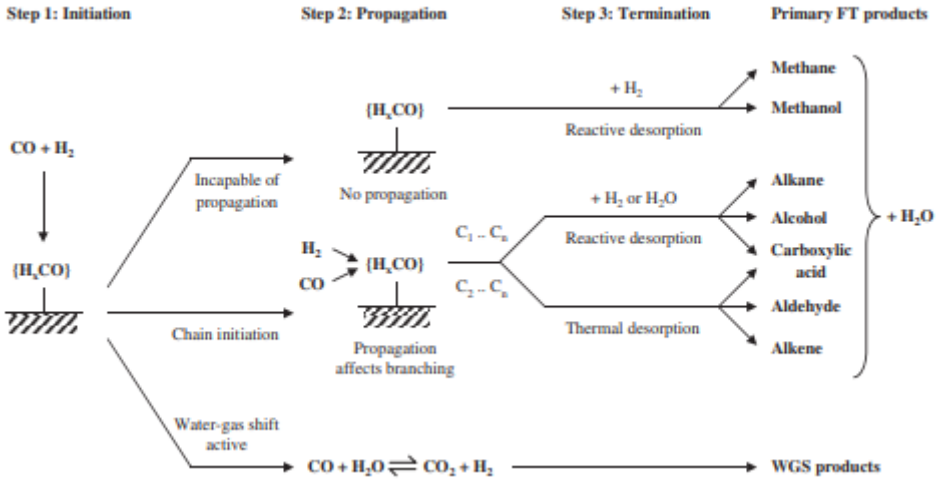

Figure 3. Reaction mechanisms of the Fischer-Tropsch process. We can notice the presence of several mechanisms, in order from top to bottom are: hydrogenation of CO, polymerization of this gas and the shift of water vapor. However, the secondary conversion reaction of the primary products of the process has not been included.

The polymerization and hydrogenation of carbon monoxide have a process similar to any other polymerization, that is, they present an accretion of the chain according to the reactions of initialization, accretion and termination.

The first step begins when the CO is adsorbed on the catalyst. Carbon monoxide is bound, dissociated and partially hydrogenated to become a chain start. The nature of the reaction intermediate is which that leads to the propagation or conversion reaction of water gas shift (reported in reaction 1):

$$CO + H_2O \rightleftharpoons H_2 + CO_2 \quad (1)$$

The following propagation step is the one that causes the growth of the chain, which occurs by adding carbon monoxide to the initiator of the chain or to a chain already growing on the surface of the catalyst. In practice, CO is added to the chain, not necessarily as carbon monoxide but as a reaction intermediate, whatever it is[4], so that the preservation of oxygen on more than one carbon is impossible and in such a way that the branching of the chain is possible.

The last step is the termination, very important with regard to the selectivity of the Fischer-Tropsch process since this determines both the number of carbon atoms of the molecule formed, and the functional group associated with the product. This step is determined both by the nature of the catalyst and by the operating conditions.

The termination can take place by thermal desorption or by reactive desorption, which are competitive with each other. The first process produces a detachment of the propagating chain due to a loosening of the bond between the catalyst and the reaction intermediate on its surface due to tempering. This process is possible only for chains with more than two carbon atoms, and the released product is unsaturated, for example, an alkene or an aldehyde is formed. The second process, on the other hand, is based on a desorption caused by a reaction that breaks the bonds between the intermediate on the surface of the catalyst and the catalyst itself. This can happen to intermediates with chains long one or more carbon atoms, and it occurs mainly by hydrogenation producing alkanes or alcohol.

Both processes can also lead to the formation of carboxylic acids.

The only reaction not yet described is that of secondary conversion of the primary products of a Fischer-Tropsch process, which occurs when a primary product is reabsorbed on the catalyst (also a hydrogenation catalyst). The reabsorbed product forms a surface intermediate capable of starting a chain, so the Fischer-Tropsch process begins again. Very often, however, the catalyst is not able to restart the process, so hydrogenation is catalyzed thus leading to the formation of saturated products. Surface concentration and competition for adsorption regulate the probability of reaction of primary products.

1.3. Carbon dioxide:

Carbon dioxide, however, is not an easy gas to split. Its linear triatomic structure characterized by double bonds between carbon and the two oxygens (figure 4[5]), makes the molecule extremely stable.

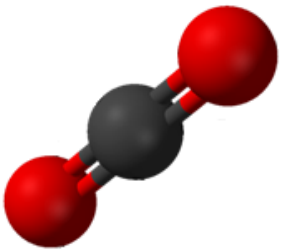

Figure 4. Ball and sticks model of carbon dioxide. The presence of double bonds between carbon and oxygens can be noted.

Oxygen atoms are more electronegative than carbon atoms (3,44 for oxygen and 2,55 for carbon according to Pauling electronegativity), which is why the outermost electrons of carbon are shifted towards oxygen, leading to the formation of a relatively low-energy state, stabilizing the molecule.

It is also interesting to note that the bond length between carbon and oxygen is 116 pm, closer to that of a triple bond (112,8 pm in carbon monoxide) rather than that of a double bond (124 pm in acetaldehyde[6]) also explaining the great stability of carbon dioxide.

The energy of the C=O bond in CO_2 is 803 kJ/mol, which is high; for a comparison, that of the O-H bond in H_2O is 463 kJ/mol. These properties could be led to the presence of two σ bonds and two π bonds (π_3^4) in the molecule. The carbon has two sp hybridized orbitals that are formed by mixing electrons in the 2s orbital with those in the $2p_x$ orbital. Each sp orbital of C and a $2p_x$ orbital of O combine to form a bond σ, and each π bond (π_3^4) is formed by the combination of a $2p_y$ or $2p_z$ orbital, two $2p_x$ orbitals, and a $2p_y$ of O[6]. The set of these properties, high symmetry, low polarity and high bond energy, brings high stability to the carbon dioxide molecule.

The CO_2 molecule is also an acidic oxide since dissolved in water it forms carbonic acid according to the following reaction:

$$CO_2 + H_2O \longrightarrow H_2CO_3 \quad (2)$$

The study will focus on the preparation and both structural and catalytic characterization of materials capable of transforming carbon dioxide into carbon monoxide.

1.4. CO_2 splitting:

The catalysis process is described as follows (figure 5[7]): the catalyst (basic oxide of a metal) is reduced at high temperature (about 1400 °C) in an inert atmosphere releasing oxygen. After this reaction, the catalyst is oxidized at a lower temperature (about 1100-1200 °C). Carbon dioxide and/or water restore the initial oxide and produce carbon monoxide and/or hydrogen. The reactions take place on the surface of the material, so it is important that the superficial area of the material is maximized, therefore the materials studied are very often pulverized.

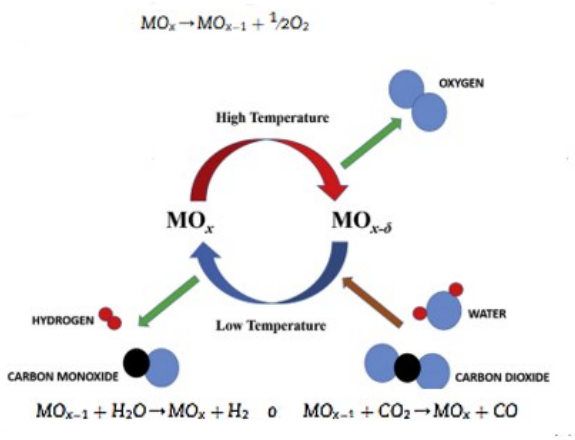

Figure 5. Catalysis process of carbon dioxide and water splitting.

1.5. Catalysts:

Several materials have been studied for this process, from lanthanum, strontium, manganese and iron perovskites (LSGM)[8] to strontium oxide[9], but iron spinel (Fe_3O_4) and ceria (CeO_2) are the materials that gave the best performance.

Both materials, however, have the same problem: they sinter at high temperatures. A sintering process lead to a decrease in the surface active area of the material and therefore to a loss of performance by the catalyst that will be able to separate less carbon dioxide than before.

To solve this problem, the focus is on supporting catalysts with inert materials [10–13], with the need of less sintering processes, and on doping them[10,13–22].

The focus of this work has been on the iron spinel because it is more reactive for the splitting of carbon dioxide and more reducible than the ceria[18]. The spinel, after the thermal reduction forms wustite (FeO)[11,12,23] with NaCl type structure[24] able to oxidize easily even with carbon dioxide and reform the starting material[25] (reaction 3, 4):

$$Fe_3O_4 \longrightarrow FeO + O_2 \quad (3)$$

$$FeO + CO_2 \longrightarrow Fe_3O_4 + CO \quad (4)$$

It should be noted that the active material for splitting carbon dioxide is not the iron spinel, but the wustite phase that is formed after its reduction.

In this work we will use both approaches: doping the spinel and supporting it. The state of the art indicates as the best catalyst for the splitting of carbon dioxide a nickel spinel doped magnesium ($Ni_{0,9}Mg_{0,1}Fe_2O_4$[21]), while as regards the support, I decided to use materials not inert, as used in the literature[11–13], but ones able to store oxygen and transport it quickly with the intent to release the surface sites of the catalyst from oxygen as fast as possible. This has been designed in order to make both oxidation and reduction reactions take place faster and to facilitate these reactions so that they react at a temperature below 1400 °C. These materials have been used with different intentions than those of this work (for chemical looping combustion in fact) however their oxygen transport properties are functional to the intent.

1.6. Supports:

The best materials according to these properties turn out to be nickel oxide and cupric oxide, as can be seen in tables 1 and 2[26].

In Table 1 it is possible to see how the best material is a cobalt oxide, which has a lot of oxygen compared to metal moles, however cobalt is an expensive metal then it has not been taken into account, focusing for cheaper options for a possible future application in the industry field. Nickel and copper oxide are, after the cobalt one, the materials with the best properties. It should also be noted that iron oxide has the worst oxygen storage.

Oxygen-carrying capacity for different metal or metal oxide pair (Hossain and de Lasa 2008)

Metal oxide	Moles of O_2/moles metal
NiO/Ni	0.5
CuO/Cu	0.5
Cu_2O/Cu	0.25
Fe_2O_3/Fe_3O_4	0.083
Mn_2O_3/MnO	0.25
Mn_3O_4/MnO	0.17
Co_3O_4/Co	0.67
CoO/Co	0.5

Table 1. Oxygen storage properties of various metal oxides placed as oxygen moles normalized for metal moles.

In Table 2, on the other hand, there are these metal oxides supported with inert materials such as alumina and silica. In this case the oxygen transport property of the materials is analyzed by R_0, indicated as:

$$R_0 = \frac{m_{ox} - m_{red}}{m_{ox}}$$

Where m_{ox} is the mass of the oxidized material and m_{red} is the reduced oxide mass (when it has lost oxygen). Materials with a higher R_0 will be those with a smaller mass of the species, so more reducible (and better for this application). Once again it can be seen how nickel and copper oxides are better than iron oxide (R_0=0,16 for nickel oxide and R_0=0,083 for copper oxide versus R_0=0,027 for ferric oxide). In this case, however, cobalt oxide does not have the best oxygen transport capacity, probably because it is supported (therefore having a metal load of less than 100% and perhaps reducing its oxygen transport properties).

Oxygen-carrying capacity of various metal oxides

Oxygen carrier	Metal loading (%)	R_o	References
NiO/SiO_2	35	0.074	Zafar et al. (2006)
NiO/Al_2O_3	20–60	0.043–0.16	Mattisson et al. (2003), Sedor et al. (2008a, b) and Hossain, and de Lasa (2007)
$NiO/NiAl_2O_4$	40–60	0.09–0.13	Mattisson et al. (2006)
$NiO/MgAl_2O_4$	37–60	0.09–0.13	Zafar et al. (2006) and Mattisson et al. (2006)
NiO/TiO_2	40–60	0.09–0.13	Mattisson et al. (2006)
CuO/SiO_2	41	0.083	Zafar et al. (2006)
CuO/Al_2O_3	14–35	0.027–0.08	Mattisson et al. (2003) and de Diego et al. (2007)
$CuO/MgAl_2O_4$	43	0.087	Zafar et al. (2006)
Fe_2O_3/SiO_2	39	0.012	Zafar et al. (2006)
Fe_2O_3/Al_2O_3	60	0.027	Cho et al. (2005) and de Diego et al. (2007)
CoO/Al_2O_3	29–35	0.07	Mattisson et al. (2003)
Mn_2O_3/SiO_2	47	0.048	Zafar et al. (2006)
$Mn_2O_3/MgAl_2O_4$	46	0.047	Zafar et al. (2006)

Table 2. Oxygen transport capacity for various metal oxides supported by inert materials.

As it is possible to see, these materials have a good oxygen storage capacity and a good oxygen conductivity. Even here, however, the materials suffers of sintering.

1.7. Aim of the thesis:

To operate an industrial scale-up, it was decided to use the industrial supports and mix them mechanically by wet ball milling with the catalysts, synthesized by sol-gel method with citric acid. Subsequently, a characterization of the materials was carried out by X-ray diffraction, scanning electron microscopy (SEM), energy dispersive X-ray diffraction (EDX) and X-ray photoelectron spectroscopy (XPS) in order to see if the resulting materials are the desired ones and the size of the powders obtained.

To study the maximum amount of oxygen that materials can lose and then reobtain, TPR (temperature-programmed reduction) and TPO (temperature-programmed oxidation) respectively are carried out.

The TPR will be carried out up to 900 °C in the atmosphere of 5 % of H_2 in He while the TPO will be carried out immediately after the TPR in an atmosphere of 5 % oxygen in helium case up to 900 °C. The temperature ramp, in both cases, is 10 °C/min.

To observe and quantify both the thermal reduction of the material and the subsequent splitting of carbon dioxide, a mass spectrometer is used, in order to study the release of oxygen by the system at 1000 °C and the production of CO at that same temperature.

Since for all the materials thermal reduction at 1000 °C does not occur, it was thought to reduce them with 5 % hydrogen at the maximum peak temperature of H_2-TPR, about 580 °C, and then carrying out the splitting of carbon dioxide at a concentration of 10 % in helium, so as to see if there is the production of carbon monoxide.

2. EXPERIMENTAL SECTION

2.1. Catalyst synthesis:

Among the various methods of synthesis for spinels[27,28], it was chosen to use the sol-gel with citrate method, using as precursors metallic iron (Fe, MM=55,85 g/mol, purity at 99,98 %), magnesium hydroxide ($Mg(OH)_2$, MM=58,32 g/mol, 95 % purity) and nickel nitrate hexahydrate ($Ni(NO_3)_2 \cdot 6H_2O$, MM=290,79 g/mol, purity 99 %), all from Aldrich. The following quantities of materials are used to ideally prepare 5 g of catalyst: 2,4186 g of Fe, inserted into a 200 mL beaker; 0,1263 g of $Mg(OH)_2$, placed in a 200 mL beaker; 5,6703 g of $Ni(NO_3)_2 \cdot 6H_2O$, placed in a less capacious beaker since, being highly hygroscopic, a low amount of water is expected to dissolve it; and 24,568 g of citric acid monohydrate $(HOC(COOH)(CH2COOH)_2 \cdot H_2O$, MM=210,14 g/mol, purity 99 %) , placed on a 1 L beaker since all cation-containing solutions will be added to this one.

To find the amount of materials to be taken to obtain an ideal 5 g of spinel, the following equations were used:

$$n_{spinel} = \frac{m_{desired}}{MM_{spinel}}$$

$$n_{cation} = n_{spinel} \cdot K_{cation}$$

$$m_{precursor} = n_{cation} \cdot MM_{precursor}$$

K indicates the stoichiometric coefficient of the given cation in the spinel formula (for example in $Ni_{0,9}Mg_{0,1}Fe_2O_4$, K_{Mg}=0,1).

Regarding the amount of citric acid monohydrate used, the following equation was used:

$$m_{citric} = \left(K_{Ni} + K_{Mg} + K_{Fe}\right) \cdot 1{,}8 \cdot MM_{citric}$$

Where a ratio of 1:1,8 was used between the moles of citric acid and the moles of cations present in the brute formula of the spinel.

All these materials were diluted with little deionized water, in addition the first two were dissolved separately with 40 mL of nitric acid (5 mL for magnesium hydroxide and 35 mL for iron) while the last one was dissolved in water. All these, to obtain a faster dissolution, were placed on a plate equipped with a magnetic stirrer and stirred (except iron since it is a ferromagnetic material).

Once clear solutions have been obtained, indicating that all the materials have dissolved, these are poured into the beaker with citric acid and left to mix at 300 rpm for about 10 minutes, obtaining a solution looking like the one in figure 6.

Figure 6. Solution containing cations and citrate. The green color is given by the presence of nickel and iron, probably complexed by the nitrates present; the magnesium in solution is colorless.

The pH is then adjusted between 6 and 7 using a 37 % ammonium solution (from Aldrich), so as to deprotonate all of the citric acid active sites (pKa_1=3,13, pKa_2=4,76, pKa_3=6,40[29]) being careful not to exceed pH 7 since otherwise it precipitates iron hydroxide ($Fe(OH)_3$), as can be seen from the Pourbaix diagram of iron in aqueous solution at 25 °C in figure 7[30], which segregates and, after calcination, becomes hematite (Fe_2O_3)[30] and not a spinel, with properties different from the ones described before. Iron is the main issue regarding the compounds that precipitate, since magnesium hydroxide and nickel oxide are formed at much higher pH (pH about 8[31] for $Mg(OH)_2$ and about 9[32] for NiO).

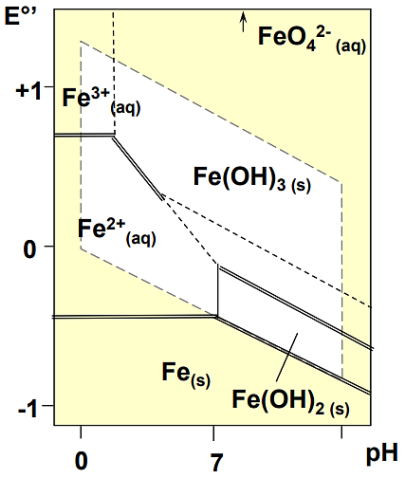

Figure 7. Pourbaix diagram of iron in aqueous solution at 25°C, showing the phases present as a function of pH (in abscissa) and applied potential (in ordinate). The potential applied in the case studied is 0 V so it can be seen how, in order not to precipitate the ferric hydroxide, it is necessary to keep a pH not exceeding 7.

As the pH is increased, the solution takes on a darker and darker color until it becomes brown (figure 8), the color of ferric hydroxide (at a pH of about 3). This is probably due to the presence of nitric acid, and complexes are formed between nitrate and Fe^{3+}. These oxides then dissolved again as the solution went green again (figure 9).

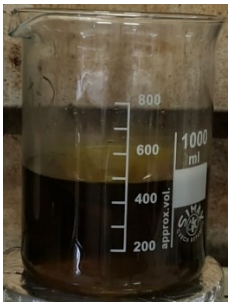

Figure 8. Brown solution obtained at a pH of about 3. The color is mainly given by the presence of ferric hydroxide probably complexed by nitric acid.

Figure 9. Green-returned solution after adding more ammonia. The iron (III) complexes probably formed are dissolved again as the solution turned at the initial color.

The solution is heated to 120 °C and left overnight to evaporate the water, after which it is heated to a temperature of about 300 °C to burn the citrate igniting a self-combustion process. The material obtained (figure 10) is pulverized with pestle and mortar and then calcined at 1000 °C for 4 hours in a muffle oven in the air, with a ramp of 10 °C min.

Figure 10. Solid obtained after burning citrate. This is then ground with a mortar and pestle to obtain the powder that have to be calcined.

2.2. Compound creation:

The catalyst obtained is mechanically mixed with industrial supports, namely nickel oxide (NiO, MM=74,59 g/mol, purity 99 %), copper oxide (CuO, MM=79,55 g/mol, purity 99 %) and zirconia (ZrO_2, MM=123,128 g/mol, purity 99 %) with water for 4 hours at 20 Hz using a ball miller.

The sample was extracted from the ball mill with the help of deionized water, then the solution was filtered and cooked for two hours at 1200 °C (with a ramp of 10 °C/min) regarding the mixing with nickel oxide and zirconia, in air in a muffle oven to bind the support and catalyst. This temperature was chosen trying to operate a slight sintering of the materials so that they would bind together and since the melting temperature of nickel oxide and zirconium oxide is very high (for NiO there is a T_{mel} of 1955 °C[33], while zirconia has a melting temperature of 2715 °C[34]). The spinel instead melts at a temperature of 1597 °C[35], so a fairly high temperature was sought to produce a sintering of one of the materials, in this case ferrite, but not so high as to melt them, thus the sintering took place at 1200 °C. As for the catalyst with copper oxide, it was placed to sinter for 2 hours at 900 °C, with a ramp of 10 °C/min in the air inside a muffle furnace. The temperature is lower than the previous ones because, following the same reasoning made previously, I tried to slightly sinter the material that melts at lower temperatures, namely copper oxide, which precisely has a T_{mel} of 1326 °C[36].

These materials were mixed together at 50 % and 20 % by weight in order to observe both how the reactivity and sintering of the material changes by varying the supports, and the effect of the latter on the catalyst at different concentrations.

2.3. Analysis of the compound:

The analysis of the synthesized compound is carried out with an X-ray diffractometer. The sample is analyzed after two reaction cycles with the same instruments.

SEM was performed with a Zeiss Sigma HD microscope, equipped with a Schottky FEG source, one detector for backscattered electrons and two detectors for secondary electrons (InLens and Everhart Thornley). The microscope is coupled to an EDX detector (from Oxford Instruments, x-act PentaFET Precision) for X-rays microanalysis, working in energy dispersive mode.

Powder X-ray diffraction was carried out on a Bruker D8 Advance Plus diffractometer at the PanLab department facility, founded by the MIUR “Dipartimenti di Eccellenza” grantNExuS. Diffraction data were

acquired in Bragg-Brentano geometry by employing the Cu Kα radiation (Cu anode supplied with 40 kV and a current of 40 mA) and a LYNEXEYE XE-T detector with 192 measuring channels in 1D mode.

2.4. Analysis of the reactivity of the compound:

The reactivity of the material is analyzed by temperature programmed reduction (TPR), temperature programmed oxidation (TPO) and mass spectrometry.

TPR is carried out using the Micromeritics Autochem 2920 instrument, flushing 50 sccm of gas (H at 5 % in He), according to a heating program that provides for the temperature increase of 10 °C/min up to 900 °C.

The TPR treatment consists in reducing the sample by constantly increasing the temperature in the reducing atmosphere, what the instrument goes to detect is the amount of hydrogen that arrives at the detector. In fact, an oxide that is reduced to hydrogen goes to form water according to reaction 5:

$$MO + H_2 \longrightarrow M + H_2O \quad (5)$$

To perform the measurement, 0,0250 g of sample is weighed on a scale and placed on a quartz tube reactor, after placing quartz wool on the tube bed so as to mechanically support the sample and so as to place it as close as possible to the thermocouple. In this way the temperature recorded by the thermocouple is nearly that of the sample.

Since the reduction leads to the formation of water, a trap is prepared for it using 2-propanol, which is inserted on a Dewar and cooled with liquid nitrogen slowly, when it reaches a consistency similar to that of honey it is inserted into the trap.

To perform the temperature programmed oxidation the same reduction program used for the TPR was used, but a subsequent step was added in which the TPR program is maintained (so with a temperature ramp of 10 °C/min) modifying the incoming gas (inserting O_2 at 5% in He) to obtain precisely the oxidation of the previously reduced material.

The catalytic test was obtained by inserting 0,0500 g of powder inside a quartz tube, supporting the powder in this case too with quartz wool that is inserted above and below the sample. A thermocouple is inserted and finally this tube is inserted into a small oven and connected to flow meters and mass spectrometer. The sample is brought to 1000 °C (the maximum temperature reachable by the oven) with a ramp of 10 °C/min in an inert atmosphere of helium at 100 sccm and this temperature is maintained for 2 hours, trying to obtain the thermal reduction of the sample. After this time, an atmosphere of 100 sccm is injected with 10 % carbon dioxide for 30 minutes to observe the splitting of this gas.

Since this didn't happen, as we will see later, I tried to observe only the splitting of CO_2 after having operated a treatment by flushing 100 sccm of hydrogen at 5 % in helium up to 600 °C, with a ramp of 10 °C/min thus emulating the temperature programmed reduction, and then bringing the sample to 1000 °C flushing 100 sccm of helium. Splitting is done under the same conditions described above, so by passing an atmosphere of 10 % carbon dioxide in helium at a rate of 100 sccm, for 30 minutes. In this case you can see how the separation of CO_2 into CO takes place.

3. RESULTS AND DISCUSSIONS

The synthesis of the catalyst obtained using a ratio between moles of metals and moles of citrate equal to 1: 1,8 led to the formation of 4,77 g of catalyst, against the 5 g expected (therefore yield of about 95 %) taking into account, however, also any loss of material during the transfer of the same in the falcons or slides, or even lost by pulverizing it in the mortar.

The wet ball milling method, on the other hand, has led to an average yield of 50 %, due both to the powders that remains attached to the walls of the mill and to filtration, since part of the compound remains attached to the filter.

To be able to compare any improvements in the performance of the various materials, an analysis of the supports was also carried out, therefore of pure nickel oxide, pure copper oxide and pure zirconia. XRD analysis of the supports was omitted as Aldrich's pure commercial compounds.

3.1. NiO:

3.1.1. Temperature Programmed Reduction:

The ability to reduce nickel oxide by H_2-TPR of 0,0501 g of material was studied. The graph of the hydrogen signal as a function of temperature is shown in figure 11.

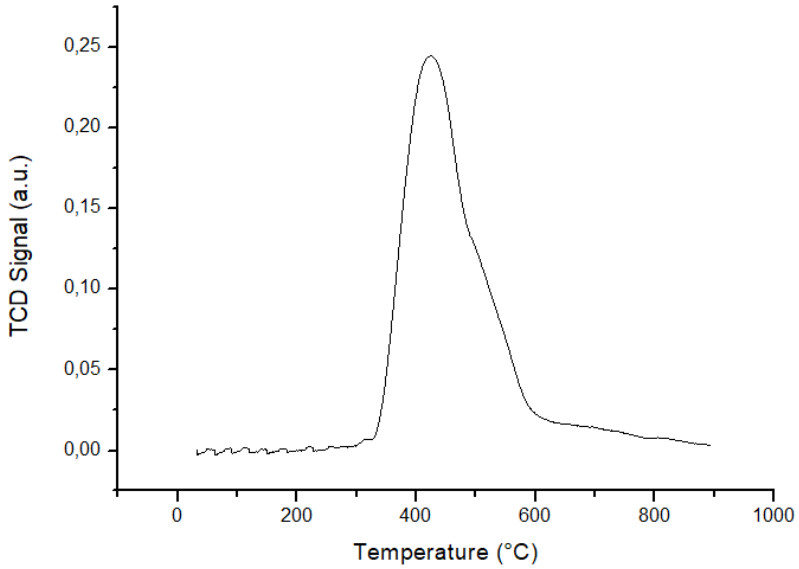

Figure 11. H_2-TPR of 0,0501 g of pure nickel oxide. In abscissa there is the temperature in degrees Celsius, while in ordinate there is the hydrogen signal read by the TCD.

The result obtained is very similar to that reported in the literature (figure 12[37]).

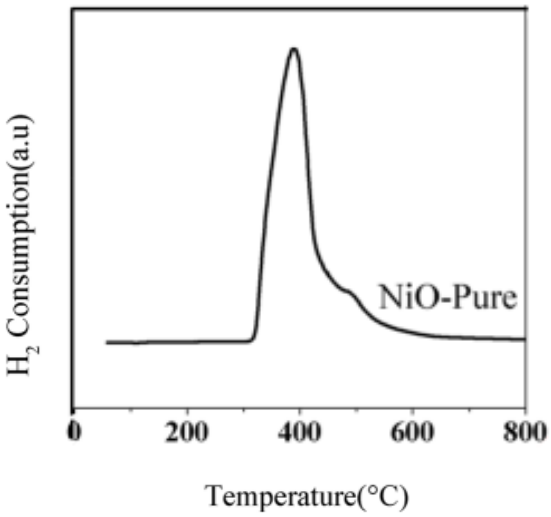

Figure 12. H_2-TPR of pure nickel oxide. As you can see the second peak (located at about 500°C) is much less intense than the experimental result.

The total area of the curve underlying the H_2-TPR is 290,96 cm^3/g STP (standard temperature and pressure), while the maximum is present at 429,9 °C. In addition, the reduction begins at about 330 °C and ends at about 770 °C. Starting from the area of the reduction curve obtained, it is possible to obtain the number of hydrogen moles that reacted with the system, therefore the number of maximum oxygen moles that the material loses. In fact, it can be found that:

$$n = \frac{Area\ of\ the\ curve}{1000\ {cm^3}/{L}} \cdot \frac{pV}{RT}$$

In this way a loss of hydrogen (and therefore oxygen) equal to $1{,}30 \cdot 10^{-2}$ mol/g is obtained. Multiplying this result by the mass of the sample (placing it equal to 50 mg for convenience, so as to compare it with the results obtained with the mass spectrometer) we obtain the number of moles of oxygen released by nickel oxide, equal to $6{,}49 \cdot 10^{-4}$ mol, corresponding to $1{,}04 \cdot 10^{-2}$ g. Counting the total oxygen present in the material, equal to the number of moles on 0,05 g of material, it is possible to derive the percentage of the total oxygen released. Nickel oxide in total has $6{,}69 \cdot 10^{-4}$ mol of oxygen, so the percentage of oxygen loss is 97%.

3.1.2. Temperature Programmed Oxidation:

Through O_2-TPO operated following the H_2-TPR I went to see if the material is reoxidized. The graph obtained (figure 13) shows how the reoxidation of the material takes place at high temperatures and also it does not seem to end within 900 °C.

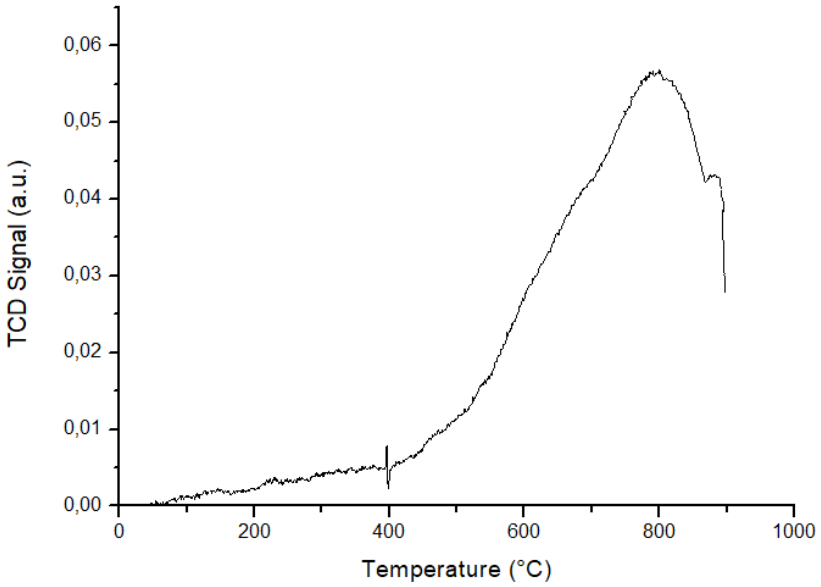

Figure 13. Trend of O_2-TPO related to nickel. It can be seen that within 900 °C the material cannot oxidize completely, in fact the peak does not end, it remains "open".

It can be seen how the oxidation of nickel begins at low temperatures (about 400 °C), however it is not completed within 900 °C, which is why it is not possible to accurately obtain the amount of oxygen used for total oxidation. The peak oxidation in this case is at 729,4 °C, which is a very high temperature.

The area of the curve, however, turns out to be 122,08 cm^3/g, taking as the end of the curve the 900 °C and extrapolating the trend of the baseline. That result corresponds to $5{,}45 \cdot 10^{-3}$ mol/g of absorbed molecular oxygen. Normalizing by 50 mg, a value of $2{,}72 \cdot 10^{-4}$ mol of molecular oxygen is obtained, so, multiplying by two, yields $5{,}44 \cdot 10^{-4}$ mol of reticular oxygen that is taken up by the material after releasing it during the reduction. Multiplying by the molar mass of oxygen gives the mass taken from nickel oxide, which corresponds to $8{,}71 \cdot 10^{-3}$ g. Once again, it is possible to obtain the percentage of oxygen compared to that released during thermal reduction, 84 %.

It is therefore seen how the material does not take back all the oxygen, crediting the hypothesis that the material does not finish its oxidation at 900 ° C.

3.2. CuO:

3.2.1. Temperature Programmed Reduction:

The cupric oxide was studied with H_2-TPR in order to observe how the behavior of the catalyst varies when it is mixed with it and vice versa. The graph from 0,0498 g is shown in figure 14.

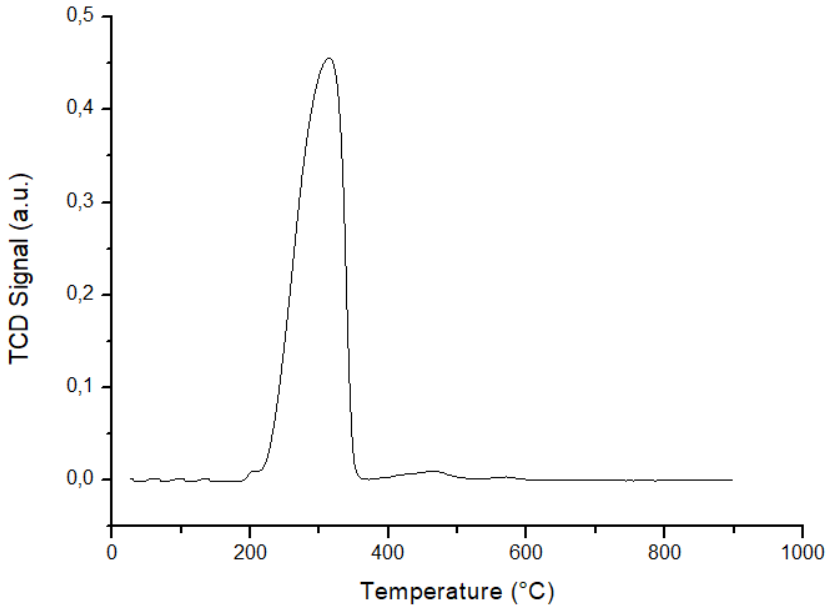

Figure 14. H_2-TPR of cupric oxide. You can see how this is reduced to very low temperatures (it starts at about 200 ° C), long before even nickel oxide and, as you will see, the spinel.

This type of oxide is very reducible, in fact its reduction begins at about 210 °C and ends at about 360 °C, long before both nickel oxide and the spinel used as a catalyst. Even the peak reduction occurs early, in fact it is positioned at 314,5 °C. Also in this case an analysis of the area of the curve was made, which turns out to be 277,84 cm^3/g STP, lower than that of nickel oxide. The oxygen released will therefore be less, in fact it turns out to be $1{,}24 \cdot 10^{-2}$ mol/g, then $6{,}20 \cdot 10^{-4}$ mol, corresponding to $9{,}92 \cdot 10^{-3}$ g. The percentage of oxygen released by the material in relation to the total is 99 %.

The H_2-TPR obtained is very similar to that reported in the literature (figure 15[38]):

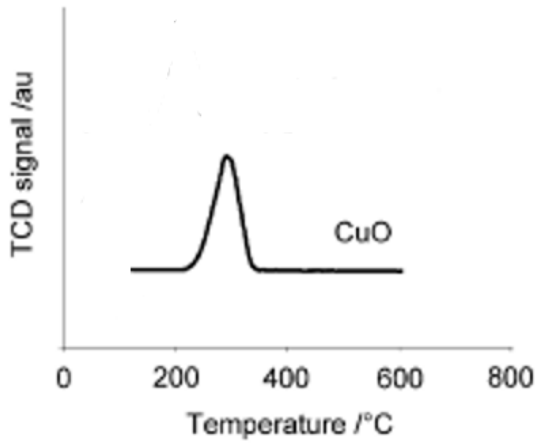

Figure 15. H_2-TPR of copper oxide. As can be seen, the experimental result is very similar to what is reported in the literature, also with regard to the location of the peak (around 300 ° C).

The result reported in the literature and the experimental one are very similar to each other, especially with regard to the position of the peak (around 300 °C), also beginning and end reduction temperatures are very close to each other.

3.1.2. Temperature Programmed Oxidation:

The O_2-TPO of the material led to the following result (figure 16):

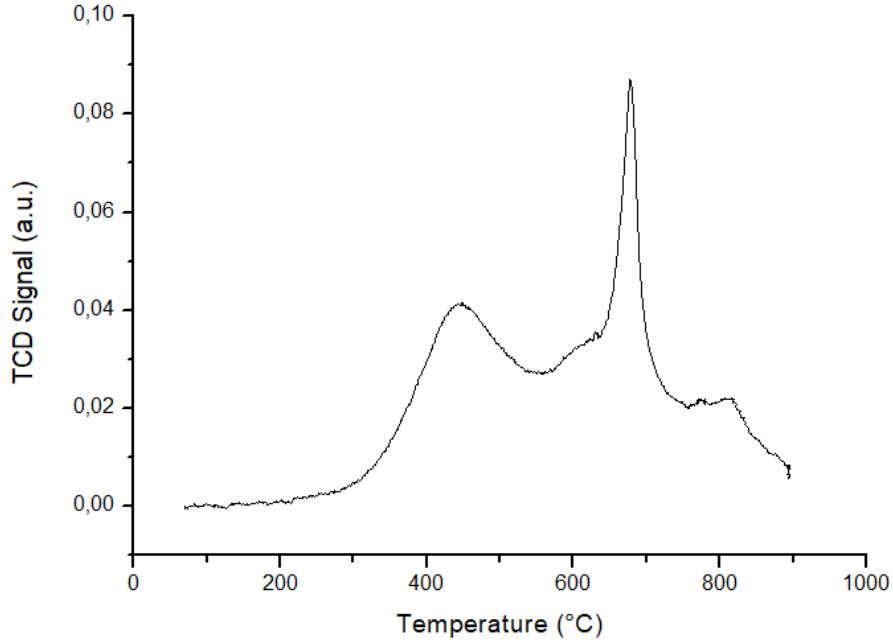

Figure 16. O_2-TPO of copper oxide previously reduced by H_2-TPR. Also with regard to oxidation, this type of oxide reacts at low temperatures.

You can see how, even for oxidation, the material begins to react at temperatures lower than those of nickel oxide and spinel (as will be seen later), at about 190 °C. The highest peak, however, is present at 677,6 °C, while the end of oxidation occurs at 900 °C.

The area underlying the oxidation curve is 124,29 cm^3/g STP, corresponding to $5{,}55 \cdot 10^{-3}$ mol/g of O_2 consumed for oxidation. Normalizing for 50 mg of sample we have that the amount of oxygen consumed is $2{,}77 \cdot 10^{-4}$ mol, then $5{,}55 \cdot 10^{-4}$ mol of reabsorbed reticular oxygen that is $8{,}87 \cdot 10^{-3}$ g. The percentage of oxygen regained by the material is 90 %.

3.3. ZrO_2:

3.3.1. Temperature Programmed Reduction:

H_2-TPR of 0,0496 g zirconia produced the following result (figure 17):

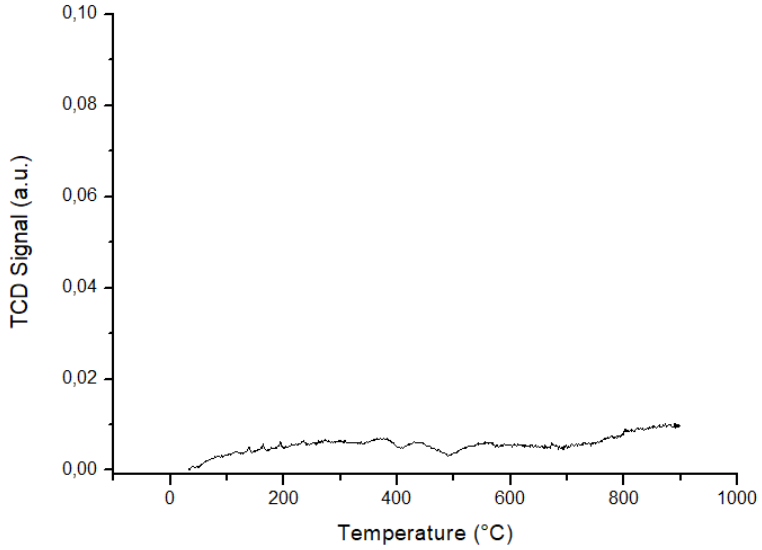

Figure 17. H_2-TPR by ZrO_2. As you can see, the material is not reduced in a hydrogen atmosphere to 5 % even within 900 ° C, so the material is considered inert.

It can be observed that, within 900 °C, zirconium oxide is not reduced even in a reducing atmosphere with 5 % hydrogen, in fact this material is considered an inert with respect to reduction. The signal increase is to be considered an instrumental artifact since it is too low, not even 0,02.

3.3.2. Temperature Programmed Oxidation:

Again, following H_2-TPR, an O_2-TPO is performed (figure 18):

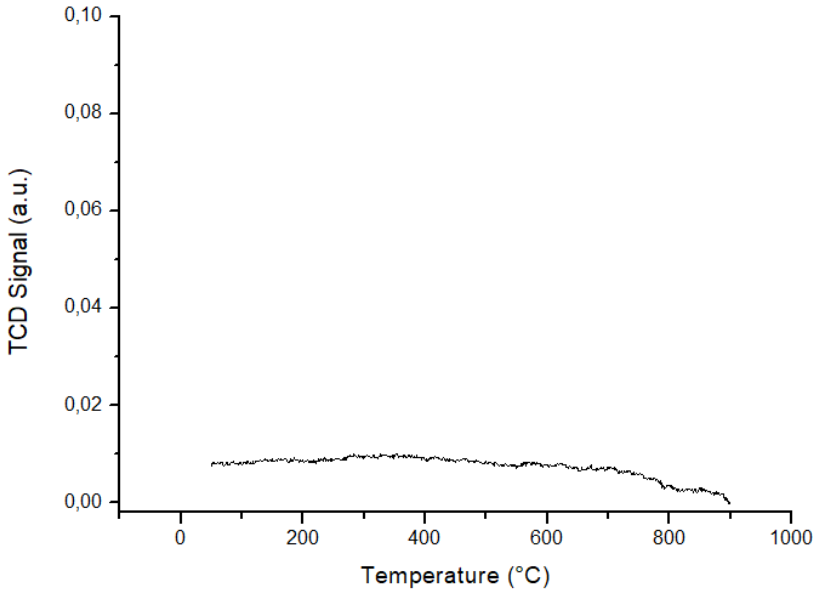

Figure 18. O_2-TPO of zirconium oxide. Given the absence of reduction previously seen by H_2-TPR this material does not oxidize even at 900 ° C, it is therefore an inert material.

Since previously the material has not reduced, this has not led to any reoxidation during O_2-TPO, so even in this case the trend of the graph is to be considered an instrumental artifact.

3.4. $Ni_{0,9}Mg_{0,1}Fe_2O_4$:

3.4.1. XRD Analysis:

The sample, studied by powder diffraction, developed the following pattern (figure 19):

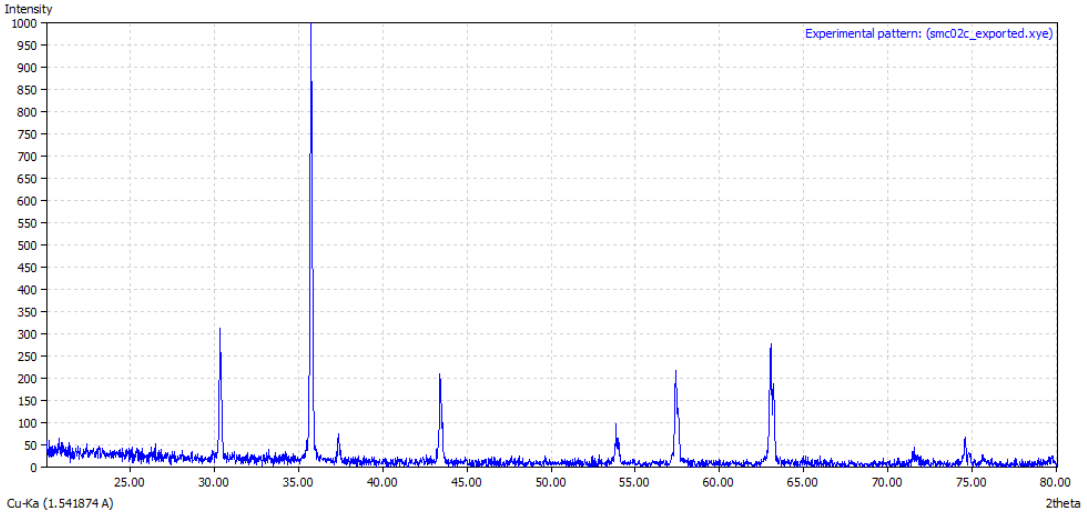

Figure 19. X-ray diffraction pattern from powders obtained from the sample, in the range between 2ϑ=20° and 2ϑ=80°.

The XRD pattern obtained is very similar to that present in the literature regard to the $Ni_{0,9}Mg_{0,1}Fe_2O_4$ spinel (figure 20[21]):

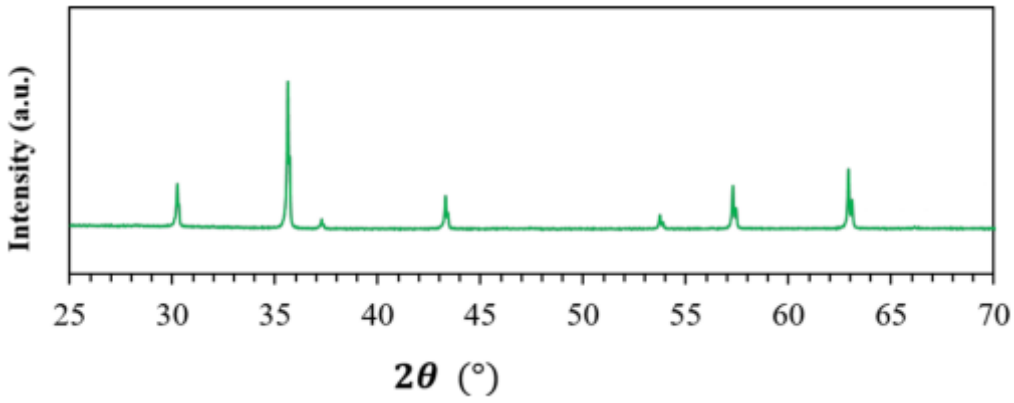

Figure 20. Pattern XRD present in the literature. As you can see, it is very similar to the one obtained experimentally, so the synthesized spinel is the one wanted, $Ni_{0,9}Mg_{0,1}Fe_2O_4$.

Therefore, we can identify the material as $Ni_{0,9}Mg_{0,1}Fe_2O_4$.

3.4.2. XPS:

The analysis through XPS led to the definition of the following survey, shown in figure 21.

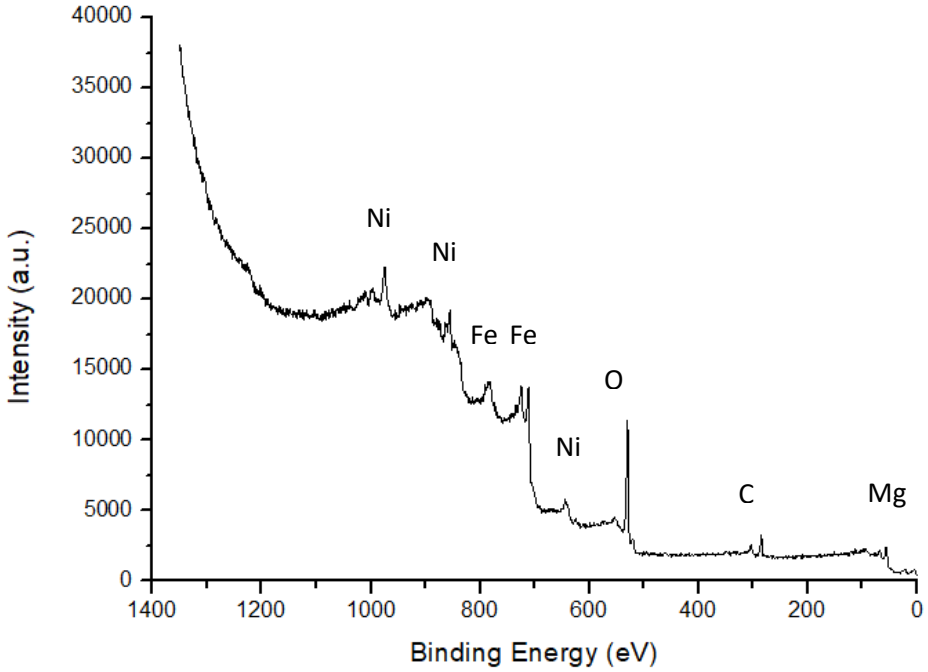

Figure 21. Survey spectrum obtained through XPS of the pure $Ni_{0,9}Mg_{0,1}Fe_2O_4$.

The species therefore present are Ni, Mg, Fe and O. A small contribution is derived from carbon, which is normalized to a position of 285 eV (corresponding to hydrocarbon contamination, always present in surface). The position of the peaks is in agreement with how expected for the cations in the corresponding oxides.

A quantitative analysis is also carried out, shown in Table 3:

Element	Concentration (%)	Expected concentration (%)
Ni	9,1	12,9
Mg	8,6	1,4
Fe	28,2	28,6
O	54,1	57,1

Table 3. Percentage concentration found by XPS against that expected for $Ni_{0,9}Mg_{0,1}Fe_2O_4$ spinel. As for oxygen and iron, the concentrations are very similar, while more magnesium is revealed than expected, and therefore less nickel.

From the quantitative analysis carried out we have a brute formula that is, approximately, $Ni_{0,67}Mg_{0,63}Fe_{2,08}O_4$. By comparing the experimental with the expected concentration, you can see how both the oxygen and iron values are very close to those obtained experimentally, however those of nickel and magnesium differ, in fact magnesium is more present than expected in the sample, while there is less nickel. Apparently, there is a small segregation of magnesium on the surface at the expense of nickel, since the XPS analysis measures a depth of up to 10 nm.

3.4. 3. SEM:

Below is the analysis by scanning electron microscopy, SEM (figure 22), at different magnifications.

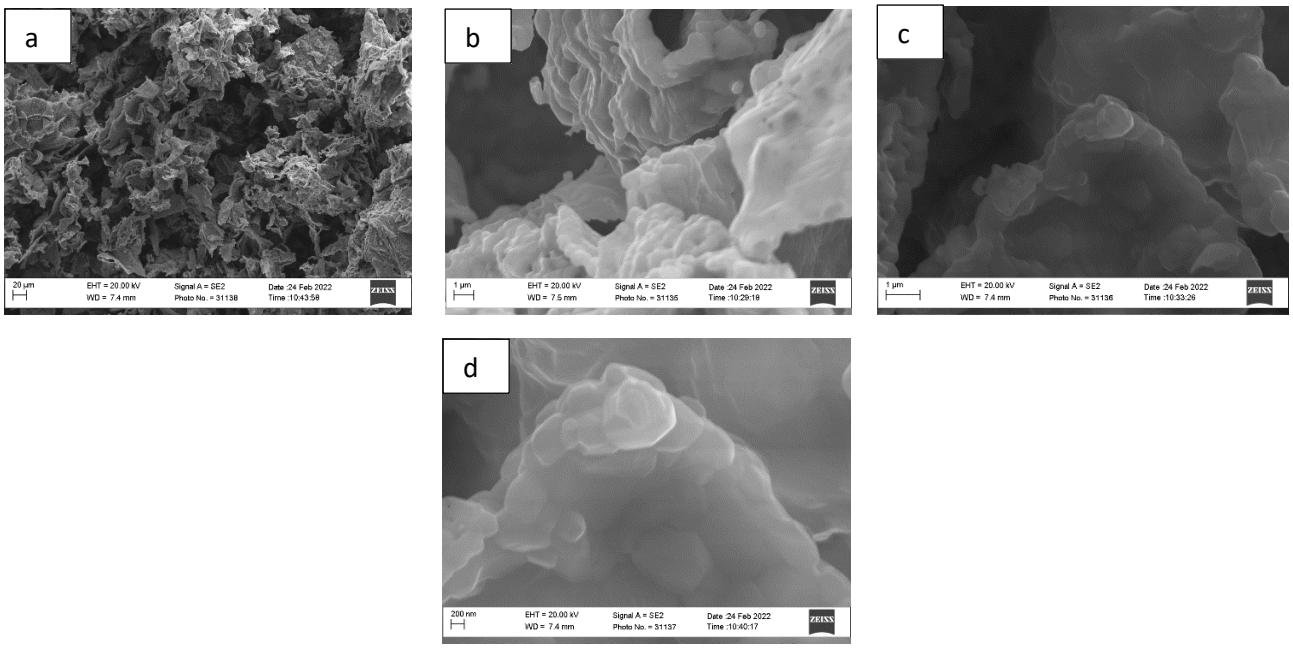

Figure 22. SEM images of $Ni_{0,9}Mg_{0,1}Fe_2O_4$. The image in figure a is at a magnification of 500x, the one in figure b is at 15000x, in figure c there is the image at 25000x, while in figure d there is the one at 50000x.

The morphology of the sample turns out to be similar to cornflakes at a magnification of 500x, moreover the particles are too packed and we can't distinguish one from the others also at a magnification of 25000x. The structure is also quite porous. A further EDX (energy dispersive X-ray spectroscopy) analysis, starting from the image obtained in figure 22,c at 25000x, led to the obtaining of the percentage composition of the sample (table 4).

Element	Concentration (%)	Expected concentration (%)
Ni	11,5	12,9
Mg	1,0	1,4
Fe	30,2	28,6
O	57,3	57,1

Table 4. Percentage concentration of elements in the spinel $Ni_{0,9}Mg_{0,1}Fe_2O_4$ obtained by EDX against the theorical one. As can be seen in this case the two concentrations are very similar to each other.

In this case the expected results and the experimental results of percentage concentration are all very close to each other. The values of nickel and magnesium are slightly lower than expected, while that of iron is slightly higher, but this may be due to the choice of the area on which to make EDX, so it can be said that in this case the material actually has the theorical brute formula, $Ni_{0,9}Mg_{0,1}Fe_2O_4$. The comparison between the XPS and EDX composition underlines that the Mg surface segregation is strictly involving the very few outer monolayers.

3.4.4. Temperature Programmed Reduction:

The temperature programmed reduction of 0,0248 g of material led to the formation of the following graphs (figure 23):

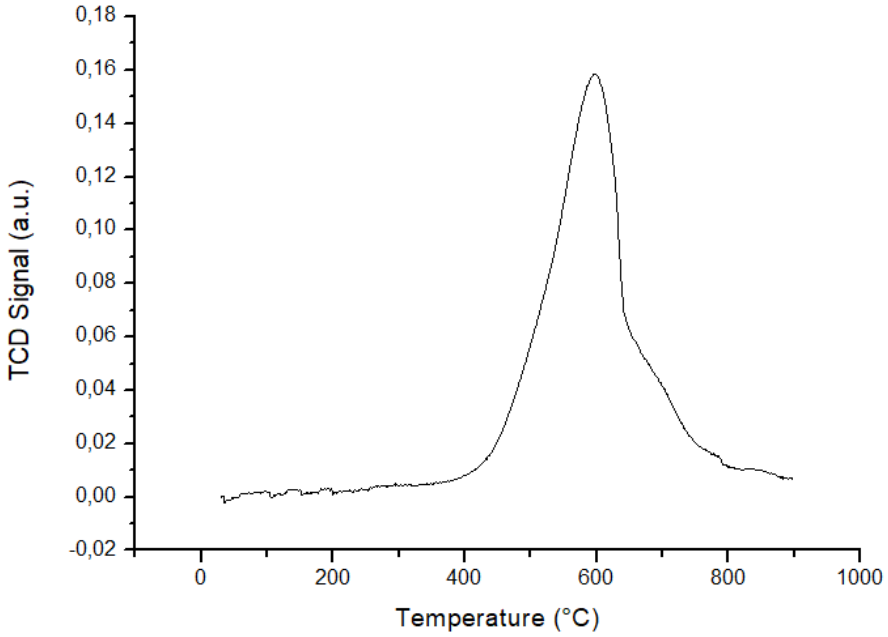

Figure 23. Graph of temperature programmed reduction (with signal vs temperature) obtained using 0,0248 g of $Ni_{0,9}Mg_{0,1}Fe_2O_4$.

From a qualitative analysis it can be seen how the material obtained is actually a spinel since there are no reduction peaks comparable to those of the oxides of the other materials present, therefore of MgO (figure 24[39]) and NiO (figure 25[37]). The absence of the first can be seen because the reduction of the sample ends at about 800 °C instead of about 750 °C, and also the magnesium present in the material is so little that a peak reduction of the same is not expected. The second oxide is not reduced in the sample because the peak reduction of nickel oxide is not seen around 400 °C. However, it can be seen that the H_2-TPR obtained is very similar to that of the spinel (figure 26[40]), except for the lack of the first peak due to hematite, Fe_2O_3, that is not present.

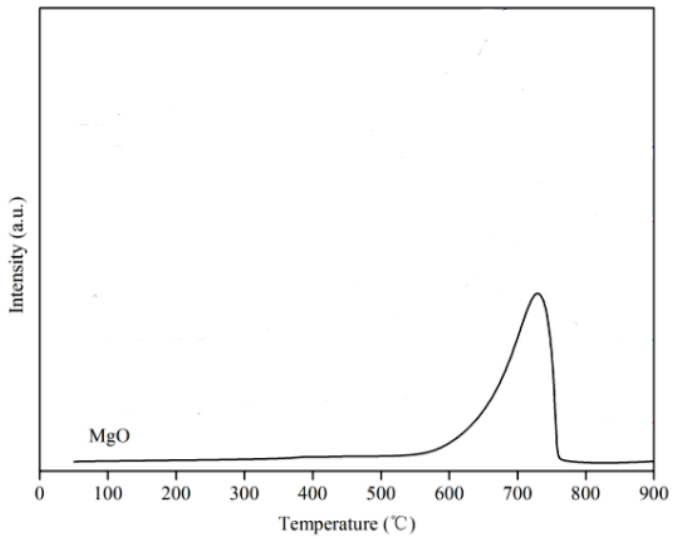

Figure 24. H_2-TPR of magnesium oxide. As you can see it is different from the TPR obtained experimentally, so there is no reduction of this material.

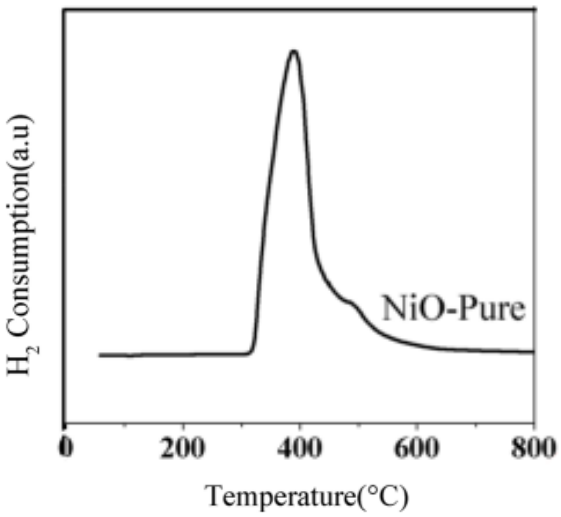

Figure 25. H_2-TPR of pure nickel oxide. Also in this case the trend is very different from the experimental one so even this material is not present, nickel is in the spinel's structure.

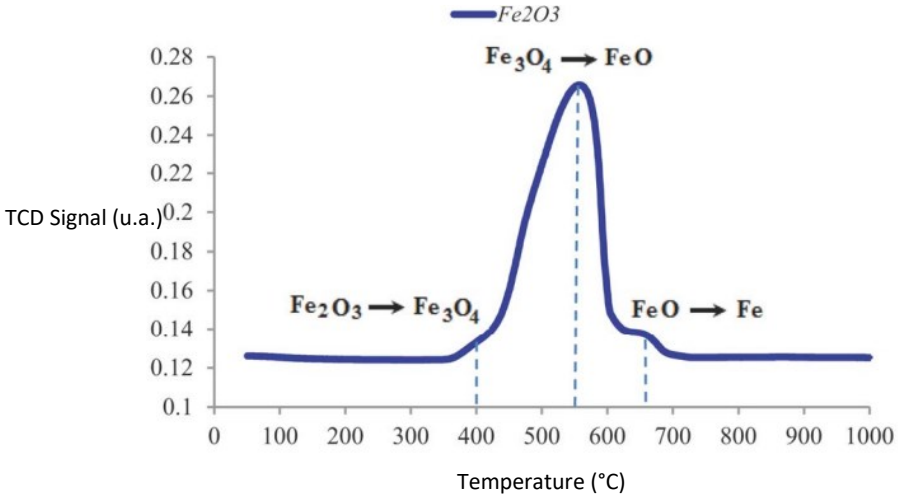

Figure 26. Hematite H_2-TPR (Fe_2O_3). As can be seen, the trend is very similar to that obtained experimentally, however in this case there isn't the peak of hematite's reduction.

As for the quantitative analysis, the area of the reduction curve was obtained, which turns out to be 346,24 cm^3/g STP, slightly higher than that of copper oxide and smaller than nickel oxide. The maximum peak reduction is at 596,3 °C, higher than both previously mentioned oxides. The beginning of the reduction is located at 330 °C, the same as nickel oxide but higher than copper oxide, while the end of the same is located at 820 °C, very high considering that this occurs in a reducing and not inert environment. This means that in an inert environment this material does not run the risk of becoming a metal with therefore low oxidation capacities. In fact, it is important that the material becomes wustite so as to be able to take the oxygen of CO_2 thanks to the oxygen vacancies present on the surface. Starting from the area of the reduction peak it is possible to derive the number of moles of oxygen released by the material, corresponding to $1{,}54 \cdot 10^{-2}$ mol/g, then to $7{,}72 \cdot 10^{-4}$ mol on 50 mg. Therefore the material loses $1{,}24 \cdot 10^{-2}$ g of oxygen. The percentage of oxygen moles released by the material compared to the total is 89 %.

3.4.5. Temperature Programmed Oxidation:

Also in this case an O_2-TPO was operated after H_2-TPR. The resulting graph is shown in Figure 27.

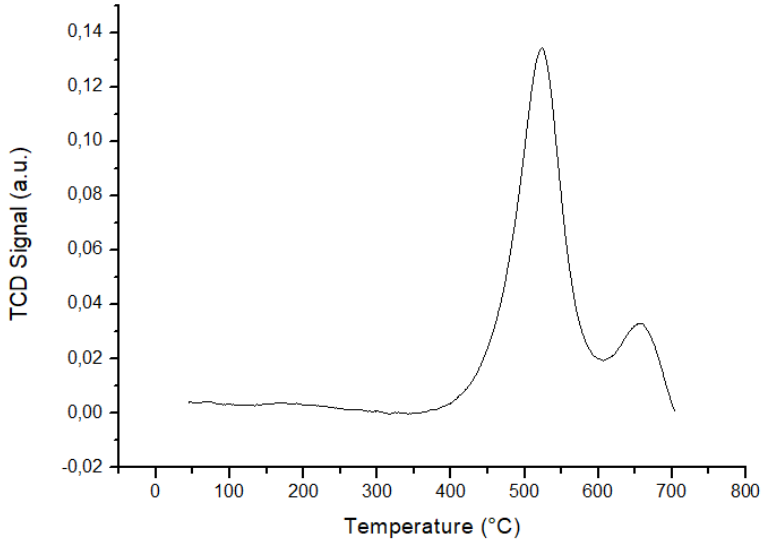

Figure 27. O_2-TPO of $Ni_{0,9}Mg_{0,1}Fe_2O_4$ spinel obtained after reduction. From the area of the two peaks it is possible to obtain how much oxygen reabsorbs the material.

In this case, the oxidation peak is present at 523,1 °C, much lower than the oxides previously studied, moreover the beginning and the end of the process also take place at lower temperatures, that is, respectively 350 °C and 700 °C approximately. In addition, the total area of the curve, determined by the oxygen gain, corresponds to 164,44 cm^3/g STP, so $7{,}34 \cdot 10^{-3}$ mol/g. Normalizing as previously we obtain the moles of molecular oxygen taken from 50 mg of sample, or $3{,}67 \cdot 10^{-4}$ mol, then, about reticular oxygen repurchased, $7{,}34 \cdot 10^{-4}$ mol, or $1{,}17 \cdot 10^{-2}$ g. The percentage of oxygen repurchase compared to that lost is of 95 %.

3.4.6. Carbon dioxide splitting:

The behavior of the material after reduction to hydrogen when flushing carbon dioxide at 1000 °C was studied to observe the splitting of this gas and its conversion to carbon monoxide.

Unfortunately, the mass spectra of CO_2, CO and O_2 have peaks 16 and 28 in common with each other, and this makes it impossible to accurately hold how much carbon monoxide is formed. Oxygen can be studied through 32, while carbon dioxide can be studied through 44, both of which are not shared by other substances. The result obtained, therefore, is as follows (figure 28):

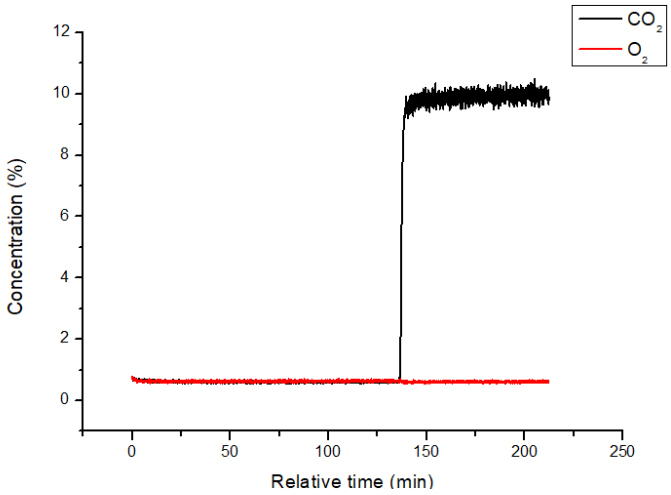

Figure 28. Trend of oxygen and carbon dioxide, after having heat treated the sample at 1000 °C for two hours in helium and passing 100 sccm of CO_2 to 10 % in helium. As you can see, oxygen always remains at zero or close to zero, its signal does not increase so the system does not release this gas during thermal reduction. The carbon dioxide signal, therefore, immediately reaches 10 %.

Since there was no actual loss of oxygen by the material during the thermal reduction step in the inert atmosphere, as can be seen in the figure (in fact the signal does not increase throughout the measurement), it was decided to use the information obtained by H_2-TPR, in order to observe only the splitting of carbon dioxide, if it actually happens, and how long and how much CO_2 is broken down. A pre-treatment up to about the maximum point of the measurement shown in figure 23 was then used in order to effectively reduce the material. For this reason, a pre-treatment similar to that developed through thermic reduction at controlled temperature was used, so I did a ramp of 10 °C/min with a 5 % flow of hydrogen in helium, up to 580 °C and then the temperature is raised to 1000 °C (ramp always of 10 °C/min) in an inert atmosphere to obtain splitting. This temperature is maintained, similarly to the previous case, for 30 min by flushing 10 % of CO_2 into helium. The result is shown in figure 29:

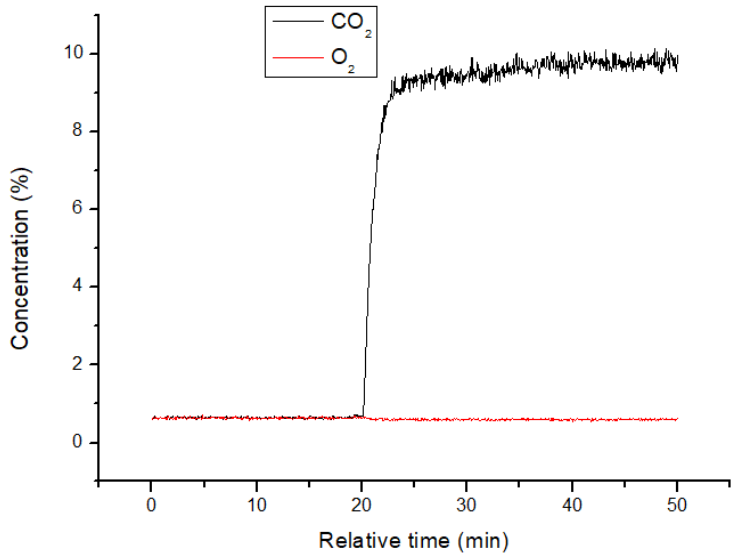

Figure 29. Trend of oxygen and carbon dioxide after having carried out a pre-treatment in 5% hydrogen, emulating the H_2-TPR, up to 600 ° C and then passing 100 sccm of CO_2 to 10% in helium. In this case the carbon dioxide signal takes some time before stabilizing and reaching 10 %, so actually the splitting of this gas takes place and carbon monoxide is formed.

As can be seen, in this case the material splits the CO_2 because the signal of this gas takes about 22 minutes before returning to being stable at 10 %, the concentration introduced. To this was added a second splitting cycle operated in the same conditions as the previous one in order to observe the effective reversibility of the spinel. Figure 30 shows the second cycle.

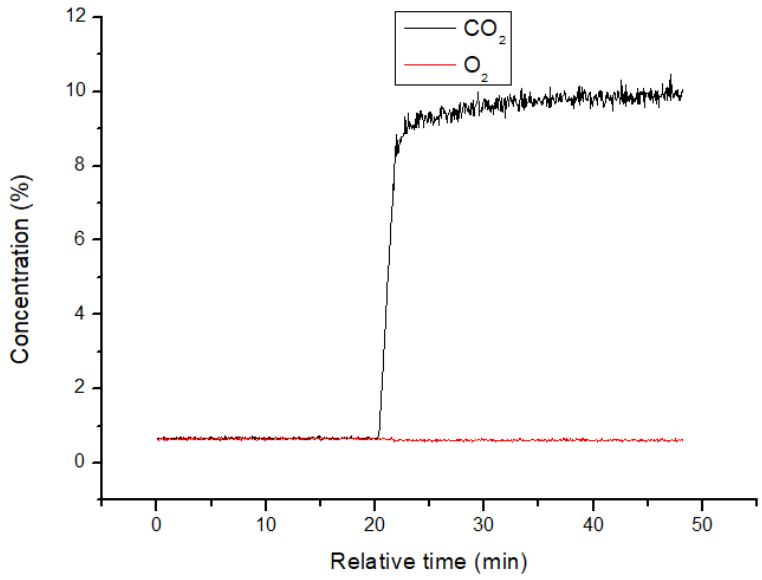

Figure 30. Trend of the second splitting cycle, obtained in an identical way to the first. Also in this case it takes time for the carbon dioxide signal to stabilize at 10 %, so the material actually manages to break down this gas into carbon monoxide.

As you can see, the trend of carbon dioxide concentration is almost the same as that seen previously, so the material regenerates during the splitting phase. Also in this case the carbon dioxide signal takes about 22 minutes before being stable around 10 %, indicating that the catalyst works in a very similar way to what was seen in the first cycle, so during the splitting of CO_2 the material actually recovers.

At the quantitative level, the area underlying the curve generated, under the same experimental conditions, by an empty tube on which carbon dioxide is passed, subtracting it from that obtained from the figure above (figure 30) was analyzed.

After that, the following equation is used, similar to the one used for H_2-TPR and O_2-TPO:

$$n = \frac{Area\ difference}{1000\ {}^{cm^3}/_{L}} \cdot \frac{pV}{RT}$$

In the first cycle, $4{,}05 \cdot 10^{-4}$ mol of carbon dioxide are split, corresponding to $6{,}48 \cdot 10^{-3}$ g of material taken, that is, since the oxygen that has been released from the CO_2 has been reabsorbed into the material, the percentage of oxygen taken from the material compared to the total one initially present in the same is at least 47 %. This can be deduced since there is no increase in the oxygen signal during the measurement, it remains constant over time.

During the second cycle, the conversion is slightly lower because $3{,}93 \cdot 10^{-4}$ mol of carbon dioxide are split, or $6{,}28 \cdot 10^{-3}$ g, so in this case the percentage of oxygen taken (and therefore released previously) is 45 %.

After the catalytic test, some other characterizations were performed, in order to see if the material would regenerate during the splitting of carbon dioxide and if it would sinter at these high temperatures. These measuring are XRD, SEM and EDX.

The XRD spectrum done after the two cycles splitting reveals that there is a segregation of metallic nickel in the structure, and this is the only one sample that presents it, so it is reported only this spectrum to see the nickel segregation, in figure 31.

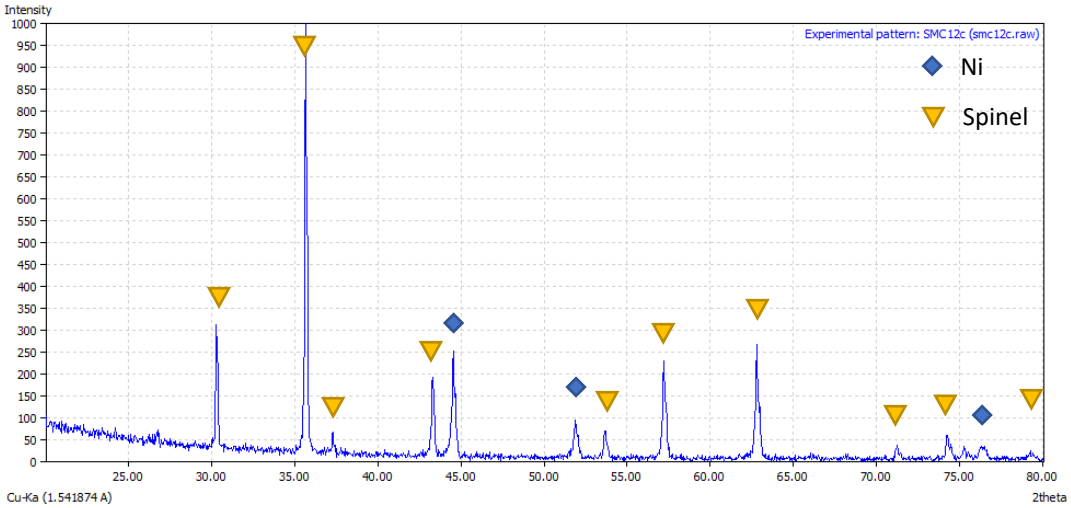

Figure 31. XRD analysis of the spinel $Ni_{0,9}Mg_{0,1}Fe_2O_4$ after two spitting tests. There is the appearance of three new reflexes at 44 °, 52 ° and 76 °, representative to segregation of metallic nickel in the spinel structure. Spinel reflexes are anyway present in the spectrum.

We can see that there are anyway spinel reflexes, but also a nickel segregation, so the structure doesn't regenerate completely.

Another SEM analysis is done with the aim of observing if there is sintering of the catalyst (figure 32).

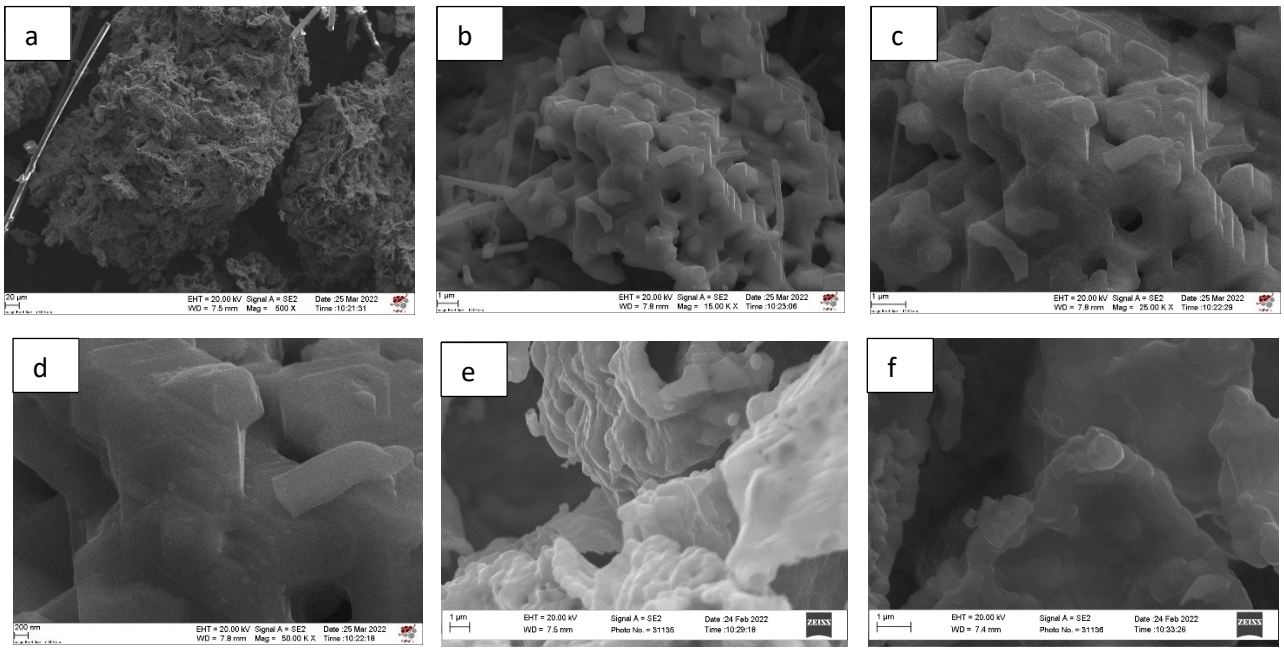

Figure 32. SEM images of the pure catalyst after two reaction cycles at 500x (a), 15000x (b), 25000x (c) and 50000x (d). It could be seen that this material tends to highly sinter during the reaction due to the very high temperatures. Images d and f are those done before these two cycles, at 15000x and 25000x respectively.

It is noticeable that this type of material is highly sintered after two splitting cycles and maybe this is the cause of the loss of performance during the second cycle, because the surface area is lower than the catalyst as synthetized. It is also interesting to see that there are structures tips-like in the surface and after an EDX analysis I saw that it is the pure spinel that apparently tends to grow in preferential directions. This high sintering doesn't allow to find the particle size. The EDX performed also shows that there weren't significant changes to the spinel's atomic percentage concentration (table 4):

Element	Expected concentration (%)	Concentration as synthetized (%)	Concentration after two splitting cycles (%)
Ni	12,9	11,5	8,8
Mg	1,4	1,0	1,2
Fe	28,6	30,2	30,2
O	57,1	57,3	59,8

Table 4. Concentration comparison between the expected one, the one obtained after synthesis and the one after two splitting cycles.

3.5. $Ni_{0,9}Mg_{0,1}Fe_2O_4$/ NiO, with 50 % NiO:

3.5.1. XRD Analysis:

The sample was analyzed by X-ray diffraction, as was the case with the catalyst (figure 33).

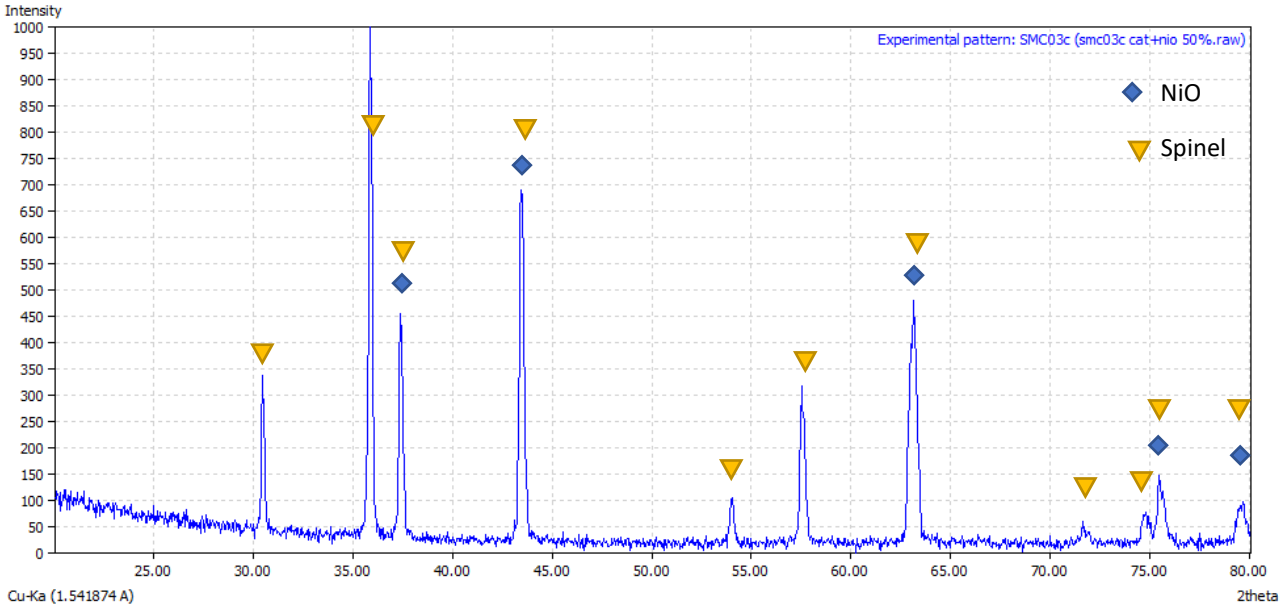

Figure 33. XRD diffractogram of the catalyst mixed with nickel oxide at 50 % in mass by ball milling and after sintering. As you can see, the XRD reflexes are identical to before (with only the catalyst, figure 19), however in this case you can notice higher reflexes, such as the third, fourth and seventh.

It has been seen that the reflexes remain unchanged, therefore the catalyst didn't react with the support. What changes are some peaks that have higher intensities than before since there is the presence of nickel oxide.

3.5.2. XPS:

A survey was carried out on the surface composition by XPS also of the compound given by spinel supported by nickel oxide, mixed at 50 % by weight (figure 34).

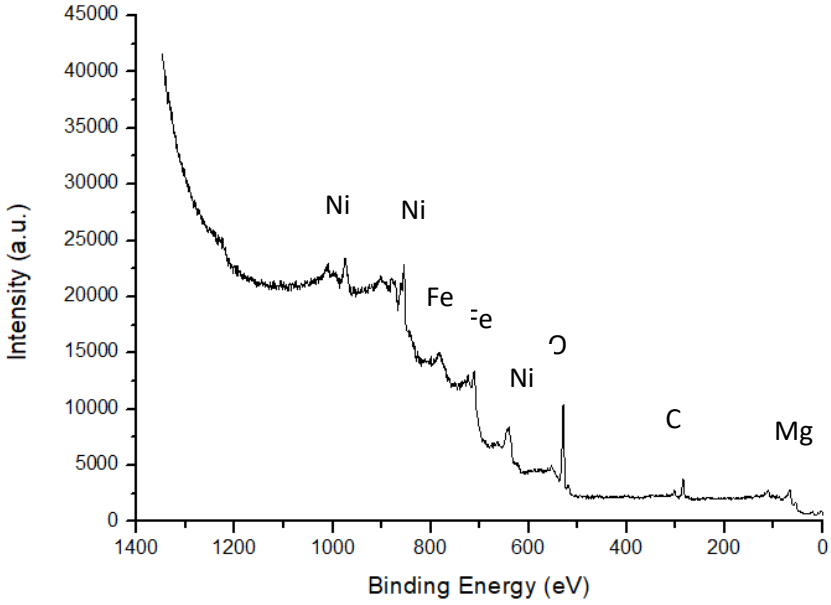

Figure 34. XPS survey given by $Ni_{0,9}Mg_{0,1}Fe_2O_4$ supported by NiO at 50 % in mass.

The peak position and shape are not modified as a consequence of the addition of NiO. With regard quantitative analysis, the following results were obtained (Table 5):

Element	Concentration (%)	Expected concentration (%)
Ni	21,3	30,2
Mg	6,5	0,8
Fe	18,8	15,2
O	53,4	53,8

Table 5. Percentage concentration experimental and theorical for $Ni_{0,9}Mg_{0,1}Fe_2O_4$ spinel mixed with 50 % in weight with nickel oxide, reported by XPS quantitative analysis.

In this case the amount of nickel is increased because this oxide is mixed with the spinel. The surface composition is consistent with the following compound: $Ni_2Mg_{0,6}Fe_{1,8}O_5$. So considering the nickel oxide support, you can find a formula of $NiMg_{0,6}Fe_{1,8}O_4$/NiO, at least on the surface. Segregation of magnesium on the surface is observed also in this case: the comparison between the experimental and expected concentration of magnesium shows that the amount of this cation is much higher than expected. As for oxygen and iron, once again the percentages are very close to each other as theorical and experimental. The species to decrease in concentration at the expense of magnesium segregation is nickel.

3.5.3. SEM:

The SEM analysis led to the following result (figure 35):

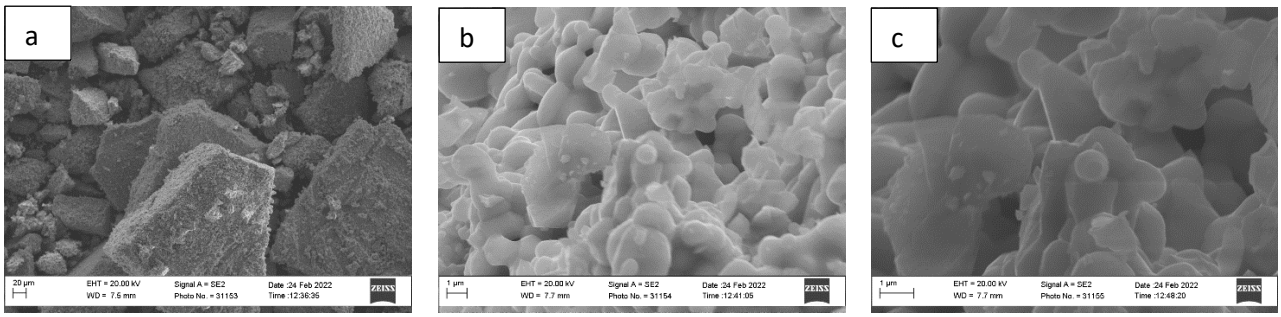

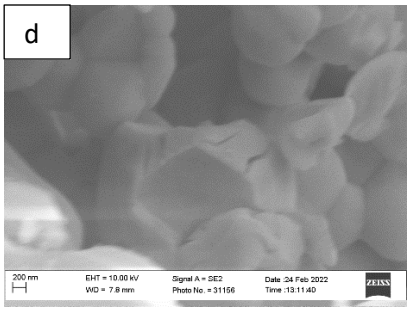

Figure 35. SEM images of the $Ni_{0,9}Mg_{0,1}Fe_2O_4$ with NiO mixed at 50% by mass. The image in figure a is at a magnification of 500x, the one in figure b is at 15000x, in figure c there is the image at 25000x, while in figure d there is the one at 50000x.

It is interesting to note how the morphology of the sample is modified by operating a ball milling, at all magnifications. Especially at 500x you can see how the macroscopical structure goes from similar to cornflake to granules, much more compact, due to mechanical forces derived from ball milling. It can also be noted that, compared to before, the material turns out to have much smaller particles, seeable at 1500x, with an average diameter of about 1,5 µm and with a quite large dispersion. A further EDX (energy dispersive X-ray spectroscopy) analysis, starting from the image obtained in figure 35,c at 25000x, led to the obtaining of the percentage composition of the sample (table 6).

Element	**Concentration (%)**	**Expected concentration (%)**
Ni	20,4	30,2
Mg	0,7	0,8
Fe	14,7	15,2
O	64,2	53,8

Table 6. Percentage atomic concentration of elements in the spinel $Ni_{0,9}Mg_{0,1}Fe_2O_4$ supported at 50 % in weight by nickel oxide, obtained by EDX against the theorical one.

Probably also in this case much depends on the selected area. In any case, the instrument detects more oxygen than necessary at the expense of nickel, while the values of iron and magnesium are very close to the theorical concentration. In this case, as in all of the systems mixed by wet ball milling, the concentration is not homogeneous as seen in the pure catalyst. This is because on a selected area there can be a particle of supporting powder but not in another different area and changes a lot the percentage of atomic concentration. All of the results reported with system mixed with ball milling, as the one on table 6, are a mean of different areas on which is done EDX.

3.5.4. Temperature Programmed Reduction:

An H_2-TPR was performed on the sample containing the nickel oxide supported catalyst, to see if it varies and in what from the same measurement carried out on the spinel and nickel oxide separately. Figure 36 shows the trend of the compound obtained after ball milling and sintering. Significant differences are observed with respect to the curve of the spinel (figure 23), or the pure nickel oxide (figure 11).

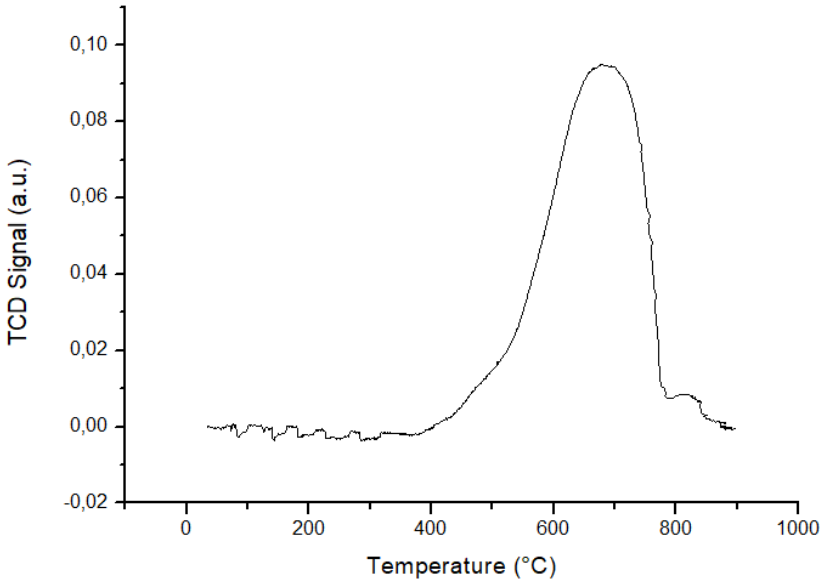

Figure 36. H_2-TPR of the system composed of $Ni_{0,9}Mg_{0,1}Fe_2O_4$ supported by NiO at 50 % in weight, after ball milling and sintering. This is different from those reported with $Ni_{0,9}Mg_{0,1}Fe_2O_4$ and NiO also.

The small peaks in the graph are considered artifacts.

In this case the area of the curve is 302,65 cm^3/g STP, while the position of the peak is at 678,9 °C, therefore higher than the previous ones. The beginning of the reduction takes place at 370 °C, very high considering the temperatures reached by the other materials. The end of the reduction is at 880 °C, again too high. The number of moles obtained is equal to $1{,}35 \cdot 10^{-2}$ mol/g, that is, for 50 mg of material, there is a number of oxygen moles released of $6{,}74\text{-}10^{-4}$ mol, equal to 87% of the total oxygen present in the sample. The grams of oxygen released will therefore be $1{,}08 \cdot 10^{-2}$ g.

3.5.5. Temperature Programmed Oxidation:

The O_2-TPO of the material gave the following result (figure 37):

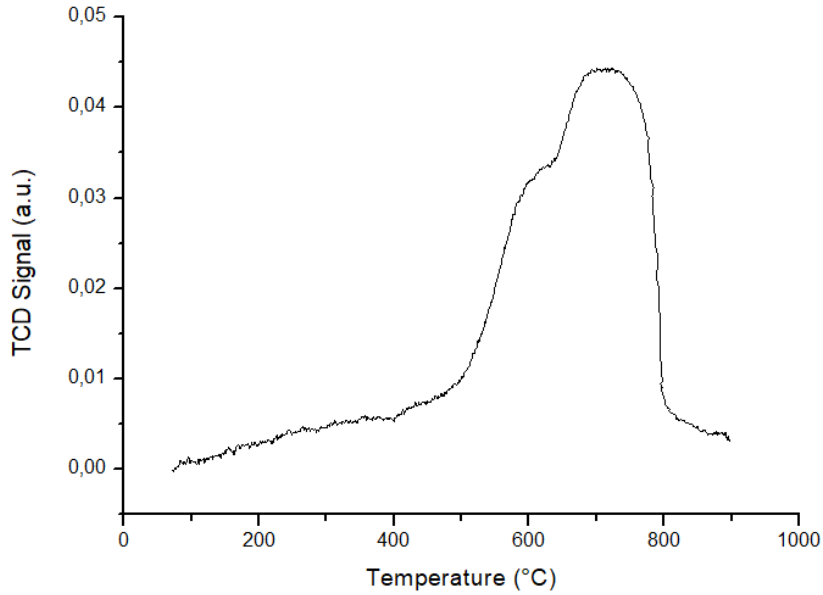

Figure 37. O_2-TPO of the system given by $Ni_{0,9}Mg_{0,1}Fe_2O_4$ supported by nickel oxide mixed at 50 % in mass. You see how the material actually reoxidizes, unlike how you rioxidize the pure catalyst.

You can see once again a different trend from the one shown in figure 27 that refers to the catalyst, so it can be said that actually this spinel is bound to nickel. Compared to the spinel alone, however, even the

reoxidation temperatures are higher as for the reduction, in fact the peak is centered at 721,7 °C. The beginning of oxidation is located at 370 °C, while its end is at about 870 °C. The area underlying the oxidation curve is 152,17 cm^3/g STP, corresponding to $6{,}79 \cdot 10^{-3}$ mol/g of molecular oxygen consumed. Normalizing for 50 mg of sample we obtain $6{,}79 \cdot 10^{-4}$ mol of reticular oxygen regained from the sample, equal to $1{,}09 \cdot 10^{-2}$ g, or 100% of oxygen taken back that had previously been released during the reduction. This material is therefore, at least as far as these measurements are concerned, very cyclable.

3.5.6. Carbon dioxide splitting:

Given that this material releases oxygen at a temperature higher than that of the spinel, and given that the spinel within 1000 °C does not release oxygen, it was thought to observe only the splitting of carbon dioxide, operating the same reducing treatment done for the pure catalyst, or emulating the TPR. A ramp of 10 °C/min was then carried out in the atmosphere of hydrogen at 5 % in helium, flowing 100 sccm, until it reached 580 °C. Then the system is brought to 1000 °C according to a ramp of 10 °C/min in the atmosphere of 100 sccm of helium, finally an atmosphere of CO_2 at 10% in helium is passed, always at 100 sccm, for 30 minutes.

The result is shown in figure 38:

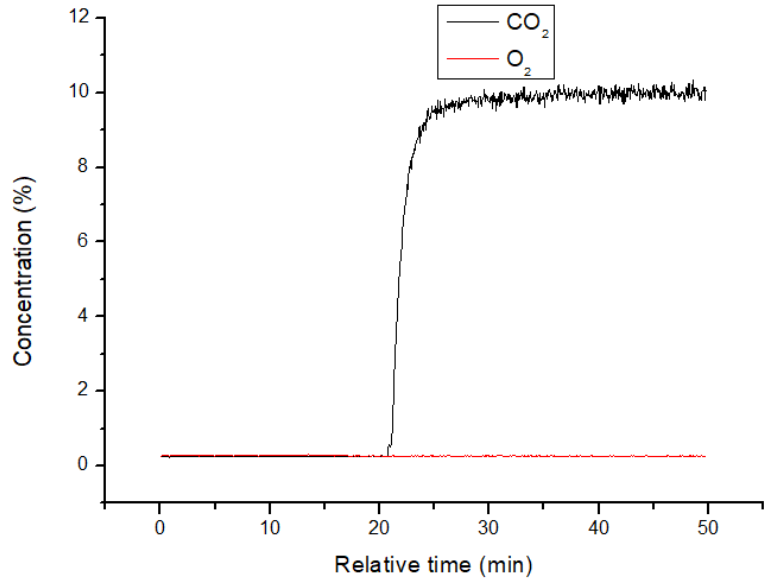

Figure 38. Trend of oxygen and carbon dioxide after having carried out a pre-treatment in 5% hydrogen up to 600 ° C and then passing CO_2 at 10% in helium. Also in this case there is splitting of carbon dioxide because the signal of this gas takes some time to stabilize at 10 %.

We see how even in this case a splitting of carbon dioxide is obtained; the signal takes about 18 min of time to return to being stable at 10 %. The oxygen signal is stable during the entire measuring, so also during the splitting there isn't release of O_2 and so the system reobtains it splitting the carbon dioxide.

Also in this case a second cycle is carried out, under the same conditions as the previous one (figure 39). The trend is very similar to the previous one, so the material regenerate itself during the breaking of CO_2.

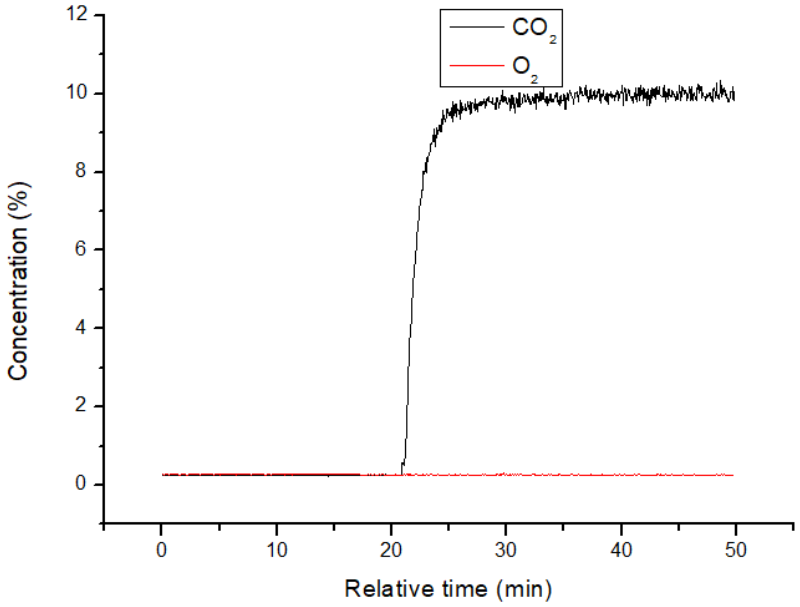

Figure 39. Trend of the second cycle of CO_2 splitting, obtained in an identical way to the first. It takes time for the carbon dioxide signal to stabilize at 10 %, so the material actually manages to break down this gas into carbon monoxide.

Also with 50 % in mass of nickel oxide the system is reversible since the results between the two cycles are comparable. Similarly to before, the splitting time is about 18 min.

Quantitatively, the system separates $3{,}42 \cdot 10^{-4}$ mol of carbon dioxide during the first cycle and $3{,}32 \cdot 10^{-4}$ during the second, corresponding to $5{,}47 \cdot 10^{-3}$ g and $5{,}31 \cdot 10^{-3}$ g of mass respectively resumed. In this case the percentage of oxygen released and taken up compared to the total oxygen present in the material is 47 % during the first cycle and 46 % during the second.

Also in this case, after the two splitting cycles, a SEM and EDX analysis were performed, in order to see if composition changes and if there is sintering.

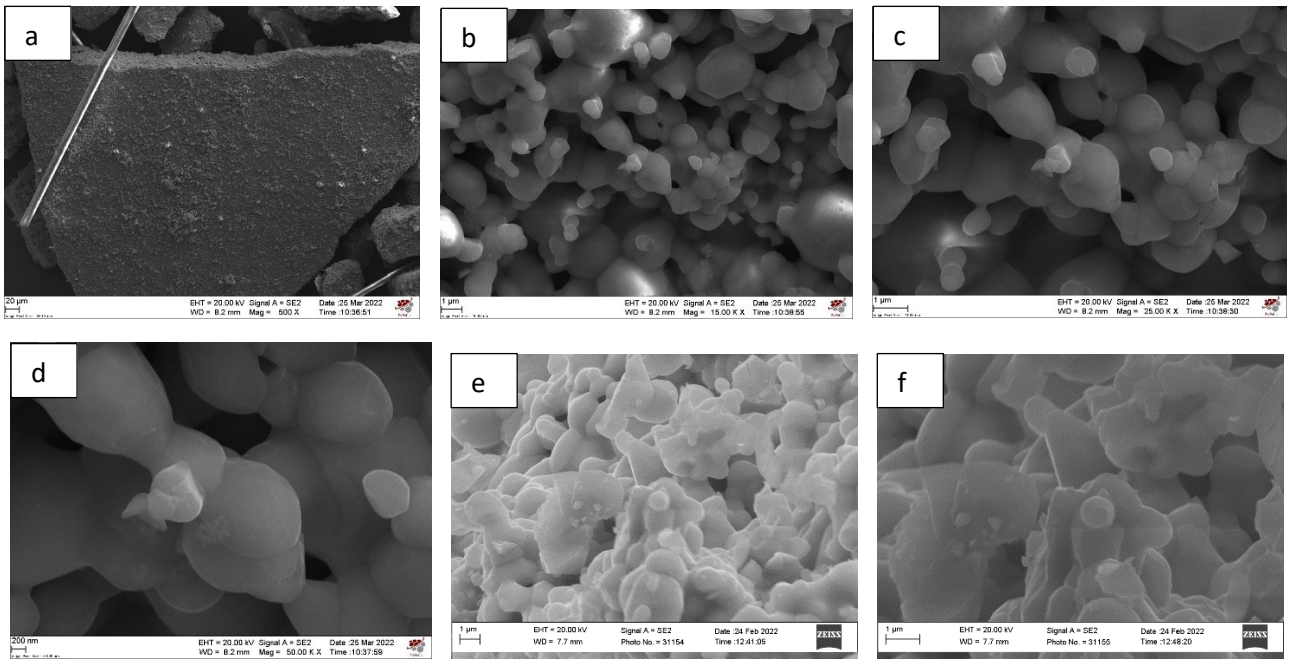

Figure 40. Catalyst mixed at 50 % in weight with nickel oxide by wet ball milling after two reaction cycles at 500x (a), 15000x (b), 25000x (c) and 50000x (d). Images e and f are those of the system as synthetized, at 15000x and 25000x.

We can see that there is a sintering of the material but it is really low compared to what happens to the pure catalyst. In this case the particle size changes from about 1,2 µm to 1,7 µm. There are some smaller particles on top of bigger ones but using EDX it could be seen that they are not different in composition to the others, probably they are so small because of Ostwald ripening present at that high splitting temperatures. An EDX analysis is performed in order to see if there were changes on the composition of the materials (table 7). Like what happens on the system as synthetized, in some places there are a bigger presence of nickel, but in others a concentration near that on pure catalyst.

Element	Expected concentration (%)	Concentration as synthetized (%)	Concentration after two splitting cycles (%)
Ni	30,2	20,4	28,1
Mg	0,8	0,7	0,7
Fe	15,2	14,7	14,1
O	53,8	64,2	57,1

Table 7. Concentration comparison of the sample made of pure catalyst mixed at 50 % in weight with NiO between the expected one, the one obtained after synthesis and the one after two splitting cycles.

The results show us that all of the concentration are near to the expected ones, more so than the as synthetized material; after two CO_2 splitting cycles there aren't changes in composition on the sample.

3.6. $Ni_{0,9}Mg_{0,1}Fe_2O_4$/ CuO with 50 % CuO:

3.6.1. XRD Analysis:

As for the system formed by catalyst and copper oxide, the XRD analysis turns out to be the following (figure 41):

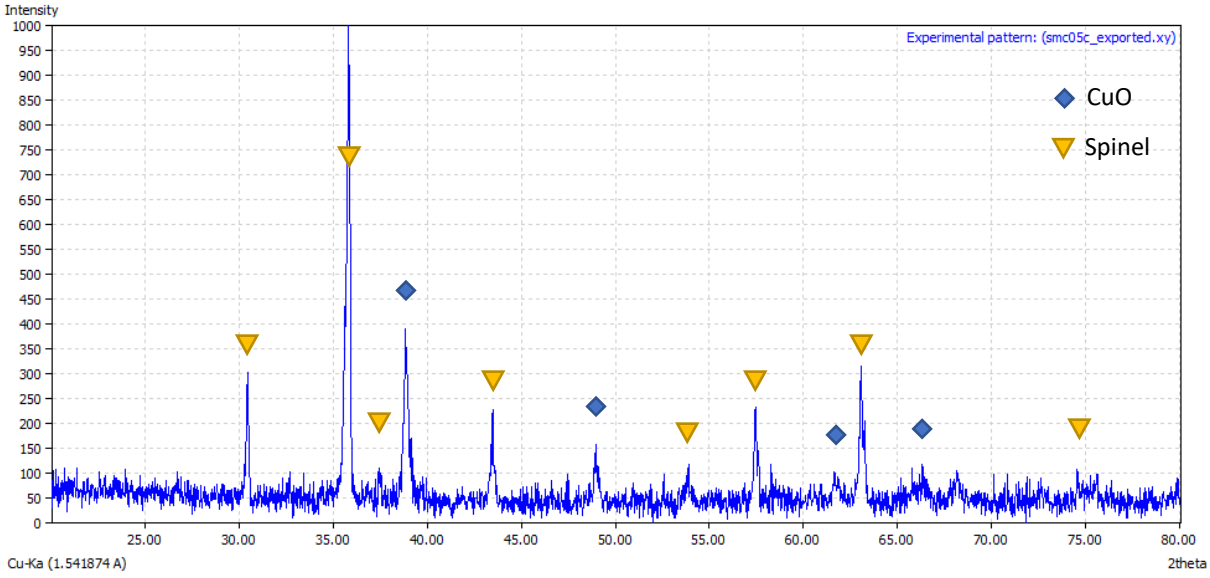

Figure 41. XRD diffractogram of the system formed by $Ni_{0,9}Mg_{0,1}Fe_2O_4$ supported by CuO at 50 % in mass. This has the same reflexes as the pure catalyst, in the same positions, however it has additional ones due to the presence of copper oxide.

It can be observed the appearance of new reflexes deriving precisely from copper oxide. Copper has not become part of the spinel structure since no shift is seen with respect to the spectrum of the pure catalyst.

3.6.2. XPS:

XPS analysis for the spinel system mixed 50 % by mass with copper oxide led to the following survey (figure 42):

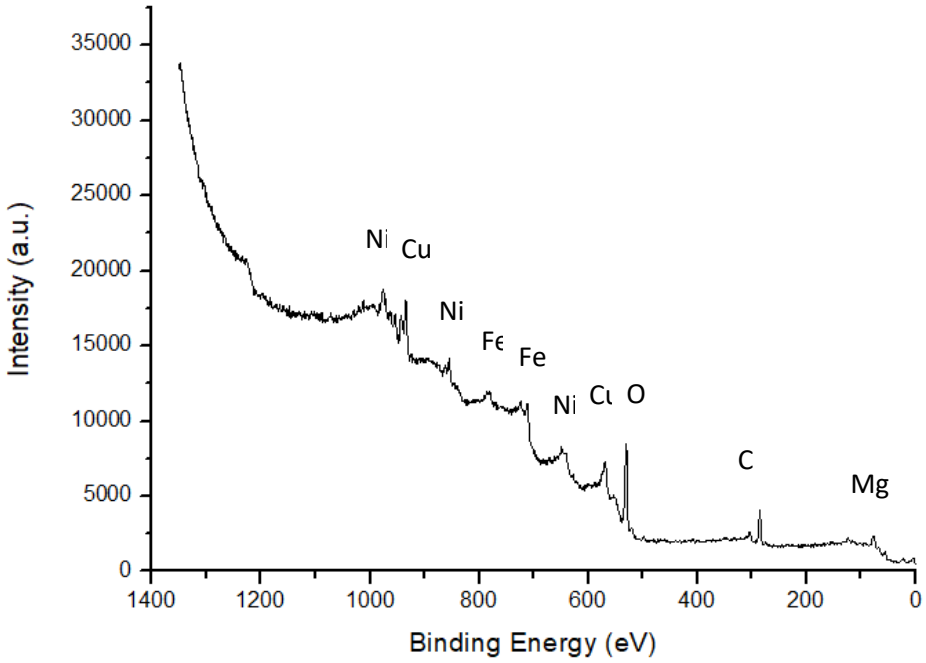

Figure 42. XPS survey given by $Ni_{0,9}Mg_{0,1}Fe_2O_4$ supported by CuO at 50 % in mass.

The quantitative analysis led to the following percentage concentrations of the elements (table 8):

Element	Concentration (%)	Expected concentration (%)
Ni	9,3	7,0
Mg	6,6	0,8
Fe	13,9	15,6
O	56,9	53,9
Cu	13,3	22,7

Table 8. Percentage concentration experimental and theorical for $Ni_{0,9}Mg_{0,1}Fe_2O_4$ spinel mixed with 50 % in weight with copper oxide, reported by XPS quantitative analysis.

As can be seen, the results also in this case doesn't correspond to the theorical concentrations. The XPS shows the presence of a lot of magnesium at the surface and a lower concentration of copper, but all other elements are at a percentage very similar to the theorical one. Also in this case the surface segregation of magnesium is observed. The resulting brute formula is $Ni_{0,8}Mg_{0,6}Fe_{1,2}Cu_{1,2}O_5$, so $Ni_{0,8}Mg_{0,6}Fe_{1,2}O_4/Cu_{1,2}O$.

3.6.3 SEM:

A SEM microscopy at different magnifications is carried out once again. Figure 43 shows the images of the sample at different magnifications: 500x, 15000x, 25000x and 50000x.

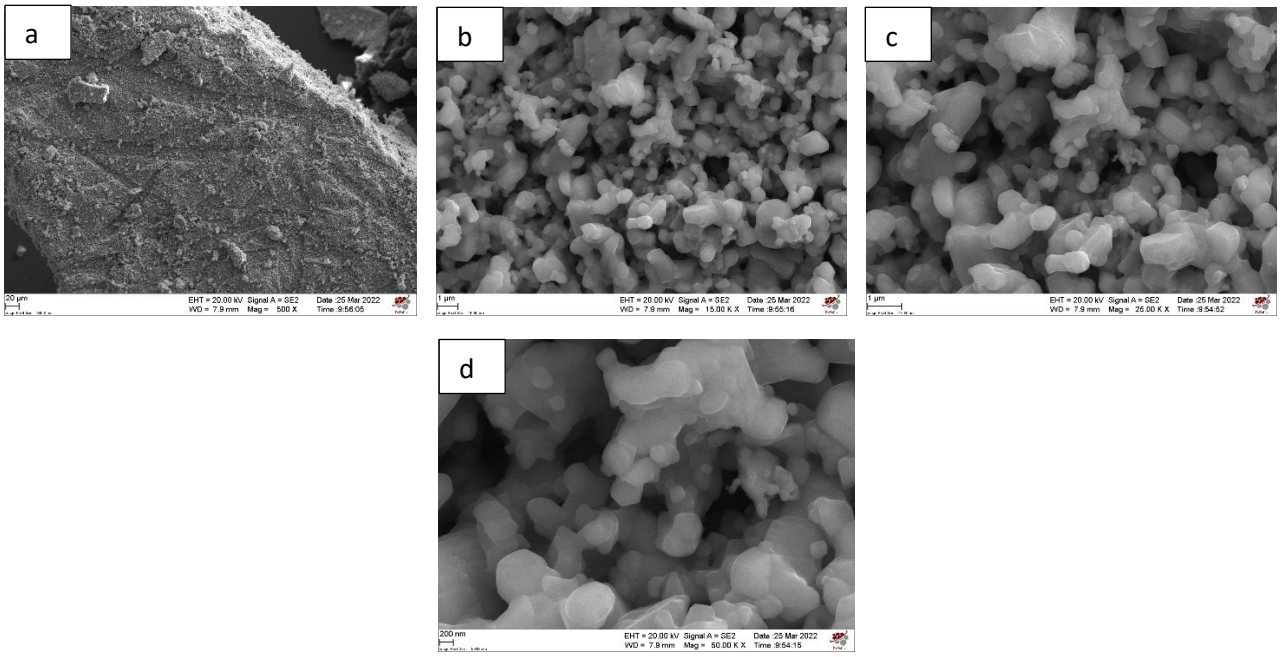

Figure 43. SEM images of the $Ni_{0,9}Mg_{0,1}Fe_2O_4$/CuO mixed at 50% by mass. The image in figure a is at a magnification of 500x, the one in figure b is at 15000x, in figure c there is the image at 25000x, while in figure d there is the one at 50000x.

Also in this case the ball milling led to a change in the morphology of the catalyst, passing once again from cornflakes-like to granular. At 15000x are visible the particles that forms the structure, and they are all pseudo-spherical, with a great dispersion of dimensions, but in average they have a diameter of about 1 µm. Also in this case the material turns out to be a good conductor of electricity since no lines are noticed in the pictures.

The EDX analysis starting from the image in figure 43,c led to the following result, in table 9.

Element	Concentration (%)	Expected concentration (%)
Ni	6,0	7,0
Mg	0,6	0,8
Fe	15,1	15,6
O	57,1	53,9
Cu	21,2	22,7

Table 9. Percentage atomic concentration of elements in the spinel $Ni_{0,9}Mg_{0,1}Fe_2O_4$ supported at 50 % in weight by copper oxide, obtained by EDX against the theoretical one.

As before, the experimental results and the theorical ones are very similar to each other, so you can see how on the surface, according to the XPS, there is a slight segregation of magnesium, while in general the composition of the material is the desired one as can be seen from the EDX measurements.

3.6.4. Temperature Programmed Reduction:

The H_2-TPR of the copper oxide supported catalyst brought the following result (figure 44):

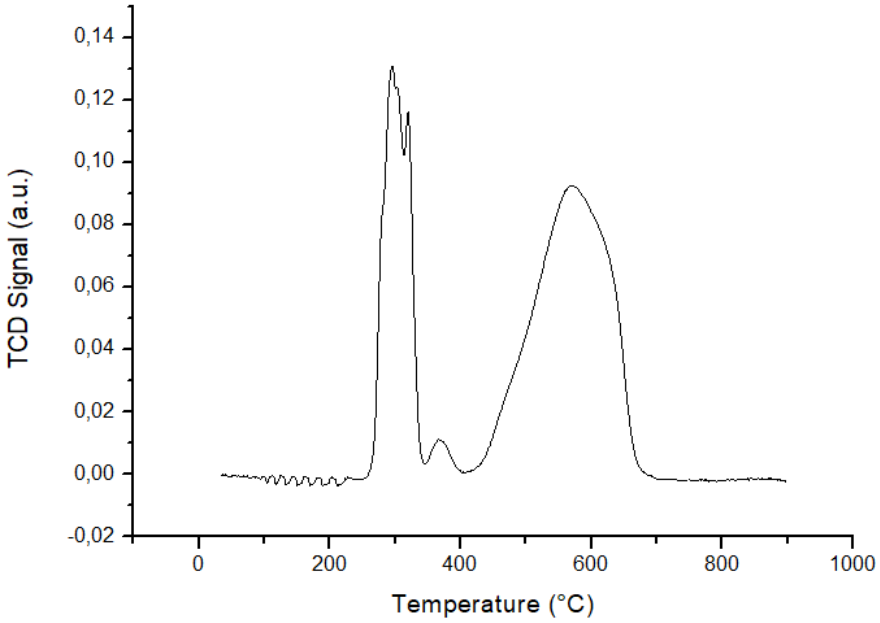

Figure 44. H_2-TPR of $Ni_{0,9}Mg_{0,1}Fe_2O_4$ supported by CuO at 50 % in mass after ball milling and sintering. You can see how the trend is different than both pure copper oxide and catalyst.

The material in this case has two main peaks: one due to copper oxide (at lower temperatures) and one due to spinel (at higher temperatures).

The total area of the reduction peaks is 325,85 cm^3/g STP, moreover the system begins to reduce to about 250 °C, before the reduction of the catalyst itself but after that of the copper oxide. The reduction ends at about 720 °C, again much earlier than the end of the reduction of the pure spinel. The highest peak is at 295,4 °C, deriving from copper, while that of the spinel is at 569,6 °C, lower than that of the pure spinel. The moles of oxygen released are $1{,}45 \cdot 10^{-2}$ mol/g so you have, for 50 mg of material, $7{,}27 \cdot 10^{-4}$ mol, equal to 97 % of the oxygen released compared to the total one. The grams of oxygen lost will then be $1{,}16 \cdot 10^{-2}$ g.

3.6.5. Temperature Programmed Oxidation:

Again, after H_2-TPR, an O_2-TPO is made (figure 45).

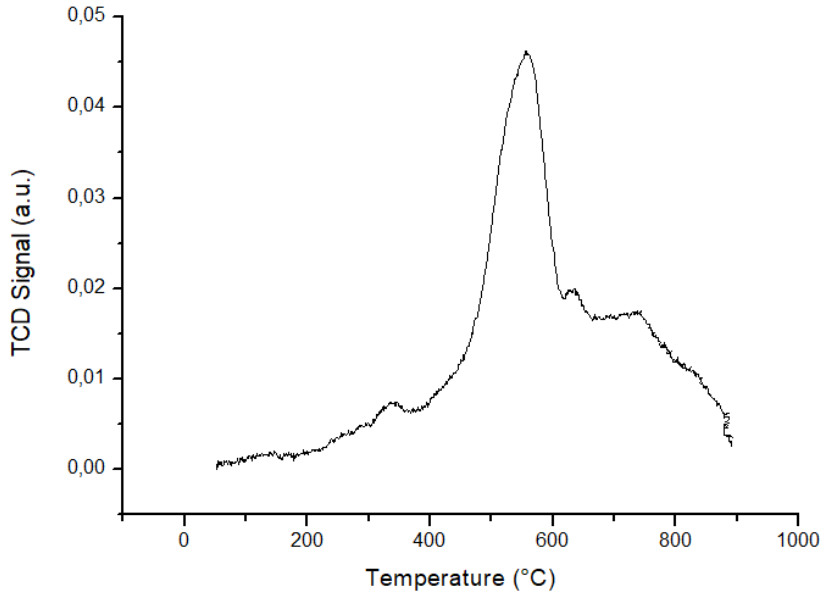

Figure 45. O_2-TPO of the system composed of a catalyst supported by copper oxide at 50 % in weight, obtained after H_2-TPR.

In this case the reoxidation begins at about 180 °C and ends at about 900 °C, while the peak oxygen consumption is at 555,4 °C. The area underlying the curve is 134,49 cm^3/g STP, corresponding to $6{,}00 \cdot 10^{-3}$ mol/g of molecular oxygen consumed, or, for 50 mg, $6{,}00 \cdot 10^{-4}$ mol of reabsorbed reticular oxygen. The percentage of oxygen regained compared to that released by H_2-TPR is 83 %. The mass is therefore increased by $9{,}60 \cdot 10^{-3}$ g.

3.6.6. Carbon dioxide splitting:

Since also this type of compound doesn't release oxygen at a temperature of 1000 °C, the same treatment was carried out as in the previous samples, so a temperature ramp of 10 °C/min flushing 100 sccm of 5 % of hydrogen into helium up to 580 °C and then, again with the same ramp, up to 1000 °C in an inert atmosphere before passing 100 sccm of CO_2 to 10 % in helium.

The result is shown in figure 46.

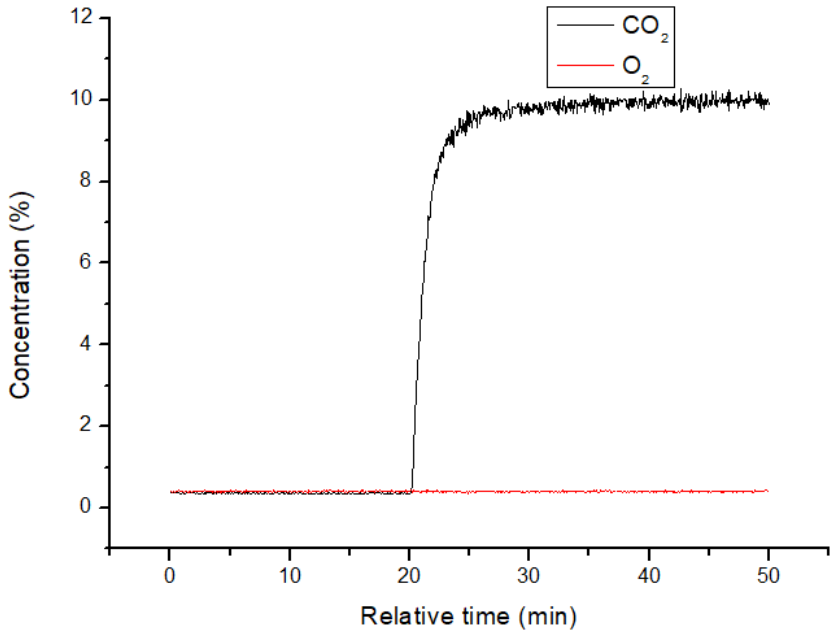

Figure 46. Trend of oxygen and carbon dioxide after having carried out a pre-treatment in 5% hydrogen up to 600 ° C and then passing CO_2 at 10% in helium.

The splitting of carbon dioxide takes place also in this case, in about 24 min, and the oxygen formed is reabsorbed in the material because the oxygen signal is stable during all the measure. The number of moles of split gases turn out to be $4{,}22 \cdot 10^{-4}$ mol, corresponding to $6{,}75 \cdot 10^{-3}$ g of oxygen taken, or the 56 % of oxygen compared to the total present in the material.

In this case, the second cycle (figure 47) isn't similar to the first one because there is a lower splitting time. In fact, carbon dioxide is now converted into 12 min, separating $2{,}59 \cdot 10^{-4}$ mol of gas, that is, taking $4{,}14 \cdot 10^{-3}$ g of oxygen or 35 %, very low considering the results obtained previously. It may be caused because of copper that is difficult to reoxidize.

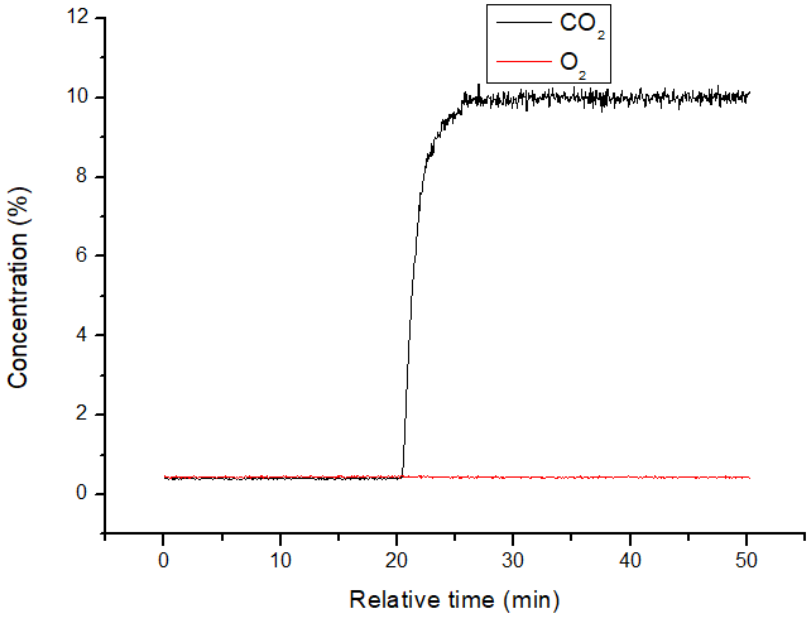

Figure 47. Trend of the second cycle of CO_2 splitting, obtained in an identical way to the first. Also in this case we can see that the material break the carbon dioxide.

A SEM analysis is performed after these two splitting cycles, in order to see if there was sintering (figure 48).

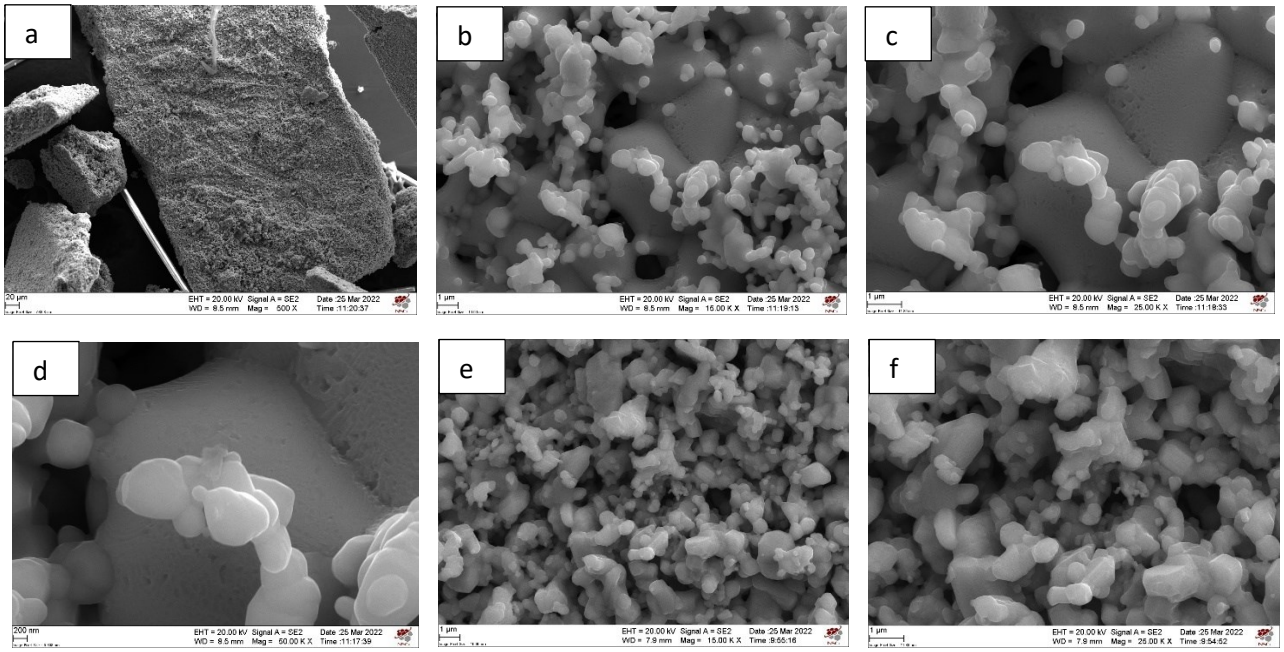

Figure 48. Catalyst mixed at 50 % in weight with copper oxide by wet ball milling after two reaction cycles at 500x (a), 15000x (b), 25000x (c) and 50000x (d). Images e and f refer to the system as synthetized at 15000x and 25000x magnifications.

It is interesting to see that there are small particles on top of very big ones, in this case there is a big sintering, so the system at 1000 °C isn't so stable and with these images is possible to understand why there is that great loss in performance of the sample during the second cycle. That happens because of this sintering and so because of that decrease in superficial area. In fact, now the mean particle size is of about 2,2 µm instead of 1 µm as synthetized. An EDX analysis reveals that the big sintering is due to copper oxide particles that melts at 1326 °C[36], because the atomic percentage composition of the particles on the background is that of CuO, but the smaller particles have the composition of the spinel. An EDX on a bigger area is performed, and the results are reported in table 10.

Element	Expected concentration (%)	Concentration as synthetized (%)	Concentration after two splitting cycles (%)
Ni	7,0	6,0	6,7
Mg	0,8	0,6	0,9
Fe	15,6	15,1	15,6
O	53,9	57,1	54,5
Cu	22,7	21,2	22,3

Table 10. Concentration comparison of the sample made of pure catalyst mixed at 50 % in weight with CuO between the expected one, the one obtained after synthesis and the one after two splitting cycles.

It can be seen that, also with this big sintering, the composition of the system is by the way unchanged with respect to the one obtained with the material before the reaction cycles.

3.7. $Ni_{0,9}Mg_{0,1}Fe_2O_4$/ ZrO_2, with at 50 % ZrO_2:

3.7.1. XRD Analysis:

X-ray diffraction analysis of the system reported the underlying pattern (figure 49):

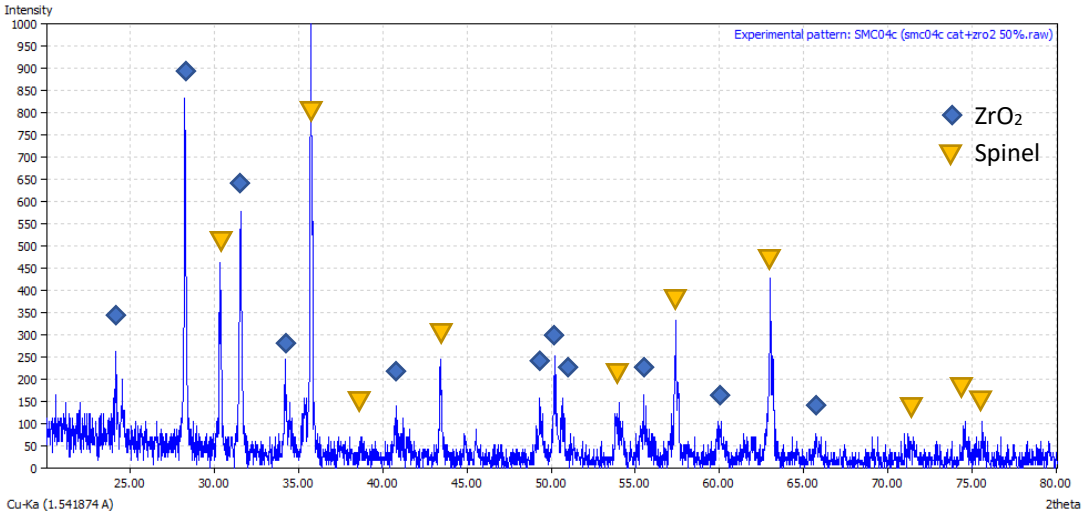

Figure 49. XRD pattern of the compound obtained by mixing by wet ball milling at 50 % by weight of zirconium oxide with the spinel used as a catalyst. The reflexes of both inserted powders are clearly visible and separated from each other, indicating that both materials did not react to each other during sintering.

As you can see, in addition to the reflexes of the spinel, shown in figure 19, there are also reflexes related to the zirconia used as a support. This suggests that the two materials did not react in the solid state.

3.7.2. XPS:

The survey done via XPS led to the following graph, shown in figure 50:

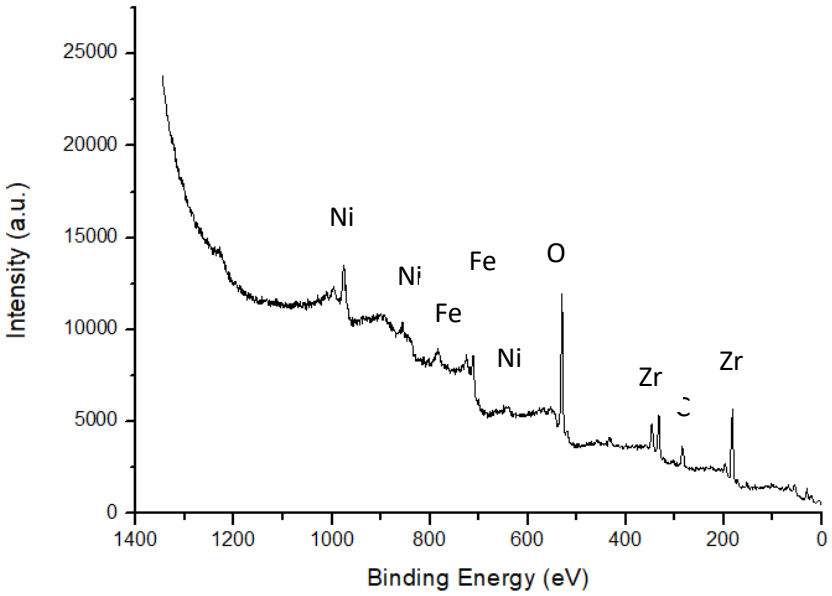

Figure 50. XPS survey given by $Ni_{0,9}Mg_{0,1}Fe_2O_4$ supported by ZrO_2 at 50 % in mass.

The quantitative analysis led to the result in table 11:

Element	Concentration (%)	Expected concentration (%)
Ni	6,7	7,1
Mg	6,3	0,8
Fe	13,6	15,8
O	60,8	61,4
Zr	12,6	14,9

Table 11. Percentage concentration experimental and theorical for $Ni_{0,9}Mg_{0,1}Fe_2O_4$ spinel mixed with 50 % in weight with zirconia, reported by XPS quantitative analysis.

We see once again the presence of segregation on the surface of magnesium, while the percentages of others are very close to the theorical ones. The brute formula turns out to be $Ni_{0,7}Mg_{0,6}Fe_{1,3}Zr_{1,2}O_6$, so $Ni_{0,7}Mg_{0,6}Fe_{1,3}O_4/Zr_{1,2}O_2$.

3.7.3. SEM:

Figure 51 shows the images at different magnifications: 500x, 15000x, 25000x and 50000x.

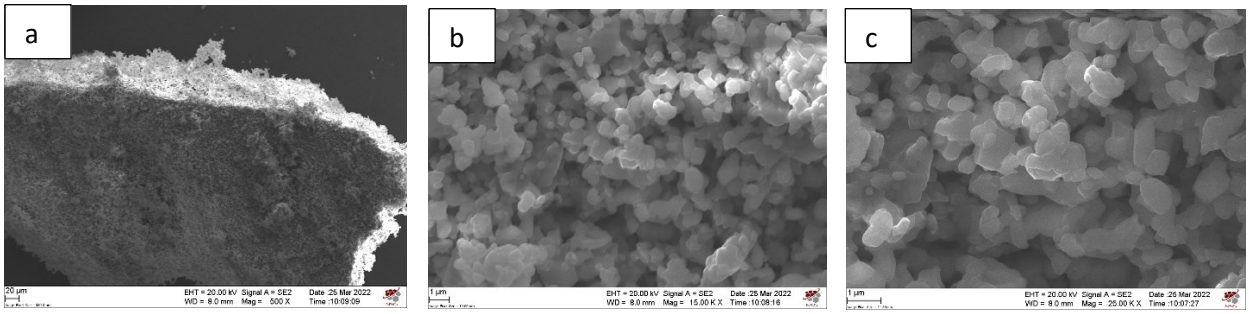

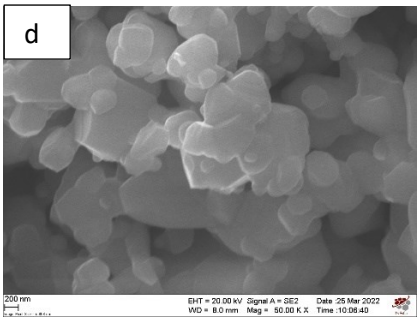

Figure 51. SEM images of the $Ni_{0,9}Mg_{0,1}Fe_2O_4$ spinel mixed at 50% by mass with ZrO_2. The image in figure a is at a magnification of 500x, the one in figure b is at 15000x, in figure c there is the image at 25000x, while in figure d there is the one at 50000x.

We can notice that the particles are present with a spherical shape and attached each other. There is a great dispersion of particle's diameter but in average it is about 0,7 µm.

The EDX analysis starting from the image in figure 50,c leads to these percentages of atoms revealed, reported in table 12:

Element	Concentration (%)	Expected concentration (%)
Ni	7,5	7,1
Mg	0,7	0,8
Fe	16,1	15,8
O	62,7	61,4
Zr	13,0	14,9

Table 12. Percentage atomic concentration of elements in the spinel $Ni_{0,9}Mg_{0,1}Fe_2O_4$ supported at 50 % in weight by zirconium oxide, obtained by EDX against the theorical one.

You can see how the theorical percentages and those obtained experimentally are again very close to each other.

3.7.4. Temperature Programmed Reduction:

The H_2-TPR obtained is shown in figure 52:

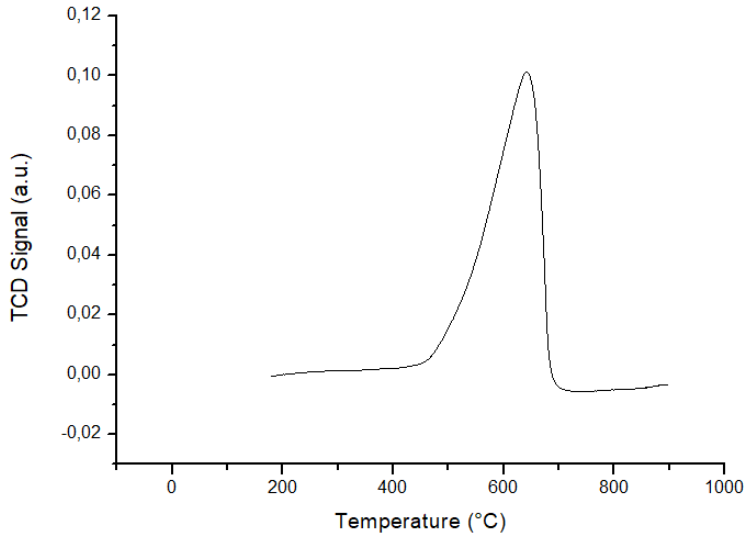

Figure 52. H_2-TPR of $Ni_{0,9}Mg_{0,1}Fe_2O_4$ supported by ZrO_2 after ball milling and sintering. In this case the trend isn't similar to that of pure spinel, though zirconia doesn't release oxygen.

The system begins its reduction at about 410 °C, while the maximum is present at 641,9 °C. The end of the curve, on the other hand, turns out to be at 730 °C. The presence of zirconia, so, have a bad impact on the reduction of the material because it increases the starting reduction temperature and also the peak temperature, even though the reduction ending temperature is lowered.

The area of the curve is 590,60 cm^3/g STP, corresponding to $8{,}50 \cdot 10^{-3}$ mol of hydrogen consumed and then oxygen released. Normalizing for 50 mg, you get $4{,}25 \cdot 10^{-4}$ mol of O_2 released or $6{,}80 \cdot 10^{-3}$ g of oxygen. The percentage of oxygen released is in this case 51 % compared to the total oxygen present in the material, which is rather low considering the others. The catalyst oxygen is at 51 % in the system and that confirm the fact that only spinel releases oxygen and zirconia is inert. This is because, as is also seen in the H_2-TPR of zirconia, this compound is inert and does not release oxygen even at 900 °C.

3.7.5. Temperature Programmed Oxidation:

The O_2-TPO of the material, obtained after H_2-TPR, is shown in figure 53.

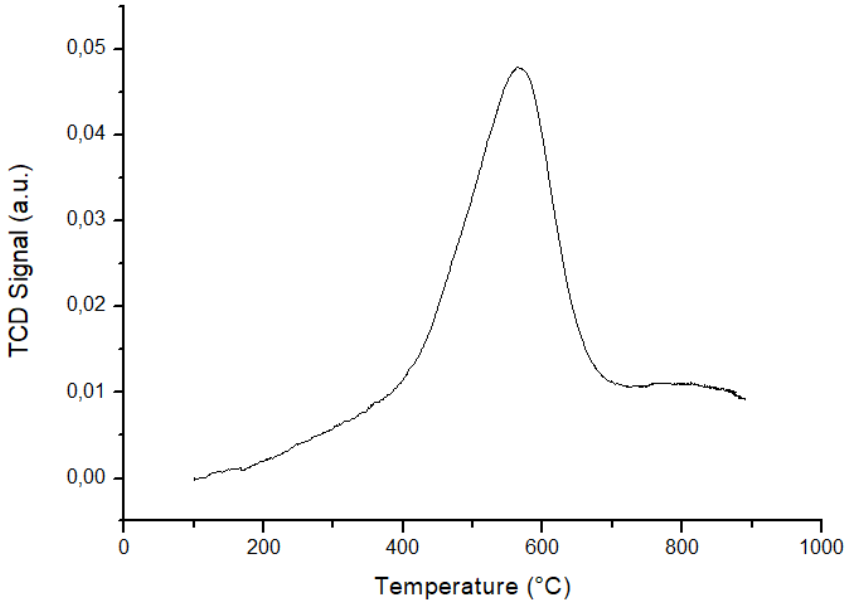

Figure 53. O_2-TPO of the system composed by the spinel and zirconia mixed at 50 % in mass, obtained after the H_2-TPR. The linear increasing of the TCD signal is due to an experimental artifact, so it isn't considered.

In this case, the oxidation starting temperature is 340 °C, a little less than the one of the catalyst, that was about 350 °C. The maximum of the peak is at 563,9 °C and the oxidation ending temperature is about 720 °C.

Quantitatively, the area of the curve in this case is 93,21 cm^3/g STP, corresponding to $4{,}16 \cdot 10^{-3}$ mol of molecular oxygen consumed. Normalizing for 50 mg, $4{,}16 \cdot 10^{-4}$ mol of O_2 or $6{,}65 \cdot 10^{-3}$ g of reticular oxygen taken from the system is obtained. The percentage of oxygen regained compared to that released is 98 %. So also in the oxidation the zirconia remains an inert (how we saw previously with the study of pure zirconia), but the spinel regain nearly all of the oxygen released during the reduction.

3.7.6. Carbon dioxide splitting:

Since the material releases oxygen at too high temperatures, as can be seen from the H_2-TPR, the measurement of carbon dioxide splitting after pre-treatment in hydrogen up to 580 °C was carried out, and then the separation of this gas into carbon monoxide is carried out at 1000 °C. The trend of the detected gases, CO_2 and O_2, is shown in figure 54.

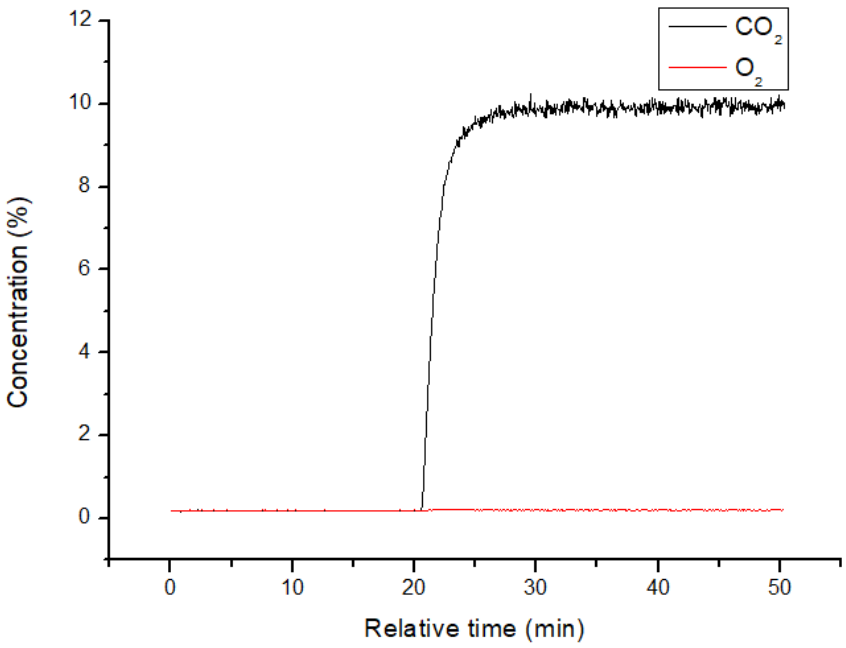

Figure 54. Trend of oxygen and carbon dioxide after having carried out a pre-treatment in 5% hydrogen up to 600 ° C and then passing CO_2 at 10% in helium for the spinel mixed at 50 % in mass with zirconium oxide.

Also in this case the actual separation of carbon dioxide takes place, in about 20 min. The number of moles of split gases turn out to be $3{,}02 \cdot 10^{-4}$ mol, corresponding to $4{,}83 \cdot 10^{-3}$ g of oxygen taken, or the 36 % of oxygen compared to the total present in the material. It can be seen that, similarly to H_2-TPR and O_2-TPO measurement, zirconia is an inert and so it reduces the total oxygen moles released and taken from the material because the only part of the system that is active is the spinel one.

In the second cycle (figure 55) the results are pretty similar to those of the first. In this cycle carbon dioxide is converted in about 18 min, separating $2{,}96 \cdot 10^{-4}$ mol of gas, that is, taking $4{,}73 \cdot 10^{-3}$ g of oxygen or 35 %. Also in this case the results are pretty low with respect to those obtained with other supports at 50 % due to the inert behaviour of zirconium oxide.

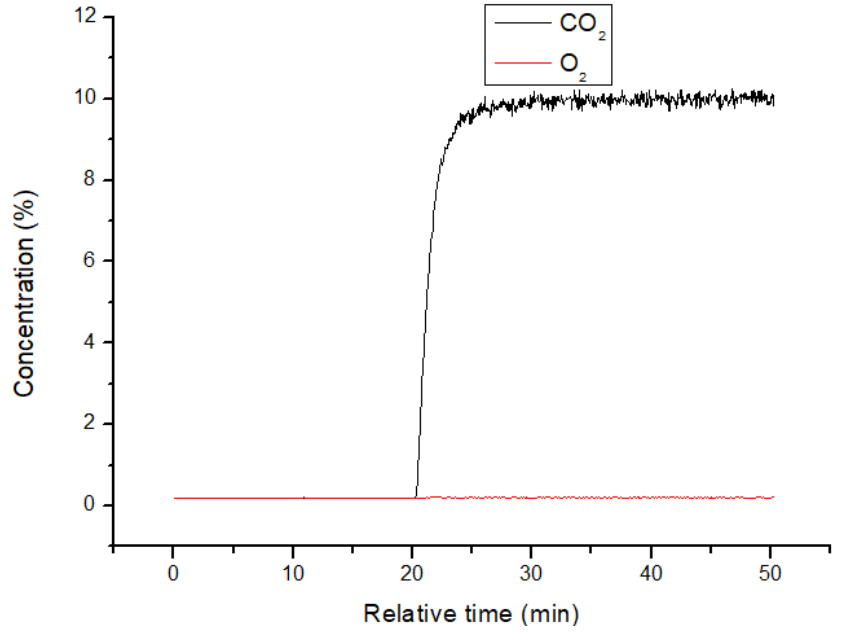

Figure 55. Second cycle of CO_2 splitting, obtained with the same pre-treatment of the first. Also in this cycle there is the splitting of carbon dioxide.

Again, a SEM analysis, reported in figure 56, is done in order to see if there is sintering of the sample's particles at the high temperature at which carbon dioxide splitting is achieved.

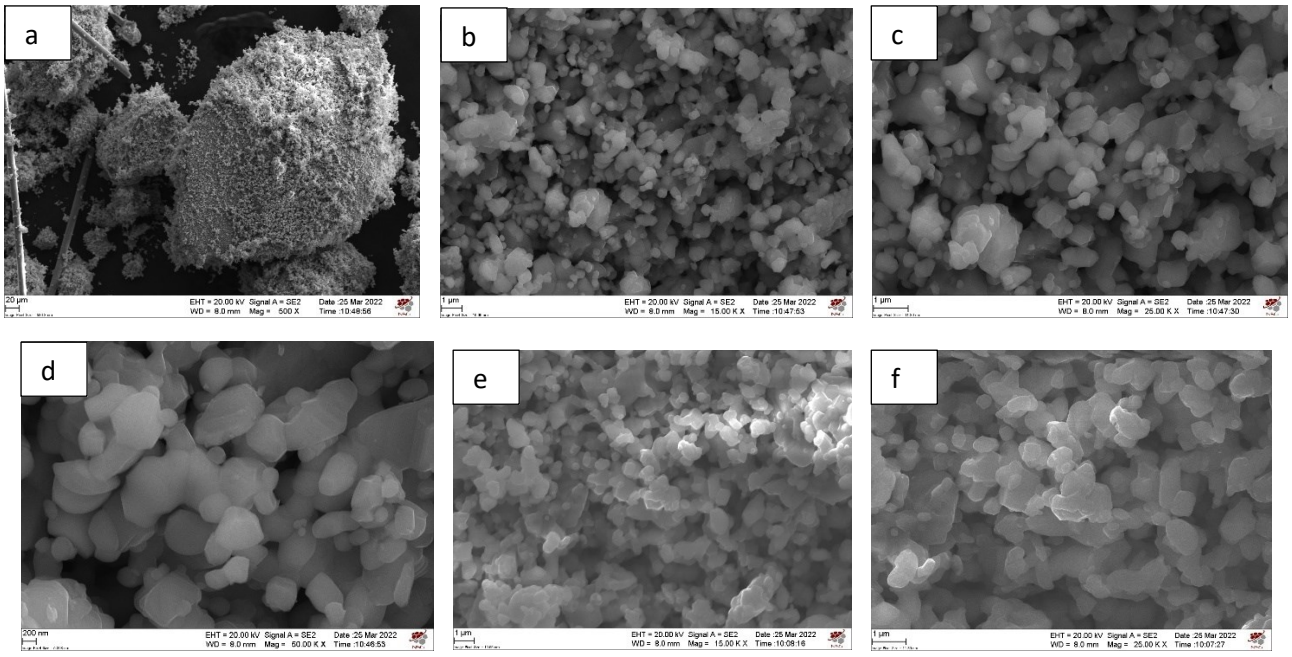

Figure 56. Catalyst mixed at 50 % in weight with zirconium oxide by wet ball milling after two reaction cycles at 500x (a), 15000x (b), 25000x (c) and 50000x (d). e and f refer to the sample before two splitting cycles.

It can be seen that supporting the catalyst with zirconium oxide leads to a very low sintering of the particles, in fact we can distinguish one particle from the other even at 50000x. The particle average dimension now is more or less 0,8 µm, very close to the mean 0,7 µm saw with the sample before the cycles. So, it can be noticed that even if catalytic property is lowered, supporting the material with zirconium oxide improve its cyclability, as seen after in carbon dioxide splitting cycles. As done before, an EDX analysis is performed and the results are reported in table 13:

Element	Expected concentration (%)	Concentration as synthetized (%)	Concentration after two splitting cycles (%)
Ni	7,1	7,5	7,2
Mg	0,8	0,7	0,7
Fe	15,8	16,1	16,7
O	61,4	62,7	62,0
Zr	14,9	13,0	13,4

Table 10. Concentration comparison of the sample made of pure catalyst mixed at 50 % in weight with ZrO_2 between the expected one, the one obtained after synthesis and the one after two splitting cycles.

The composition, so, doesn't change after two splitting cycles but is very similar to the theoretical one and to the composition of the sample before the catalytic activity.

3.8. $Ni_{0,9}Mg_{0,1}Fe_2O_4$/ NiO, with 20 % NiO:

3.8.1 XRD Analysis:

The XRD analysis of the new system composed of catalyst and 20 % by mass of nickel oxide mixed by wet ball milling brought the same results obtained using 50 % by mass of NiO, that is the raising of some spikes of the spinel deriving from the presence of nickel oxide, obviously less than the previous mixing since the amount of nickel oxide inserted is less (figure 57).

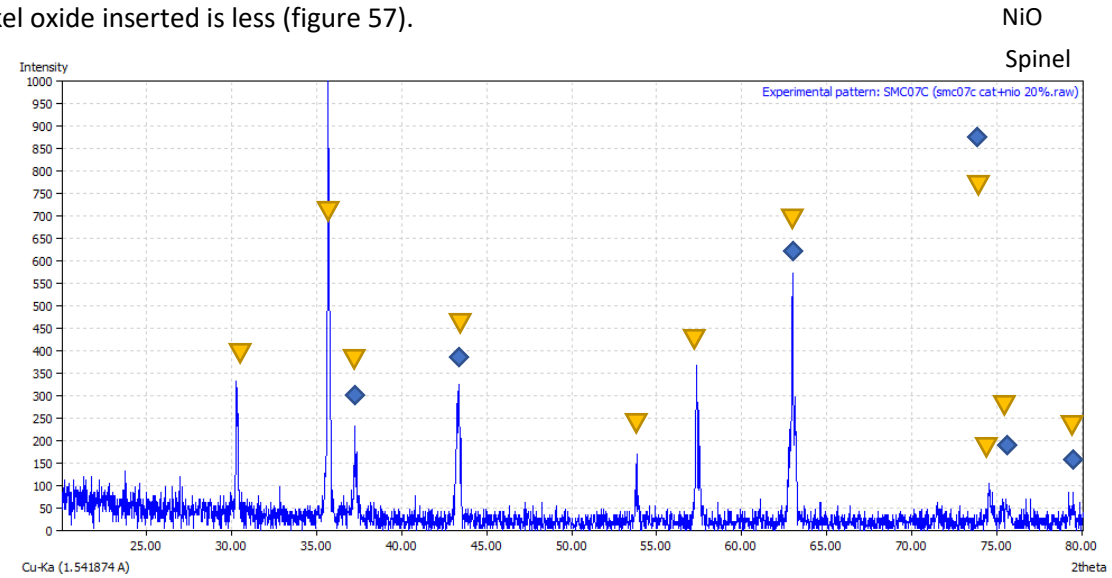

Figure 57. XRD pattern of the compound obtained by mixing by wet ball milling 20 % by weight of nickel oxide with the spinel used as a catalyst. The nickel oxide reflexes are once again superimposed on those of the spinel, but the absence of shift of the same is an indication of the fact that both materials did not react to each other during sintering.

The absence of shifts of the reflexes suggests that the two powders have not reacted, as in previous cases.

3.8.2. XPS:

XPS survey led to the following graph, shown in figure 58:

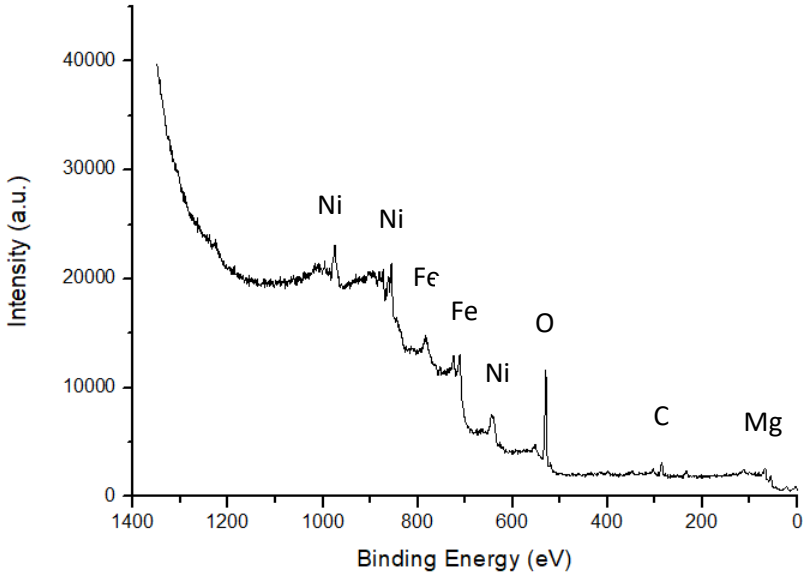

Figure 58. XPS survey given by $Ni_{0,9}Mg_{0,1}Fe_2O_4$ supported by NiO at 20 % in mass.

The quantitative analysis led to the result in table 14:

Element	Concentration (%)	Expected concentration (%)
Ni	20,6	19,6
Mg	9,0	1,2
Fe	19,2	23,4
O	51,2	55,8

Table 14. Percentage concentration experimental and theorical for $Ni_{0,9}Mg_{0,1}Fe_2O_4$ spinel mixed with 20 % in weight with nickel oxide, reported by XPS quantitative analysis.

Magnesium is also in this case at a higher percentage concentration with respect to that expected, while the percentages of other atoms are very close to the theorical ones. The brute formula turns out to be $Ni_2Mg_{0,9}Fe_{1,9}O_5$, that is $NiMg_{0,9}Fe_{1,9}O_4$/NiO.

3.8.3. SEM:

Figure 59 shows the images at different magnifications: 500x, 15000x, 25000x and 50000x.

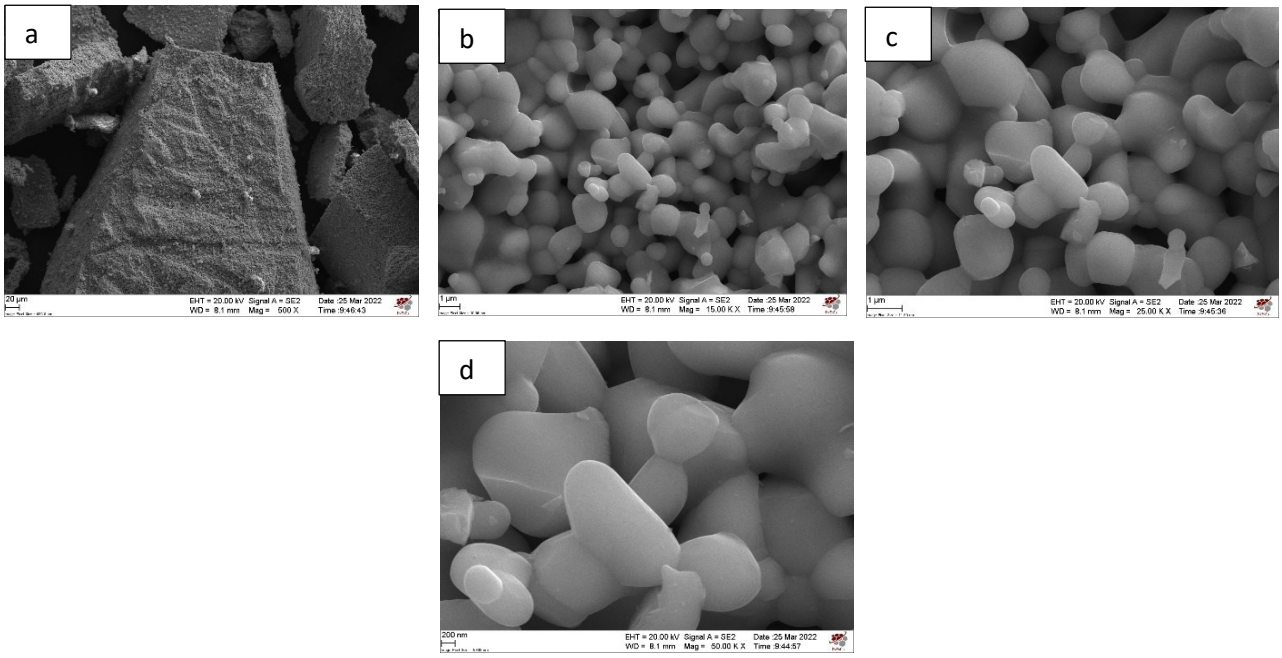

Figure 59. SEM images of the $Ni_{0,9}Mg_{0,1}Fe_2O_4$ spinel mixed at 20% by mass with NiO. The image in figure a is at a magnification of 500x, the one in figure b is at 15000x, in figure c there is the image at 25000x, while in figure d there is the one at 50000x.

We can see especially at 50000x that now particles are smaller than the one seen with spinel mixed at 50 % with nickel oxide, in fact we can now distinguish between two particles even at a magnification of 50000x. The mean diameter of the particles is now of about 1,0 µm.

The EDX analysis starting from the image in figure 58,c leads to these percentages of atoms revealed, reported in table 15 below:

Element	Concentration (%)	Expected concentration (%)
Ni	18,9	19,6
Mg	2,1	1,2
Fe	20,8	23,4
O	58,2	55,8

Table 15. Percentage atomic concentration of elements in the spinel $Ni_{0,9}Mg_{0,1}Fe_2O_4$ supported at 20 % in weight by nickel oxide, obtained by EDX against the theorical one.

Theoretical percentages and those obtained experimentally are again very close to each other.

3.8.4. Temperature Programmed Reduction:

H_2-TPR led to the following result (figure 60):

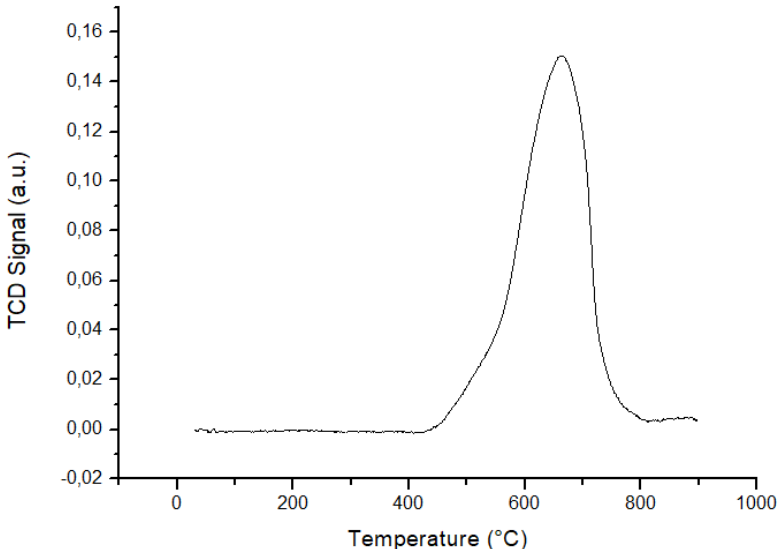

Figure 60. H_2-TPR of $Ni_{0,9}Mg_{0,1}Fe_2O_4$/ NiO, with NiO mixed at 20% by mass, after ball milling and sintering. This is different from those reported with $Ni_{0,9}Mg_{0,1}Fe_2O_4$, NiO pure and both mixed at 50%.

It can be noted that, compared to the mixing of 50 % nickel oxide and catalyst, the beginning of the reduction of the system is shifted to higher temperatures, about 430 ° C, even worse than the pure spinel. The end of the reduction is at 830 °C, while the peak is at 669,7 °C. Quantitatively, the area of the curve is 340,80 cm^3/g, therefore the moles are $1{,}52 \cdot 10^{-2}$ mol/g, considering the 50 mg of the system we arrive at a release of $7{,}60 \cdot 10^{-4}$ mol of oxygen, then at $1{,}22 \cdot 10^{-2}$ g. The release of oxygen is 92 % of the total present in the system.

3.8.5. Temperature Programmed Oxidation:

Following H_2-TPR, an O_2-TPO was carried out, which led to the following result (figure 61):

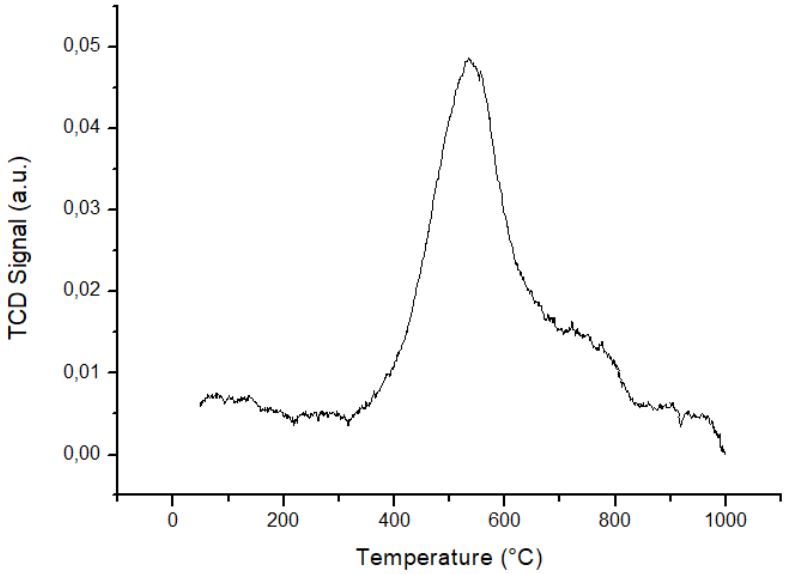

Figure 61. O_2-TPO of $Ni_{0,9}Mg_{0,1}Fe_2O_4$/NiO, with NiO mixed at 20% by mass, obtained after H_2-TPR. Also in this case it is different from those reported with $Ni_{0,9}Mg_{0,1}Fe_2O_4$, NiO pure and both mixed at 50 %.

The system begins its oxidation at about 310 °C, and ends it at about 840 °C. The maximum oxidation is located at 535,2 °C, very close to the oxidation point of the pure spinel. The area underlying the curve is 150,51 cm^3/g STP, corresponding to $6{,}72 \cdot 10^{-3}$ mol/g. Normalizing for 50 mg results in a consumption of $6{,}72 \cdot 10^{-4}$ mol of atomic oxygen entering the lattice, corresponding to 88 % of regained oxygen compared to that previously released. The grams of oxygen taken are $1{,}07 \cdot 10^{-2}$ g.

3.8.6. Carbon dioxide splitting:

Since also with 20 % in weight of nickel oxide the material releases oxygen at too high temperatures, as can be seen from the H_2-TPR, the splitting was carried up after pre-treatment in hydrogen up to 580 °C, and then the separation of this gas is done at 1000 °C. The trend of the detected gases, CO_2 and O_2, is shown in figure 62.

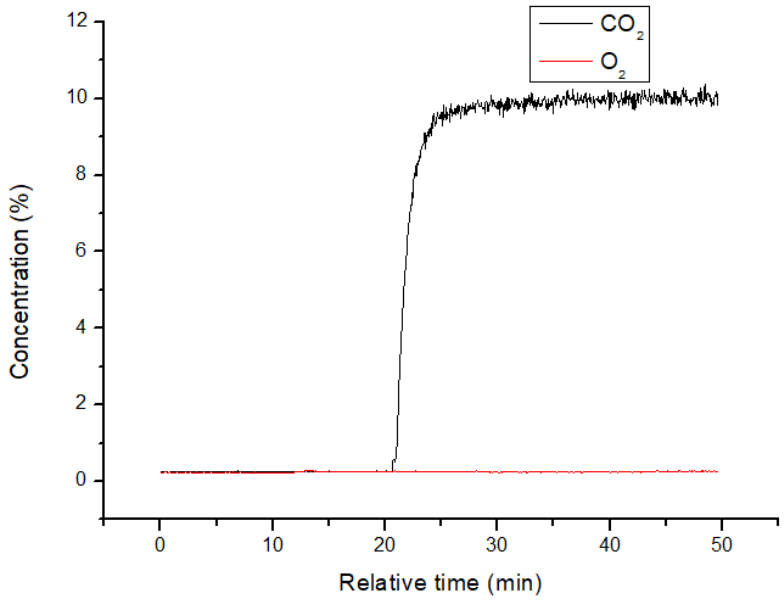

Figure 62. Trend of oxygen and carbon dioxide after having carried out a pre-treatment in 5% hydrogen up to 600 ° C and then passing CO_2 at 10% in helium for the spinel mixed at 20 % in mass with nickel oxide.

As you can see, the actual separation of carbon dioxide takes place, in 20 min more or less. The number of moles of split gas turn out to be $3{,}67 \cdot 10^{-4}$ mol, corresponding to $5{,}89 \cdot 10^{-3}$ g of oxygen taken, or the 44 % of oxygen compared to the total present in the material.

In the second cycle, similarly to the first, carbon dioxide is converted into about 20 min, separating $3{,}58 \cdot 10^{-4}$ mol of gas and so taking $5{,}72 \cdot 10^{-3}$ g of oxygen or the 43 % of the total oxygen that is present on the sample.

Below is reported the graph obtained (figure 63):

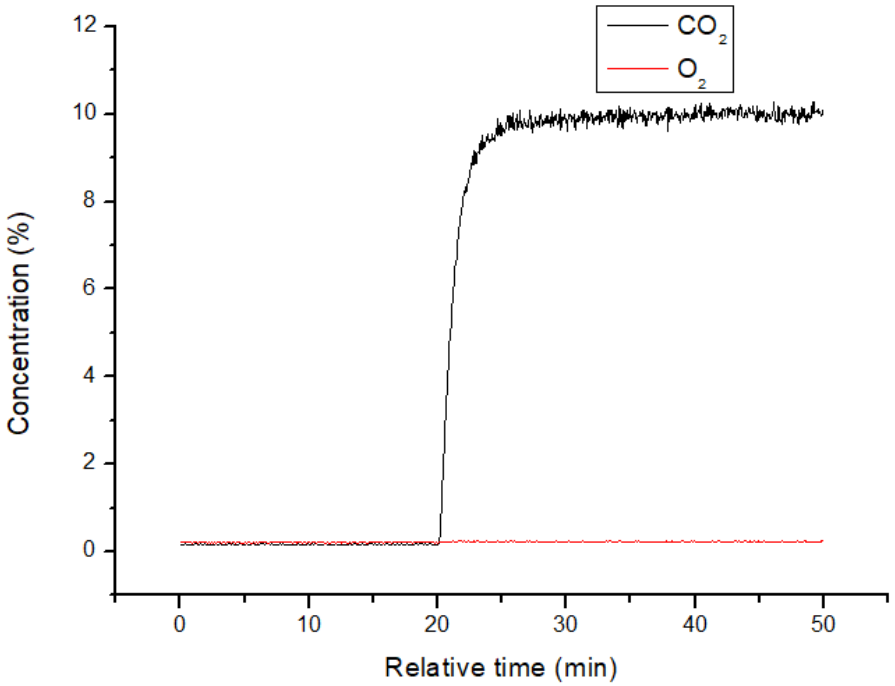

Figure 63. Second cycle of CO_2 splitting, that is very similar to the first one. We can see that also in this case the carbon monoxide is formed.

The SEM images are reported below, at figure 64:

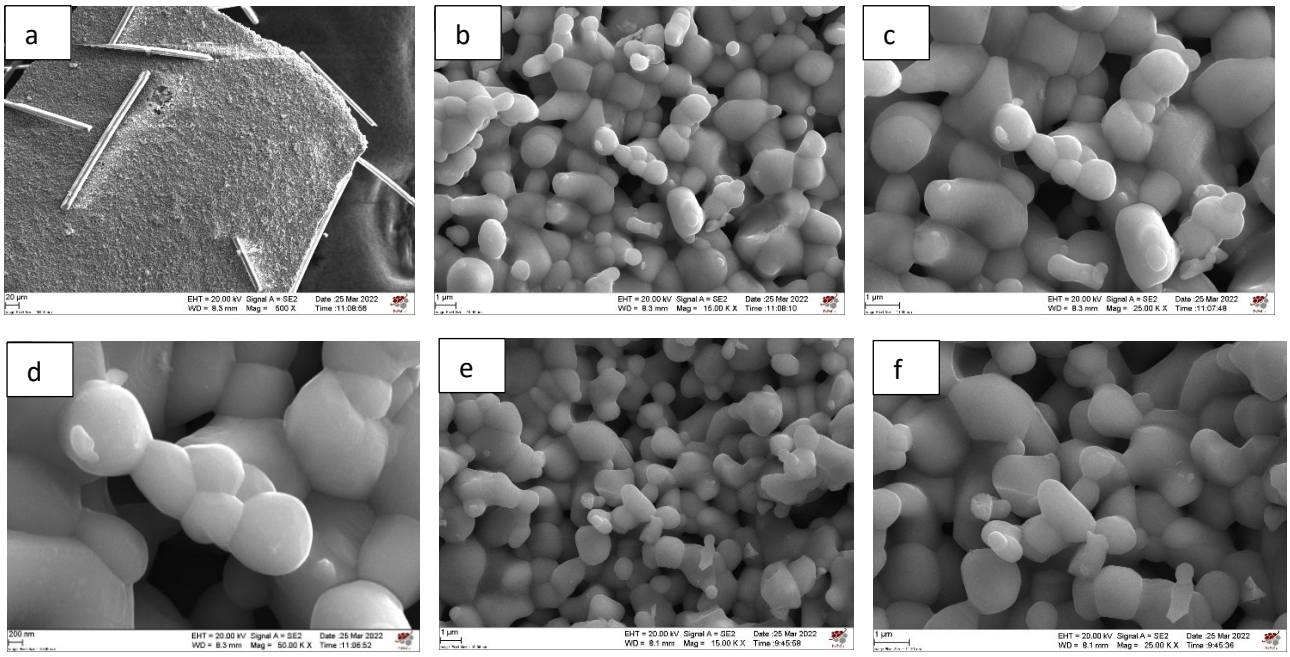

Figure 64. Catalyst mixed at 20 % in weight with nickel oxide by wet ball milling after two reaction cycles at 500x (a), 15000x (b), 25000x (c) and 50000x (d). There are reported also images e and f that are those obtained before the treatment, at 15000x and 25000x.

The structure similar to pins also in this case present at a magnification of 500x is quartz wool used as a mechanical support for when the sample is inserted in the reactor.

It could be seen the presence of sintering, especially at a magnification of 50000x, but it is very low with respect to that noticed with 50 % of nickel oxide. We can see spherical particles well distinguishable also at magnification of 25000x; the average diameter is of nearly 1,2 µm, pretty higher than that measured for the

system before splitting activity. In table 16 are present percentage concentration theorical, as synthetized and post cycles of the sample. It can be seen that they are all very similar to each other.

Element	Expected concentration (%)	Concentration as synthetized (%)	Concentration after two splitting cycles (%)
Ni	19,6	18,9	20,4
Mg	1,2	2,1	1,9
Fe	23,4	20,8	20,2
O	55,8	58,2	57,5

Table 16. Concentration comparison of the sample made of pure catalyst mixed at 20 % in weight with NiO between the expected one, the one obtained after synthesis and the one after two splitting cycles.

3.9. $Ni_{0,9}Mg_{0,1}Fe_2O_4$/ CuO, with 20 % CuO:

3.9.1. XRD Analysis:

XRD analysis of the system composed of spinel and copper oxide at 20 % by mass led to the following result (figure 65):

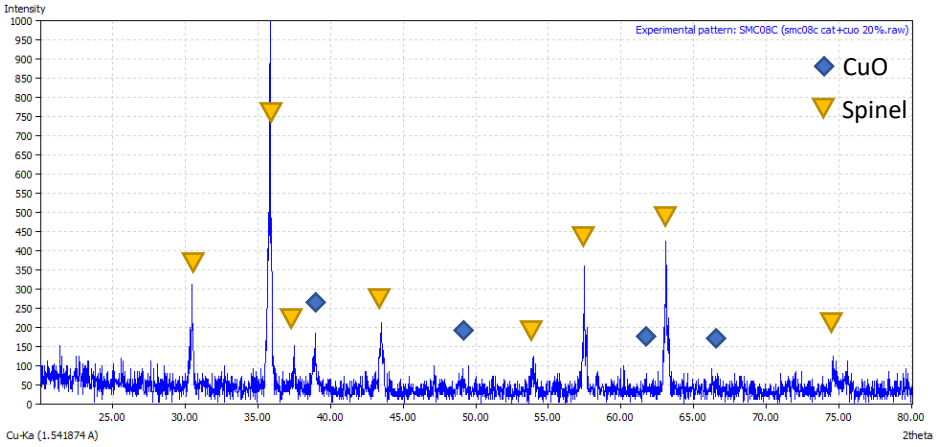

Figure 65. XRD diffractogram of the compound obtained by mixing by wet ball milling 20 % by weight of copper oxide with the spinel used as a catalyst. The reflexes of both inserted powders can be observed, indicating once again that both materials did not react to each other during sintering.

As for the mixing at 50 % by mass, also in this case the reflexes related to the cupric oxide appear, albeit with lower intensities precisely because less of this powder has been mixed. Again, the shift of the reflexes is not present, which is why it is possible to think that no reaction to the solid state has occurred.

3.9.2. XPS:

The survey via XPS led to the following graph, shown in figure 66:

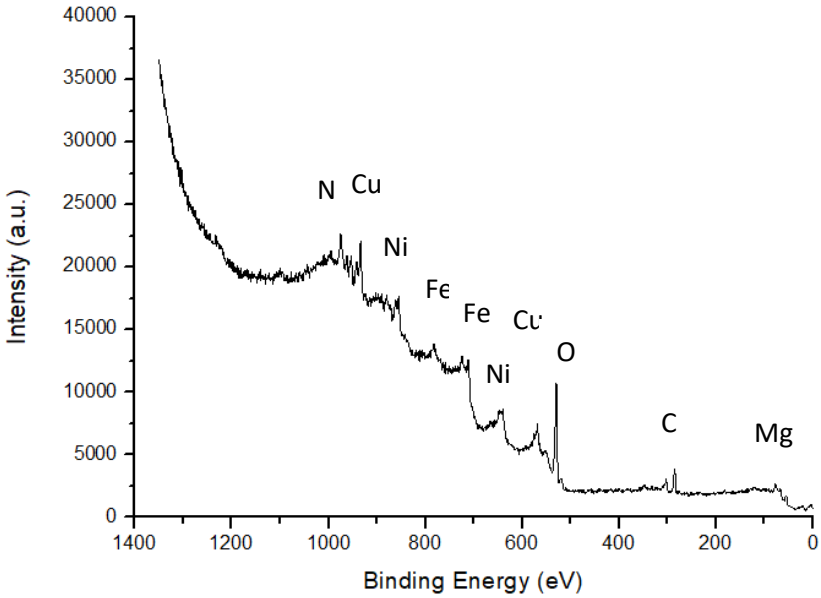

Figure 66. XPS survey given by $Ni_{0,9}Mg_{0,1}Fe_2O_4$ supported by CuO at 20 % in mass.

The quantitative analysis led to the result in table 17:

Element	Concentration (%)	Expected concentration (%)
Ni	12,6	10,7
Mg	6,9	1,2
Fe	22,8	23,7
O	50,2	55,9
Cu	7,5	8,5

Table 17. Percentage concentration experimental and theorical for $Ni_{0,9}Mg_{0,1}Fe_2O_4$ spinel mixed with 20 % in weight with copper oxide, reported by XPS quantitative analysis.

Except for the usual high concentration of magnesium, all other percentage are very close to the theorical ones. The resulting formula is $Ni_{1,3}Mg_{0,7}Fe_{2,3}Cu_{0,7}O_5$, so $Ni_{1,3}Mg_{0,7}Fe_{2,3}O_4/Cu_{0,7}O$.

3.9.3. SEM:

Figure 67 shows the images at different magnifications: 500x, 15000x, 25000x and 50000x.

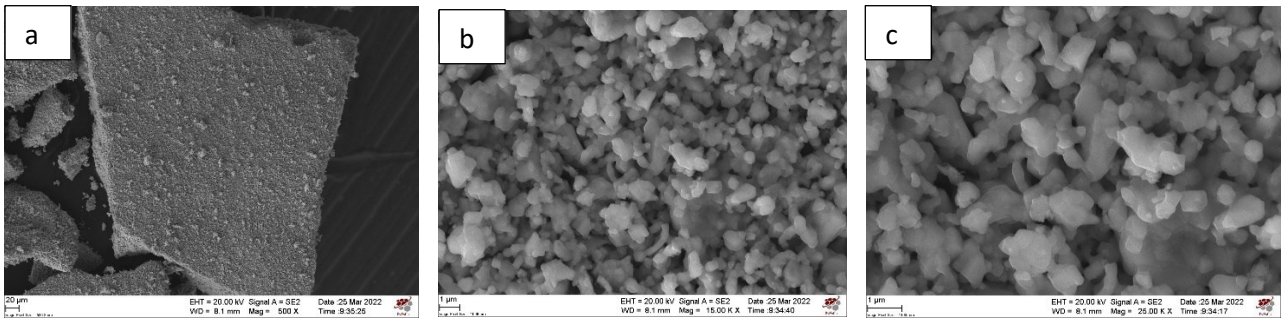

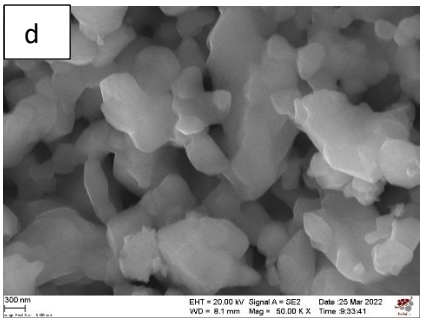

Figure 67. SEM images of the $Ni_{0,9}Mg_{0,1}Fe_2O_4$ spinel mixed at 20% by mass with CuO. The image in figure a is at a magnification of 500x, the one in figure b is at 15000x, in figure c there is the image at 25000x, while in figure d there is the one at 50000x.

The SEM images are very similar to that obtained mixing 50 % of copper oxide with the spinel; also the average particle size is like before, in fact it is nearly 1 µm.

The EDX analysis starting from the image in figure 66,c leads to these percentages of atoms revealed, in table 18:

Element	Concentration (%)	Expected concentration (%)
Ni	8,7	10,7
Mg	1,3	1,2
Fe	21,3	23,7
O	59,0	55,9
Cu	9,7	8,5

Table 18. Percentage atomic concentration of elements in the spinel $Ni_{0,9}Mg_{0,1}Fe_2O_4$ supported at 20 % in weight by copper oxide, obtained by EDX against the theorical one.

You can see how the theorical percentages and those obtained experimentally are again very close to each other.

3.9.4. Temperature Programmed Reduction:

The H_2-TPR obtained is shown in figure 68:

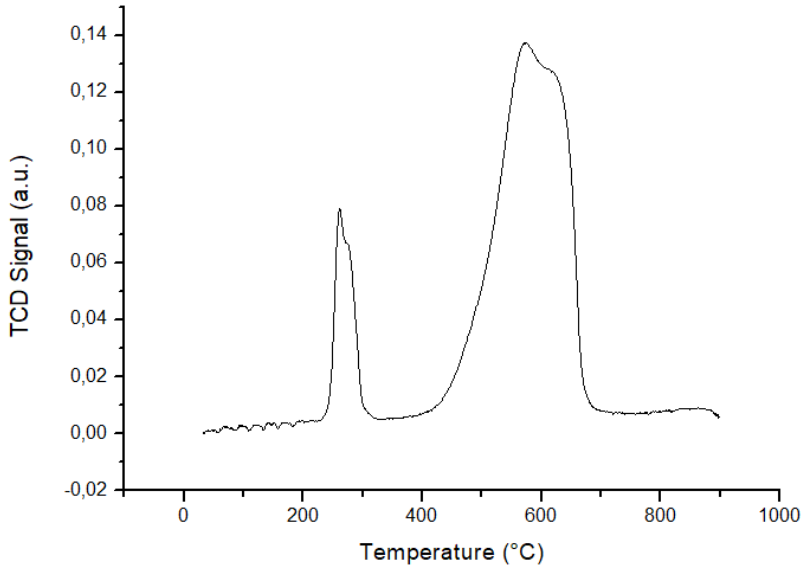

Figure 68. H_2-TPR of $Ni_{0,9}Mg_{0,1}Fe_2O_4$/CuO, with CuO mixed at 20% by mass, after ball milling and sintering. We can see that the figure is different from the one reported in figure 44, with CuO mixed at 50 % in mass with the spinel.

The system begins its reduction at about 230 °C, while the maximum is present at 571,9 °C, in this case probably derived from the spinel's peak. Copper oxide's peak probably is the one at 261,3 °C. The end of the curve, on the other hand, turns out to be at 710 °C, so also with 20 % in mass of copper oxide, the system is reduced before the spinel.

The area of the curve is 352,17 cm^3/g STP, corresponding to $1{,}57 \cdot 10^{-2}$ mol of hydrogen consumed and then oxygen released by the system. Normalizing for 50 mg, you get $7{,}86 \cdot 10^{-4}$ mol of O released or $1{,}26 \cdot 10^{-2}$ g of oxygen. The percentage of oxygen released is in this case 96 % compared to the total present in the material.

3.9.5. Temperature Programmed Oxidation:

The O_2-TPO of the material, obtained after H_2-TPR, is shown in figure 69.

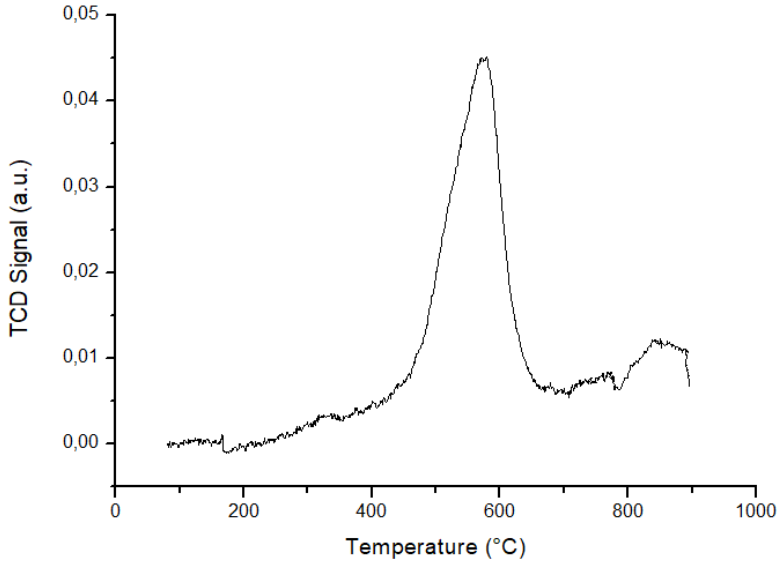

Figure 69. O_2-TPO of $Ni_{0,9}Mg_{0,1}Fe_2O_4$/CuO, with CuO mixed at 20% by mass, obtained after H_2-TPR. Also in this case it is different from those reported with $Ni_{0,9}Mg_{0,1}Fe_2O_4$, CuO pure and both mixed at 50 %.

The oxidation take place at 190 °C and the peak of oxygen consumption is at 577,8 °C. As we can see later, the percentage of oxygen regained is too low, about 57 %, so probably the oxidation doesn't end at 900 °C.

The area of the curve in this case is 139,63 cm^3/g STP, corresponding to $6{,}23 \cdot 10^{-3}$ mol of molecular oxygen consumed. Normalizing for 50 mg, $3{,}11 \cdot 10^{-4}$ mol of O_2 or $9{,}97 \cdot 10^{-3}$ g of reticular oxygen taken from the system is obtained. The percentage of oxygen regained compared to that released is 79 %, which is rather low considering the other materials. This is probably because of copper oxide, that doesn't regain all of the released oxygen lost during the H_2-TPR nether at 900 °C, how we saw in figure 16.

3.9.6. Carbon dioxide splitting:

To compare the results of carbon dioxide splitting between the various materials, the same treatment was carried out as in the previous samples, so a temperature ramp of 10 °C/min flushing 100 sccm of 5 % of hydrogen into helium up to 580 °C and then, again with the same ramp, up to 1000 °C in an inert atmosphere before passing 100 sccm of CO_2 to 10 % in helium.

The result is shown in figure 70:

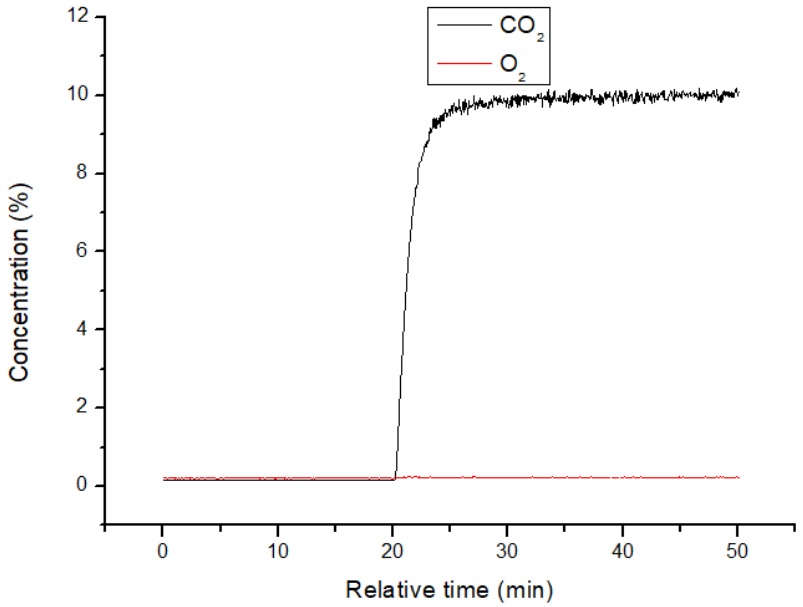

Figure 70. Oxygen and carbon dioxide signals at mass spectrum. After the splitting cycle a pre-treatment using hydrogen at 5% in helium from ambient temperature to 600 °C and then splitting the carbon dioxide at 1000 °C.

Also in this case the actual separation of carbon dioxide takes place, in 15 min, in carbon monoxide and oxygen, which is taken up by the material since the signal of this remains stable over time. The number of moles of split gases turn out to be $4{,}20 \cdot 10^{-4}$ mol, corresponding to $6{,}71 \cdot 10^{-3}$ g of oxygen taken, or the 51 % of oxygen compared to the total present in the material.

Like happened for the sample with copper oxide mixed at 50 % in weight with the catalyst also in this case there is a loss in performance during the second cycle (figure 71). In fact, carbon dioxide is converted in less time than the first, in about 10 min, and also the moles separated are $3{,}61 \cdot 10^{-4}$ mol of gas, that is, taking $5{,}78 \cdot 10^{-3}$ g of oxygen or the 44 %.

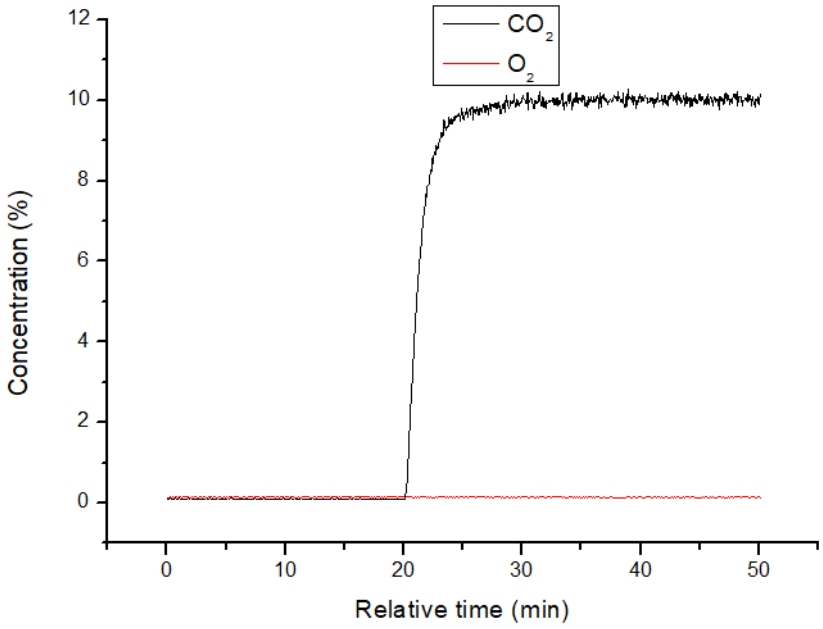

Figure 71. Second cycle of CO_2 splitting. We can see that also in this case the carbon monoxide is formed.

The SEM images acquired after these two cycles are reported in figure 72:

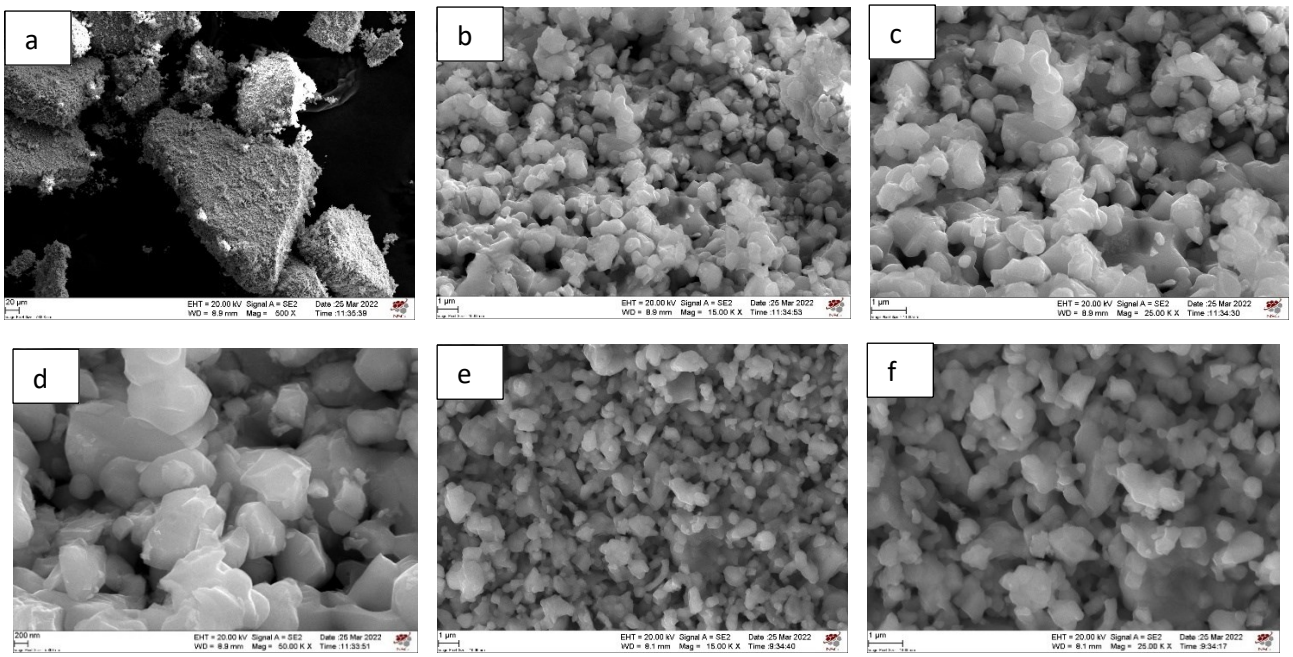

Figure 72. Catalyst mixed at 20 % in weight with copper oxide by wet ball milling after two reaction cycles at 500x (a), 15000x (b), 25000x (c) and 50000x (d). Images e and f are obtained at magnification of 15000x and 25000x before the cycles.

Reducing the quantity of copper inserted leads to a lower sintering, in fact we don't see that big particles that were formed after two splitting cycles in the sample with copper oxide mixed at 20 % in mass with wet ball milling (figure 48). There is also in this case sintering, but in a very lower way, in fact the mean particle diameter is now of 1,5 µm, from 1 µm, instead of the 2,2 µm calculated for the other sample.

The EDX results are reported in table 19:

Element	Expected concentration (%)	Concentration as synthetized (%)	Concentration after two splitting cycles (%)
Ni	10,7	8,7	8,0
Mg	1,2	1,3	1,7
Fe	23,7	21,3	20,2
O	55,9	59,0	61,6
Cu	8,5	9,7	8,5

Table 19. Concentration comparison of the sample made of pure catalyst mixed at 20 % in weight with CuO between the expected one, the one obtained after synthesis and the one after two splitting cycles.

Trough EDX we can see that all concentrations are very similar each other also in this case.

3.10. $Ni_{0,9}Mg_{0,1}Fe_2O_4$/ ZrO_2, with 20 % ZrO_2:

3.10.1. XRD Analysis:

X-ray diffraction analysis of the system reported the underlying pattern (figure 73):

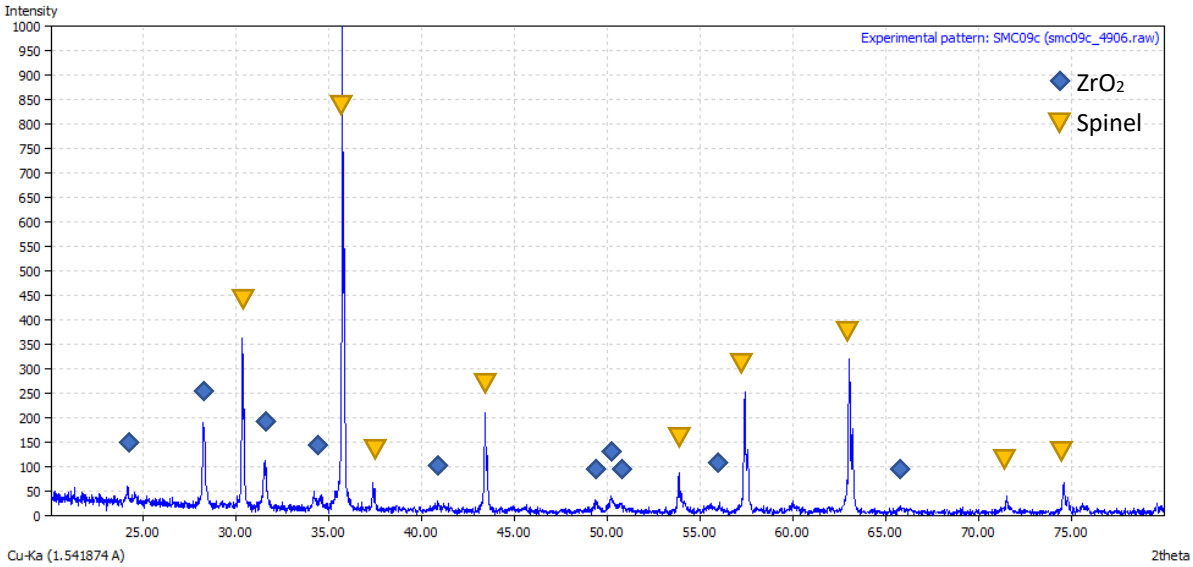

Figure 73. XRD pattern of the compound obtained by mixing by wet ball milling 20 % by weight of zirconia with the catalyst. The reflexes of both inserted powders can be observed, indicating once again that both materials did not react to each other during sintering.

As you can see, also in this case there are also reflexes related to zirconia used as a support, as in figure 49. However, given that now that zirconium oxide is present at 20 % by mass, the reflexes for this compound are less intense.

3.10.2. XPS:

The XPS survey led to the following graph, shown in figure 74:

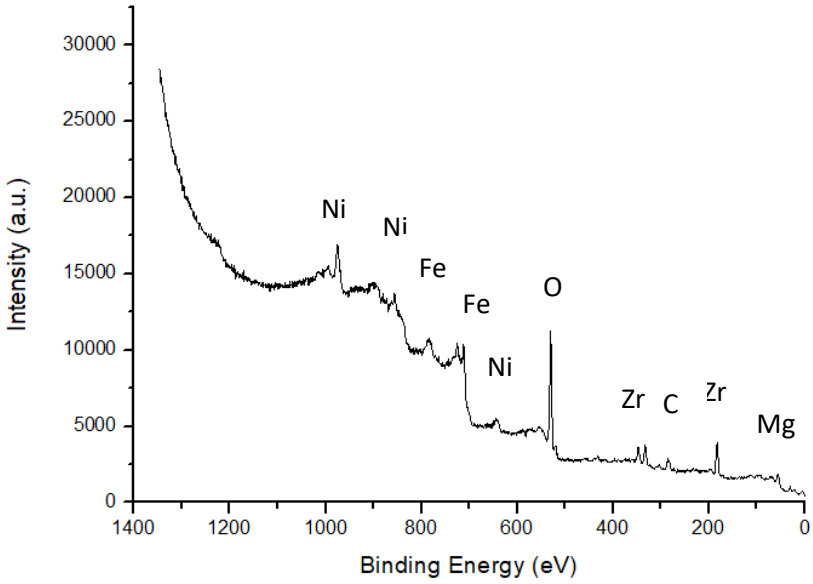

Figure 74. XPS survey given by $Ni_{0,9}Mg_{0,1}Fe_2O_4$ supported by ZrO_2 at 20 % in mass.

The quantitative analysis led to the result in table 20:

Element	Concentration (%)	Expected concentration (%)
Ni	10,4	10,7
Mg	7,0	1,2
Fe	19,7	23,8
O	58,1	58,7
Zr	4,8	5,6

Table 20. Percentage concentration experimental and theorical for $Ni_{0,9}Mg_{0,1}Fe_2O_4$ spinel mixed with 20 % in weight with zirconium oxide, reported by XPS quantitative analysis.

We see once again the presence of segregation on the surface of magnesium, while the percentages of other atoms are very close to the theorical ones. The brute formula turns out to be $Ni_{1,1}Mg_{0,7}Fe_2Zr_{0,5}O_6$, so $Ni_{1,1}Mg_{0,7}Fe_2O_4/Zr_{0,5}O_2$.

3.10.3. SEM:

Figure 75 shows the images at different magnifications: 500x, 15000x, 25000x and 50000x.

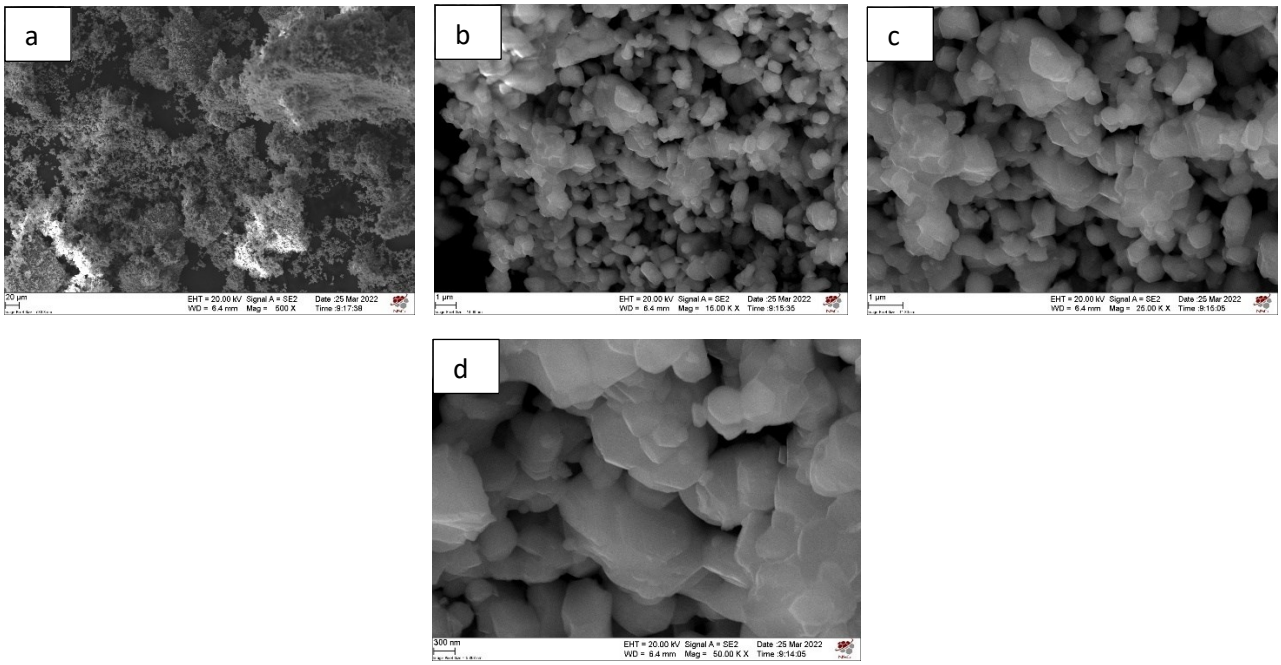

Figure 75. SEM images of the $Ni_{0,9}Mg_{0,1}Fe_2O_4$ spinel mixed at 20% by mass with ZrO_2. The image in figure a is at a magnification of 500x, the one in figure b is at 15000x, in figure c there is the image at 25000x, while in figure d there is the one at 50000x.

At 500x the morphology is different from the other sample on which wet ball milling was operated, in this case it seems to be at cornflakes as the pure spinel. At higher magnification, however, it can be seen that the SEM images are very similar to that obtained with other sample after ball milling. In fact we can see clearly the spherical particles from 15000x to 50000x. The average particle diameter is about 0,9 µm, more or less like the one obtained mixing these two oxides at 50 % in weight.

The EDX analysis starting from the image in figure 75,c leads to these percentages of atoms revealed (table 21):

Element	Concentration (%)	Expected concentration (%)
Ni	8,6	10,7
Mg	0,8	1,2
Fe	20,7	23,8
O	65,1	58,7
Zr	4,8	5,6

Table 21. Percentage atomic concentration of elements in the spinel $Ni_{0,9}Mg_{0,1}Fe_2O_4$ supported at 20 % in weight by zirconium oxide, obtained by EDX against the theorical one.

You can see how the theorical percentages and those obtained experimentally are again very close to each other.

3.10.4. Temperature Programmed Reduction:

The H_2-TPR obtained is shown in figure 76:

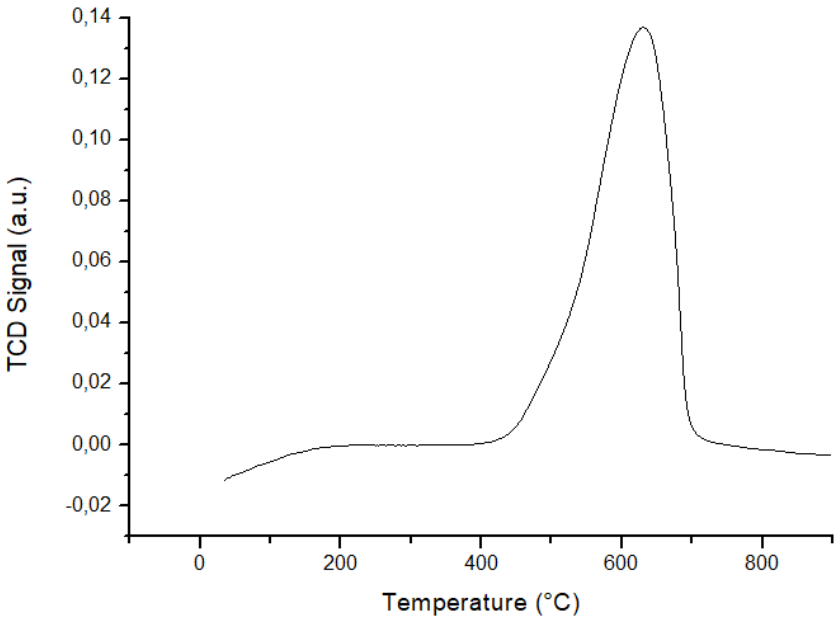

Figure 76. H_2-TPR of $Ni_{0,9}Mg_{0,1}Fe_2O_4/ZrO_2$, with ZrO_2 mixed at 20% by mass, after ball milling and sintering. In this case the measure is very similar to that obtained mixing zirconia and spinel at 50 % in mass.

The system begins its reduction at about 390 °C, while the maximum is present at 629,6 °C. The end of the curve, on the other hand, turns out to be at 740 °C.

The area of the curve is 303,89 cm^3/g STP, corresponding to $1,36 \cdot 10^{-2}$ mol of hydrogen consumed and then oxygen released. Normalizing for 50 mg, you get $6,78 \cdot 10^{-4}$ mol of O released or $1,08 \cdot 10^{-2}$ g of oxygen. The percentage of release of oxygen is in this case 79 % compared to the total oxygen present in the material, which is rather low considering the others. This is because as is also seen in the H_2-TPR of zirconia, this compound is inert even at 900 ° C. As we did for the system mixed at 50 % in mass, if we consider only the oxygen released by spinel, we obtain a theorical 81 % on the total present as percentage, near to that experimentally found, so also in this case zirconia is an inert support.

3.10.5. Temperature Programmed Oxidation:

The O_2-TPO of the material, obtained after H_2-TPR, is shown in figure 77.

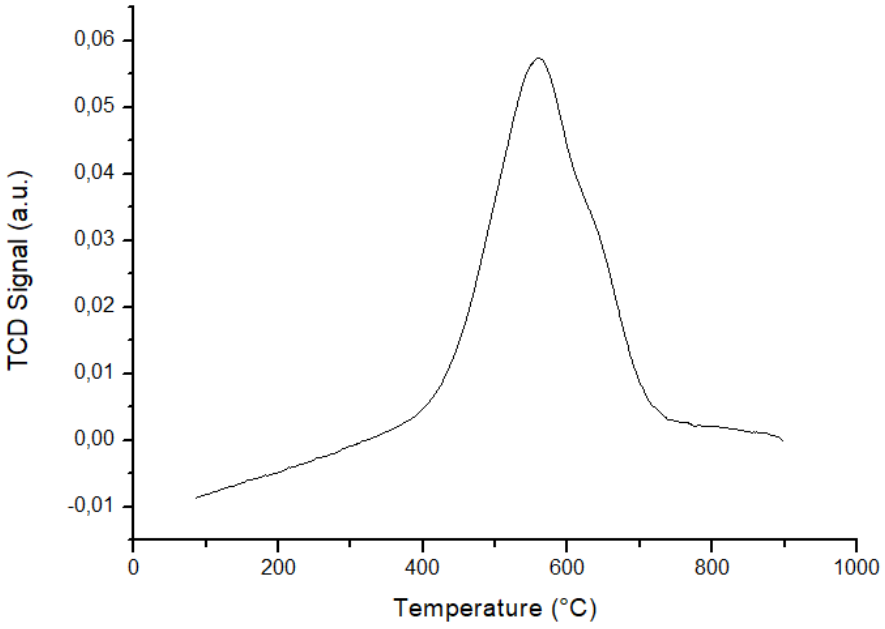

Figure 77. O_2-TPO of $Ni_{0,9}Mg_{0,1}Fe_2O_4/ZrO_2$, with the support mixed at 20% by mass, obtained after H_2-TPR. Also in this case the graph is similar to that obtained mixing 50 % of powders in mass.

The area of the curve in this case is 150,08 cm^3/g STP, corresponding to $6{,}70 \cdot 10^{-3}$ mol of molecular oxygen consumed. Normalizing for 50 mg, $3{,}35 \cdot 10^{-4}$ mol of O_2 or $1{,}07 \cdot 10^{-3}$ g of reticular oxygen taken from the system is obtained. The percentage of reobtained oxygen regained compared to that released is 99 %.

3.10.6. Carbon dioxide splitting:

Since the material releases oxygen at too high temperatures, as can be seen from the H_2-TPR, the measurement of carbon dioxide splitting after pre-treatment in hydrogen up to 580 °C was carried out, and then the separation of this gas into carbon monoxide is done at 1000 °C. The trend of the detected gases, CO_2 and O_2, is shown in figure 78.

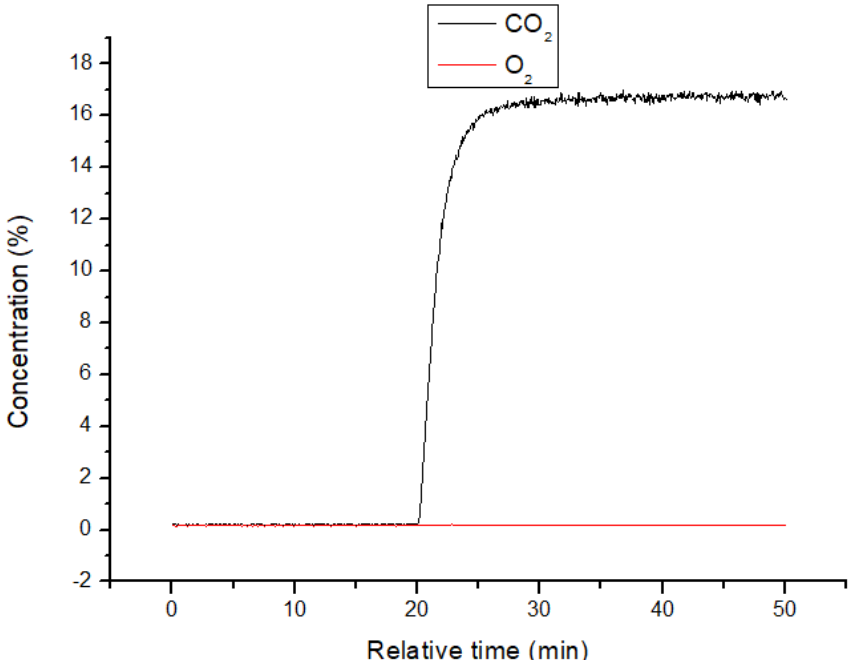

Figure 78. Trend of oxygen and carbon dioxide after having carried out a pre-treatment in 5% hydrogen up to 600 ° C and then passing CO_2 at 10% in helium.

As you can see, the actual separation of carbon dioxide takes place, in nearly 18 min. The number of moles of split gases turn out to be $3{,}75 \cdot 10^{-4}$ mol, corresponding to $6{,}00 \cdot 10^{-3}$ g of oxygen taken, or the 44 % of oxygen compared to the total present in the material, a little less than the percentage of pure $Ni_{0,9}Mg_{0,1}Fe_2O_4$ but still more than the one saw with zirconium oxide mixed at 50 % in mass with the spinel.

In the second cycle the results are very similar to those of the first (figure 79). In this cycle, similarly to the first, carbon dioxide is converted into 17 min, separating $3{,}66 \cdot 10^{-4}$ mol of gas, that is, taking $5{,}86 \cdot 10^{-3}$ g of oxygen or 43 %.

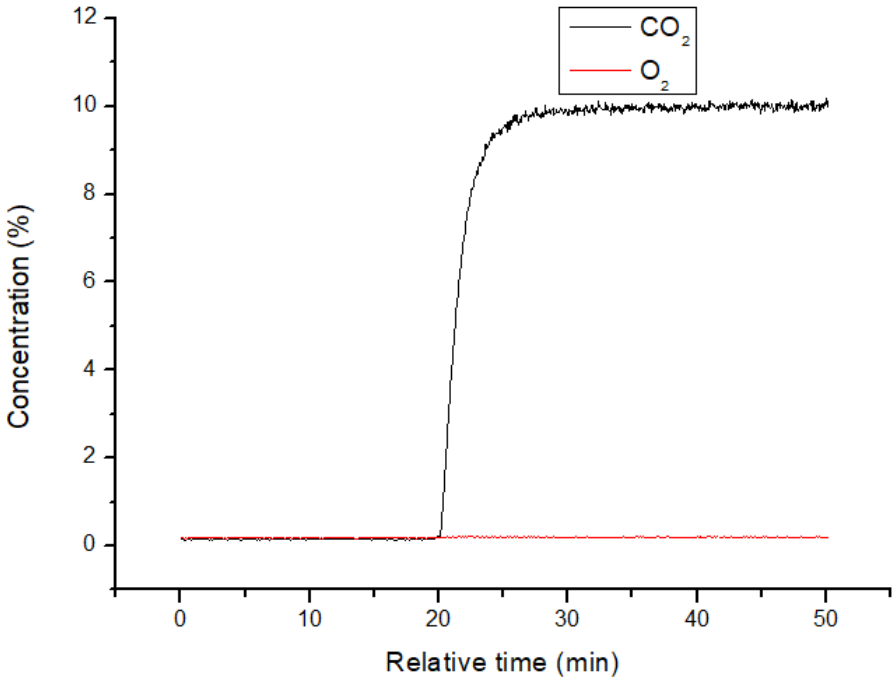

Figure 79. Second cycle of CO_2 splitting, very similar to the first one. We can see that also in this case the carbon monoxide is formed.

The SEM images are reported in figure 80, below:

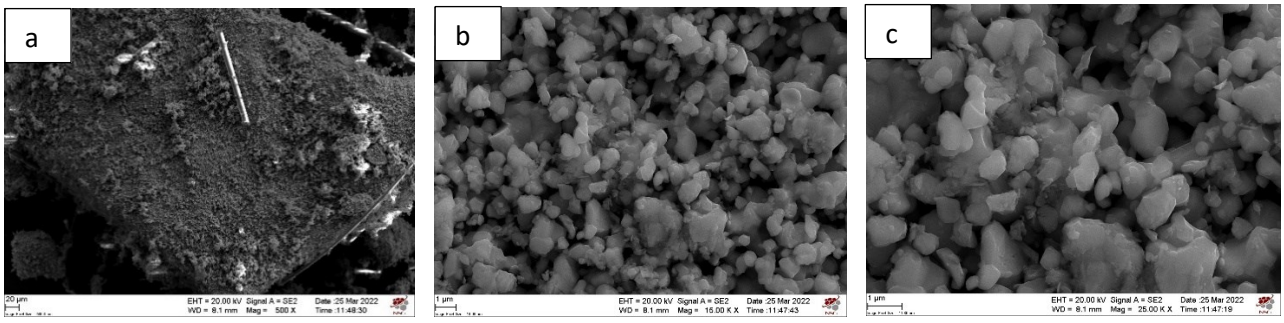

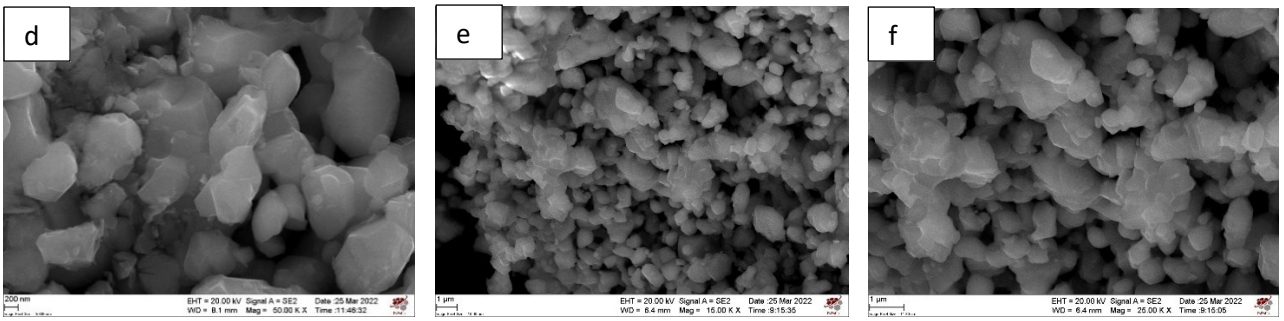

Figure 80. Catalyst mixed at 20 % in weight with zirconium oxide by wet ball milling after two reaction cycles at 500x (a), 15000x (b), 25000x (c) and 50000x (d). e and f are referred to those obtained before these two cycles, at 15000x and 25000x.

In this case it isn't noticeable any sintering, the particles aren't sintered and so it seems that they never had two cycles of splitting. This system so is very reversible also in terms of sintering and not only in terms of CO_2 moles splitted; the mean particle size remains about 0,9 µm. The EDX analysis is reported below (table 22):

Element	Expected concentration (%)	Concentration as synthetized (%)	Concentration after two splitting cycles (%)
Ni	10,7	8,6	9,3
Mg	1,2	0,8	1,3
Fe	23,8	20,7	22,0
O	58,7	65,1	62,5
Zr	5,6	4,8	4,9

Table 22. Concentration comparison of the sample made of pure catalyst mixed at 20 % in weight with ZrO_2 between the expected one, the one obtained after synthesis and the one after two splitting cycles.

Expected, as synthetized and after two splitting cycles atomic percentages are very close each other for all of the elements present on the sample so there aren't changes on concentration during the splitting.

3.11. Differences between supports:

3.11.1. Influence of the percentage concentration by mass of nickel oxide on the catalyst:

3.11.1.1. H_2-TPR and O_2-TPO:

The measurements made by H_2-TPR and O_2-TPO are used as a basis to get an idea of the possible performance of the studied material, regarding a possible release of oxygen at a temperature lower than 1400 °C and a greater amount of oxygen released and taken up by the system, when it will be used for the catalytic activity of carbon dioxide's thermal splitting into carbon monoxide. That is why these measurements turn out to be very useful. Figure 81 shows the graph of the H_2-TPR of $Ni_{0,9}Mg_{0,1}Fe_2O_4$ mixed by wet ball milling with NiO at different percentages by mass, as well as pure nickel oxide and spinel.

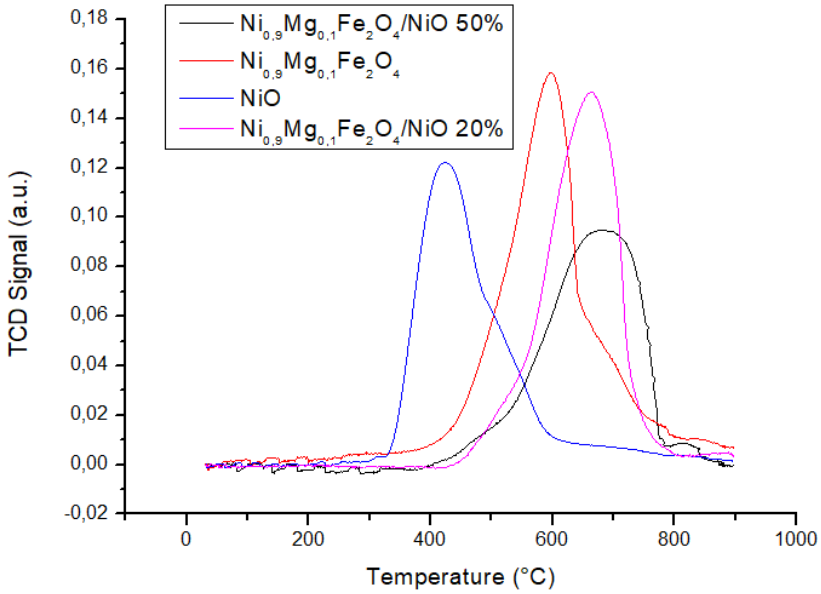

Figure 81. H_2-TPR comparison between nickel oxide (blue line), spinel (red line), nickel oxide and spinel mixed together at 50 % by mass (black line) and nickel oxide mixed at 20 % by mass with the catalyst (pink line). The measurements were normalized by sample mass introduced.

It is interesting to note that mixing the two oxides leads to an increase of the oxygen release temperature, among other things mixing 20 % in mass nickel oxide and spinel leads to a significant increase in the starting temperature of oxygen release into the reducing atmosphere, while at 50 % the beginning is at a temperature very close to that of the pure spinel. Another noteworthy thing is the fact that by increasing the percentage by mass of nickel oxide, the maximum of reduction moves to higher temperatures.

Below is a table comparing the main information obtainable from temperature-controlled thermal reductions (table 23).

System	Total O moles in the material (mol)	Moles reticular O released (mol)	Lost mass (g)	Moles lost O (%)	T start reduction (°C)	Maximum reduction T (°C)	T end reduction (°C)
NiO	$6{,}69\cdot10^{-4}$	$6{,}49\cdot10^{-4}$	$1{,}04\cdot10^{-2}$	97	330	429,9	770
$Ni_{0,9}Mg_{0,1}Fe_2O_4$	$8{,}66\cdot10^{-4}$	$7{,}72\cdot10^{-4}$	$1{,}24\cdot10^{-2}$	89	330	596,3	820
$Ni_{0,9}Mg_{0,1}Fe_2O_4$/NiO 50% by mass	$7{,}68\cdot10^{-4}$	$6{,}74\cdot10^{-4}$	$1{,}08\cdot10^{-2}$	88	370	678,9	880
$Ni_{0,9}Mg_{0,1}Fe_2O_4$/NiO 20% by mass	$8{,}27E\cdot10^{-4}$	$7{,}60\cdot10^{-4}$	$1{,}22\cdot10^{-2}$	92	430	669,7	830

Table 23. Main information noticeable by H_2-TPR of pure nickel oxide, pure $Ni_{0,9}Mg_{0,1}Fe_2O_4$ and the systems composed by these two oxides mixed at 50 % in mass and 20 % in mass of support oxide.

As for the percentage of oxygen release, the best material turns out to be nickel oxide, which releases almost all the oxygen present. Between pure catalyst and spinel mixed with this oxide, the material that releases the most quantity of oxygen of all is the one with NiO mixed at 20 % by mass with the catalyst, however this turns out to be the worst material regard to the temperature of the reduction's beginning. In general, the worst material, both in terms of oxygen release and temperatures in which it is released, is the 50 % mixed system. As for the reduction, therefore, using nickel oxide worsens the characteristics of the spinel studied, this will

most likely be reflected during the thermal reduction in an inert atmosphere where the material will not be able to release oxygen within 1000 ° C.

The measurements obtained by O_2-TPO, shown in figure 82, are also compared:

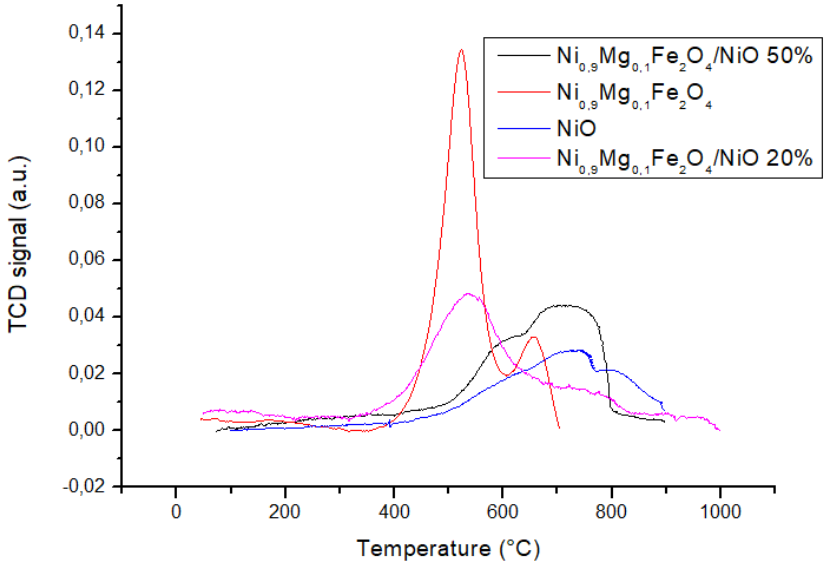

Figure 82. O_2-TPO of comparison between nickel oxide (blue line), spinel (red line), nickel oxide and spinel mixed together at 50 % by mass (black line) and nickel oxide mixed at 20 % by mass with the catalyst (pink line). Also in this case the graphs were normalized for the mass of sample inserted.

You can see how the pure catalyst has a very intense peak of oxidation, while the other materials have less intense but much wider peaks, indicating that reoxidation takes place in more time and at higher temperatures.

A comparison table between the results obtained is again shown (table 24):

System	Total moles O in the material (mol)	Moles reticular O reobtained (mol)	Recovery mass (g)	Moles O reobtained (%)	T start oxidation (°C)	Maximum oxidation T (°C)	T end oxidation (°C)
NiO	$6{,}69\cdot10^{-4}$	$5{,}45\cdot10^{-4}$	$8{,}71\cdot10^{-3}$	84	400	729,4	/
$Ni_{0,9}Mg_{0,1}Fe_2O_4$	$8{,}66\cdot10^{-4}$	$7{,}34\cdot10^{-4}$	$1{,}17\cdot10^{-2}$	95	350	523,1	700
$Ni_{0,9}Mg_{0,1}Fe_2O_4$/NiO 50% by mass	$7{,}68\cdot10^{-4}$	$6{,}79\cdot10^{-4}$	$1{,}09\cdot10^{-2}$	100	370	721,7	870
$Ni_{0,9}Mg_{0,1}Fe_2O_4$/NiO 20% by mass	$8{,}27\cdot10^{-4}$	$6{,}72\cdot10^{-4}$	$1{,}07\cdot10^{-2}$	88	310	535,2	840

Table 24. Information noticeable by O_2-TPO of pure nickel oxide, pure $Ni_{0,9}Mg_{0,1}Fe_2O_4$ and the systems composed by these two oxides mixed at 50 % in mass and 20 % in mass of support oxide made after H_2-TPR.

About the amount of oxygen taken up by the system, the material composed by the spinel and the support mixed at 50 % takes up 100 % of oxygen. However, it turns out to oxidate at very high temperatures, since the peak is positioned at 721,7 °C and the reaction ends at 870 °C. The beginning of oxidation is anticipated with respect to 20 % mixing, it is positioned at lower temperatures than even pure spinel, and the peak position is very close to that of the spinel. Since the main focus was on anticipating the reduction of the material, in general the use of nickel worsens the characteristics of the system. Among all the systems

reported, therefore, the best is the pure spinel, which releases and takes back more moles of oxygen than the others.

3.11.1.2. Splitting of carbon dioxide:

Since the pure spinel, at 1000 °C, is not thermally reduced because it doesn't release oxygen, and that mixing with nickel oxide does not anticipate the beginning of the reduction, for these materials only pre-treatment with 100 sccm of inert gas with 5 % hydrogen up to 580 °C (with a ramp of 10 °C/min) took place, and then the splitting of a mixture of 100 sccm of gas with 10 % carbon dioxide in inert at 1000 °C.

Table 25 summarizes the results obtained:

System	Total moles O in the material (mol)	CO_2 moles splitted I cycle (mol)	Recovery mass (g)	moles O reobtained (%)	CO_2 moles splitted II cycle (mol)	recovery mass (g)	moles O reobtained (%)
$Ni_{0,9}Mg_{0,1}Fe_2O_4$	$8{,}66\cdot10^{-4}$	$4{,}05\cdot10^{-4}$	$6{,}48\cdot10^{-3}$	47	$3{,}92\cdot10^{-4}$	$6{,}28\cdot10^{-3}$	45
$Ni_{0,9}Mg_{0,1}Fe_2O_4$/NiO 50% by mass	$7{,}68\cdot10^{-4}$	$3{,}42\cdot10^{-4}$	$5{,}47\cdot10^{-3}$	45	$3{,}32\cdot10^{-4}$	$5{,}31\cdot10^{-3}$	43
$Ni_{0,9}Mg_{0,1}Fe_2O_4$/NiO 20% by mass	$8{,}27\cdot10^{-4}$	$3{,}70\cdot10^{-4}$	$5{,}92\cdot10^{-3}$	45	$3{,}58\cdot10^{-4}$	$5{,}73\cdot10^{-3}$	43

Table 25. Catalytic activity tests information obtained using a mass spectrometer. These compounds are pure $Ni_{0,9}Mg_{0,1}Fe_2O_4$ and this spinel mixed at different percentage by ball milling with nickel oxide.

The carbon dioxide splitted moles correspond to the oxygen moles taken from the material and also to the carbon monoxide moles released. It can be seen that for the same pre-treatment, the material that separates the most quantity of carbon dioxide is the pure spinel, so the effect of nickel oxide in this case isn't very good. The materials presented demonstrate to have the same stability between two cycles because all of them lose a 2 % of moles reobtained during the second cycle. After a SEM analysis it can be seen that this decrease is because of sintering, by the way this process is lower when the spinel is supported with nickel oxide than when it is not.

3.11.2. Influence of the percentage concentration by mass of copper oxide on the catalyst:

3.11.2.1. H_2-TPR and O_2-TPO:

With regard to the use of copper oxide as a support, figure 83 shows the H_2-TPR of pure catalyst, CuO and the systems comprising these two powders mixed by wet ball milling at 50 % by mass and 20 % by mass.

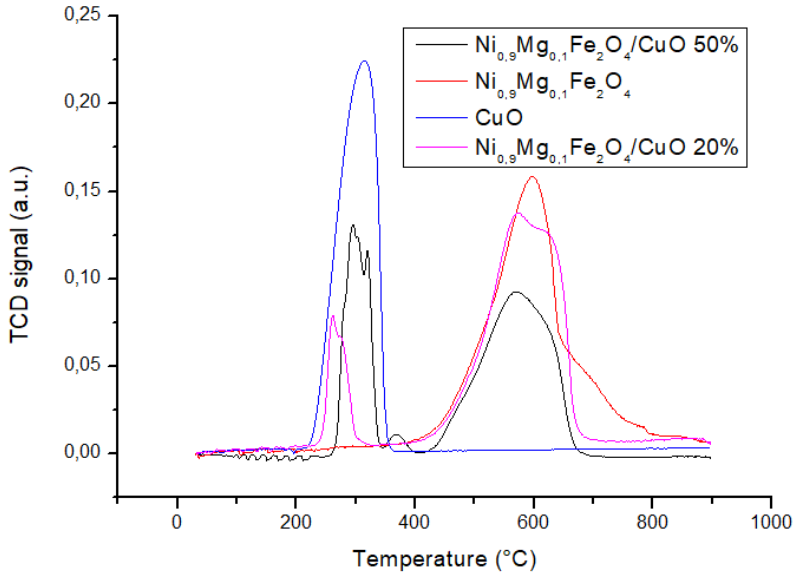

Figure 83. H_2-TPR comparison between copper oxide (blue line), spinel (red line), copper oxide and spinel mixed together at 50 % by mass (black line) and copper oxide mixed at 20 % by mass with the catalyst (pink line). The measurements were normalized by sample mass introduced.

It can be seen that, in the graph of the copper oxide mixed with 50 % in weight with the catalyst, there is a little peak at nearly 370 °C, while in the others this peak there isn't. In terms of curves' form we can see that when these two powders are mixed there are two contributions: one derived to copper oxide, at lower temperatures, and the other derived to the spinel's one. It is noticeable also that in the sample with the two oxides mixed at 20 % in weight there is a little shoulder. When the copper oxide is mixed at 20 % in weight with the catalyst, the contribution of the spinel in the curve starts at 330 °C, like the pure $Ni_{0,9}Mg_{0,1}Fe_2O_4$, but when they are mixed at 50 % this contribution starts at 405 °C, so the temperature of reduction of the spinel is increased. We can say that probably cupric oxide used as support and catalyst interact because the CuO part of the graph never starts at the same temperature but using more copper oxide shifts it at higher temperatures.

Table 26 summarizes the main data that can be obtained from these measurements.

System	Total O moles in the material (mol)	Moles reticular O released (mol)	Lost mass (g)	Moles lost O (%)	T start reduction (°C)	Maximum reduction T (°C)	T end reduction (°C)
CuO	$6{,}29\cdot10^{-4}$	$6{,}20\cdot10^{-4}$	$9{,}92\cdot10^{-2}$	99	210	314,5	360
$Ni_{0,9}Mg_{0,1}Fe_2O_4$	$8{,}66\cdot10^{-4}$	$7{,}72\cdot10^{-4}$	$1{,}24\cdot10^{-2}$	89	330	596,3	820
$Ni_{0,9}Mg_{0,1}Fe_2O_4$/CuO 50% by mass	$7{,}47\cdot10^{-4}$	$7{,}27\cdot10^{-4}$	$1{,}16\cdot10^{-2}$	97	250	569,6	720
$Ni_{0,9}Mg_{0,1}Fe_2O_4$/CuO 20% by mass	$8{,}19\cdot10^{-4}$	$7{,}86\cdot10^{-4}$	$1{,}26\cdot10^{-2}$	96	230	571,9	710

Table 26. Main information noticeable by H_2-TPR of pure copper oxide, pure $Ni_{0,9}Mg_{0,1}Fe_2O_4$ and the systems composed by these two oxides mixed at 50 % in mass and 20 % in mass of support oxide.

We can notice that increasing copper oxide content in the system leads to a higher percentage of oxygen moles released respect to the pure catalyst. The best material seems to be copper oxide mixed with

$Ni_{0,9}Mg_{0,1}Fe_2O_4$ at 20 % in mass in terms of starting and ending of reduction temperature and also the temperature of the peak is pretty low respect to the one of the pure spinel.

Once again, the measurements obtained by O_2-TPO are compared, shown in figure 84:

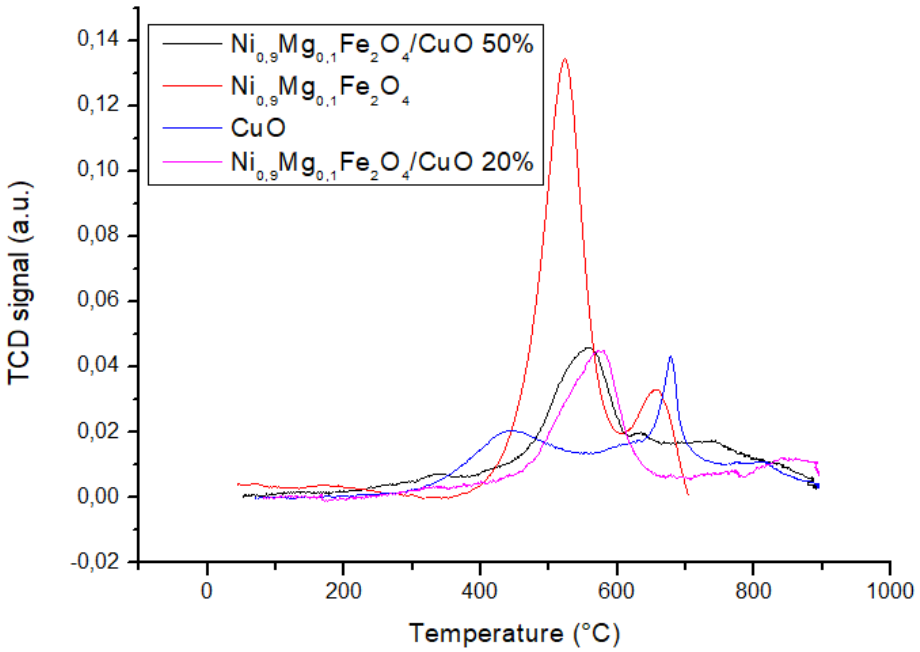

Figure 84. O_2-TPO of comparison between copper oxide (blue line), spinel (red line), copper oxide and spinel mixed together at 50 % by mass (black line) and copper oxide mixed at 20 % by mass with the catalyst (pink line). Also in this case the graphs were normalized for the mass of sample inserted.

We can see that there is a very high peak due to the pure spinel and that the other materials show smaller peaks but very large. The starting temperature of oxidation is lowered using CuO as support, but the oxidation is very slow and includes a wide range of temperatures.

The table including the various results is given in table 27, as follows:

System	Total moles O in the material (mol)	Moles reticular O reobtained (mol)	Recovery mass (g)	Moles O reobtained (%)	T start oxidation (°C)	Maximum oxidation T (°C)	T end oxidation (°C)
CuO	$6,29 \cdot 10^{-4}$	$5,55 \cdot 10^{-4}$	$8,87 \cdot 10^{-3}$	90	190	677,6	900
$Ni_{0,9}Mg_{0,1}Fe_2O_4$	$8,66 \cdot 10^{-4}$	$7,34 \cdot 10^{-4}$	$1,17 \cdot 10^{-2}$	95	350	523,1	700
$Ni_{0,9}Mg_{0,1}Fe_2O_4$/CuO 50% by mass	$7,47 \cdot 10^{-4}$	$6,00 \cdot 10^{-4}$	$9,60 \cdot 10^{-3}$	83	180	555,4	/
$Ni_{0,9}Mg_{0,1}Fe_2O_4$/CuO 20% by mass	$8,19 \cdot 10^{-4}$	$6,23 \cdot 10^{-4}$	$9,97 \cdot 10^{-3}$	79	190	577,8	/

Table 27. Information noticeable by O_2-TPO of pure copper oxide, pure $Ni_{0,9}Mg_{0,1}Fe_2O_4$ and the systems composed by these two oxides mixed at 50 % in mass and 20 % in mass of support oxide made before H_2-TPR.

It can be seen that in the case of O_2-TPO the use of copper oxide as supporting material for the spinel is not as good as using it for the reduction because process temperatures are higher and also the total oxidation is not obtained even at 900 °C, so it regains less oxygen respect to the pure $Ni_{0,9}Mg_{0,1}Fe_2O_4$.

3.11.2.2. Carbon dioxide splitting:

The measurements obtained following hydrogen pre-treatment and then carbon dioxide split are shown in table 28.

System	Total moles O in the material (mol)	CO_2 moles splitted I cycle (mol)	Recovery mass (g)	moles O reobtained (%)	CO_2 moles splitted II cycle (mol)	recovery mass (g)	moles O reobtained (%)
$Ni_{0,9}Mg_{0,1}Fe_2O_4$	$8,66 \cdot 10^{-4}$	$4,05 \cdot 10^{-4}$	$6,48 \cdot 10^{-3}$	47	$3,92 \cdot 10^{-4}$	$6,28 \cdot 10^{-3}$	45
$Ni_{0,9}Mg_{0,1}Fe_2O_4$/CuO 50% by mass	$7,47 \cdot 10^{-4}$	$4,22 \cdot 10^{-4}$	$6,75 \cdot 10^{-3}$	56	$2,59 \cdot 10^{-4}$	$4,14 \cdot 10^{-3}$	35
$Ni_{0,9}Mg_{0,1}Fe_2O_4$/CuO 20% by mass	$8,19 \cdot 10^{-4}$	$4,19 \cdot 10^{-4}$	$6,71 \cdot 10^{-3}$	51	$3,62 \cdot 10^{-4}$	$5,78 \cdot 10^{-3}$	44

Table 28. Catalytic activity tests information obtained using a mass spectrometer. Sample are pure $Ni_{0,9}Mg_{0,1}Fe_2O_4$ and this spinel mixed at different percentage by ball milling with copper oxide.

It can be noticed that copper oxide mixed at 50 % in weight with the spinel gives the best performance during the first cycle, but it loses it because of the high sintering, how we saw with SEM images post-cycles. During the second cycle, in fact, it has the worst percentage of moles reobtained. At 20 % in mass, the stability of the system is increased but there is also in this case sintering and so a lowering of carbon dioxide moles splitted. We can say that cupric oxide is a very good support regarding only the first cycle, but the worst during the second. Mixing it at 20 % in mass, by the way, seems to be a quite good compromise between reactivity and cyclability.

3.11.3. Influence of the percentage concentration by mass of zirconium oxide on the catalyst:

3.11.3.1. H_2-TPR and O_2-TPO:

Figure 85 shows the graph of the temperature programmed reductions in hydrogen of the various systems consisting of pure zirconium oxide and spinel, and these two mixed at 50 % and 20 % by mass by wet ball milling:

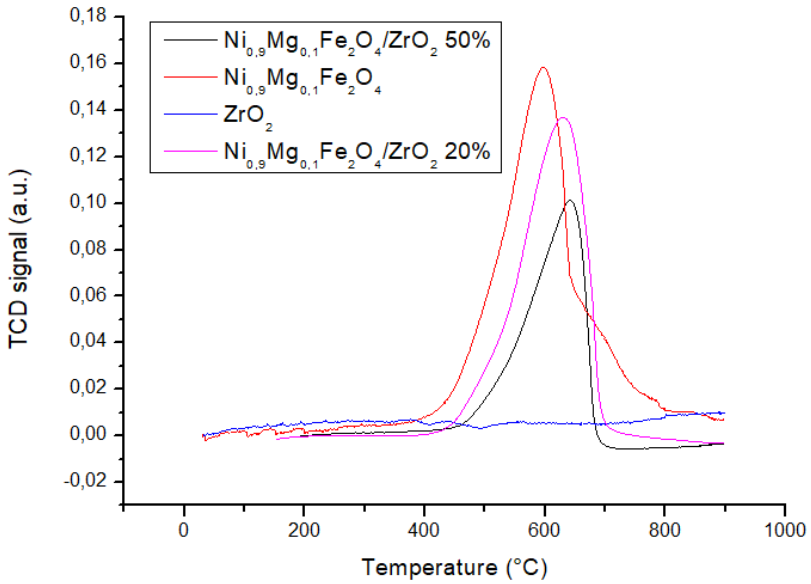

Figure 85. H_2-TPR comparison between zirconium oxide (blue line), spinel (red line), zirconia and spinel mixed together at 50 % by mass (black line) and zirconia mixed at 20 % by mass with the catalyst (pink line).

We can see how, using higher concentration of zirconia, the reduction curve gets lower, because there is a lower amount of active specie, so the spinel one, and the maximum peak shifts through higher temperatures. By the way, the end of reduction is at lower temperature when this material is supported.

The summary table is shown below (table 29):

System	Total O moles in the material (mol)	Moles reticular O released (mol)	Lost mass (g)	Moles lost O (%)	T start reduction (°C)	Maximum reduction T (°C)	T end reduction (°C)
ZrO_2	$8{,}12\cdot10^{-4}$	/	/	0	/	/	/
$Ni_{0,9}Mg_{0,1}Fe_2O_4$	$8{,}66\cdot10^{-4}$	$7{,}72\cdot10^{-4}$	$1{,}24\cdot10^{-2}$	89	330	596,3	820
$Ni_{0,9}Mg_{0,1}Fe_2O_4/ZrO_2$ 50% by mass	$8{,}39\cdot10^{-4}$	$4{,}25\cdot10^{-4}$	$6{,}80\cdot10^{-3}$	51	410	641,9	730
$Ni_{0,9}Mg_{0,1}Fe_2O_4/ZrO_2$ 20% by mass	$8{,}55\cdot10^{-4}$	$6{,}78\cdot10^{-4}$	$1{,}08\cdot10^{-2}$	79	390	629,6	740

Table 29. Main information noticeable by H_2-TPR of pure $Ni_{0,9}Mg_{0,1}Fe_2O_4$ and the systems composed by this spinel mixed with zirconium oxide. ZrO_2 is mixed at different percentage in mass in order to see how performance changes varying quantity of support used.

We can notice that the use of an inert material as support leads to a decrease of oxygen moles released and so to a decrease in percentage of lost oxygen moles with respect to the total oxygen in the material because, how we saw previously, it is only the spinel the part that is reduced.

About temperatures, we can see that in both cases the zirconia gets starting reducing temperatures and peak temperature higher, but the ending temperature is lowered. By the way, regards to the catalytic activity, ZrO_2 has not a good effect on the spinel.

Below, in figure 86, are reported the O_2-TPO of the spinel, zirconium oxide, and system made by mixing of these two powders at different percentage in weight.

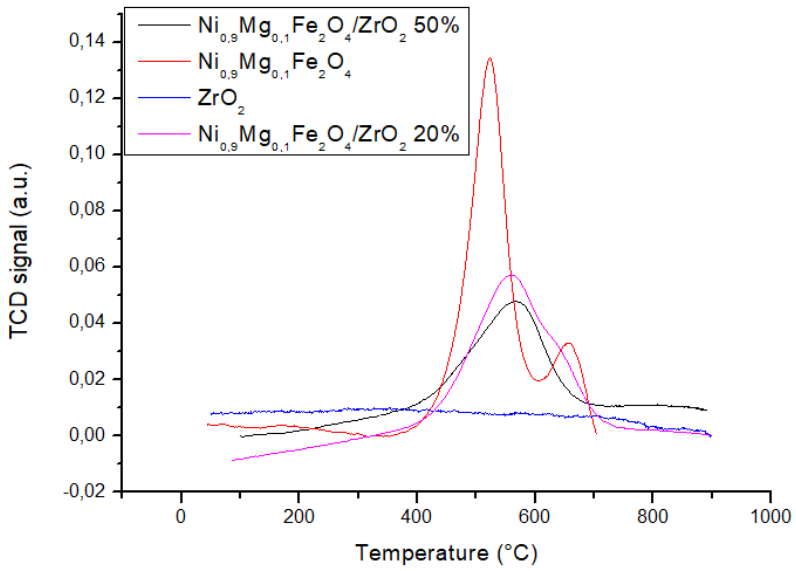

Figure 86. Comparison of O_2-TPO between zirconium oxide (blue line), spinel (red line), zirconium oxide and spinel mixed together at 50 % by mass (black line) and at 20 % by mass with the catalyst (pink line).

We can see how, also in this case, supporting the spinel with zirconia leads to a decrease in curve's area because of the inert behaviour of ZrO_2. Like we noticed with other supports, the peak intensity decreases but it widens when ferrite is supported.

Table 30 summarizes all the information obtained from these measurements:

System	Total moles O in the material (mol)	Moles reticular O reobtained (mol)	Recovery mass (g)	Moles O reobtained (%)	T start oxidation (°C)	Maximum oxidation T (°C)	T end oxidation (°C)
ZrO_2	$6{,}69\cdot10^{-4}$	/	/	0	/	/	/
$Ni_{0,9}Mg_{0,1}Fe_2O_4$	$8{,}66\cdot10^{-4}$	$7{,}34\cdot10^{-4}$	$1{,}17\cdot10^{-2}$	95	350	523,1	700
$Ni_{0,9}Mg_{0,1}Fe_2O_4/ZrO_2$ 50% by mass	$8{,}39\cdot10^{-4}$	$4{,}16\cdot10^{-4}$	$6{,}65\cdot10^{-3}$	98	340	563,9	720
$Ni_{0,9}Mg_{0,1}Fe_2O_4/ZrO_2$ 20% by mass	$8{,}55\cdot10^{-4}$	$6{,}70\cdot10^{-4}$	$1{,}07\cdot10^{-2}$	99	380	559,8	750

Table 30. Information noticeable by O_2-TPO of pure zirconium oxide, pure $Ni_{0,9}Mg_{0,1}Fe_2O_4$ and the systems composed by these two oxides mixed at 50 % in mass and 20 % in mass of support oxide made before H_2-TPR.

Also regarding O_2-TPO, zirconium oxide effect on the spinel is not as good as that saw with other supports. The percentage of moles reobtained is higher than the one of $Ni_{0,9}Mg_{0,1}Fe_2O_4$ but, about number of oxygen moles regained, we can notice that they are lower than the one of pure spinel.

Zirconium oxide effect is also to increase almost every working temperatures considered, such as starting oxidation temperature, peak temperature and ending temperature and the more of this inert is on the system, higher is the maximum peak temperature.

3.11.3.2. Carbon dioxide splitting:

With these materials, only hydrogen pre-treatment up to 580 °C was used, and then splitting at 1000 °C. Table 31 summarizes the data obtained through these measurements:

System	Total moles O in the material (mol)	CO_2 moles splitted I cycle (mol)	Recovery mass (g)	moles O reobtained (%)	CO_2 moles splitted II cycle (mol)	recovery mass (g)	moles O reobtained (%)
$Ni_{0,9}Mg_{0,1}Fe_2O_4$	$8,66 \cdot 10^{-4}$	$4,05 \cdot 10^{-4}$	$6,48 \cdot 10^{-3}$	47	$3,92 \cdot 10^{-4}$	$6,28 \cdot 10^{-3}$	45
$Ni_{0,9}Mg_{0,1}Fe_2O_4/ZrO_2$ 50% by mass	$8,39 \cdot 10^{-4}$	$3,02 \cdot 10^{-4}$	$4,83 \cdot 10^{-3}$	36	$2,96 \cdot 10^{-4}$	$4,73 \cdot 10^{-3}$	35
$Ni_{0,9}Mg_{0,1}Fe_2O_4/ZrO_2$ 20% by mass	$8,55 \cdot 10^{-4}$	$3,75 \cdot 10^{-4}$	$6,00 \cdot 10^{-3}$	44	$3,66 \cdot 10^{-4}$	$5,86 \cdot 10^{-3}$	43

Table 31. Information obtained by catalytic activity tests, using a mass spectrometer. These compounds are pure $Ni_{0,9}Mg_{0,1}Fe_2O_4$ and this spinel mixed at different percentage by ball milling with zirconium oxide.

In this case we can see how, using zirconia as a support for the spinel, there is an increase on the cyclability of the material because the results obtained during the second cycle are very similar to that obtained by the first. This fact is caused by the very low sintering that occurs on these samples how we saw with SEM images post-cycles. The usage of too much zirconia, by the way, leads to a big loss in performances because it is an inert material and it doesn't interact with the system and with the oxygen. The material with 20 % of zirconium oxide seems to be the best because it has good reversibility, the same that is obtained using 50 % by weight of zirconia, but also acceptable performances, since less than that of pure spinel.

3.11.4. Influence of the type of support mixed at 50 % with the catalyst:

3.11.4.1. H_2-TPR and O_2-TPO:

Below is the graph (figure 87) with all the reduction curves obtained by H_2-TPR of the systems consisting of pure catalyst and the same spinel mixed at 50 % by mass with the supports used (NiO, CuO, ZrO_2) by wet ball milling:

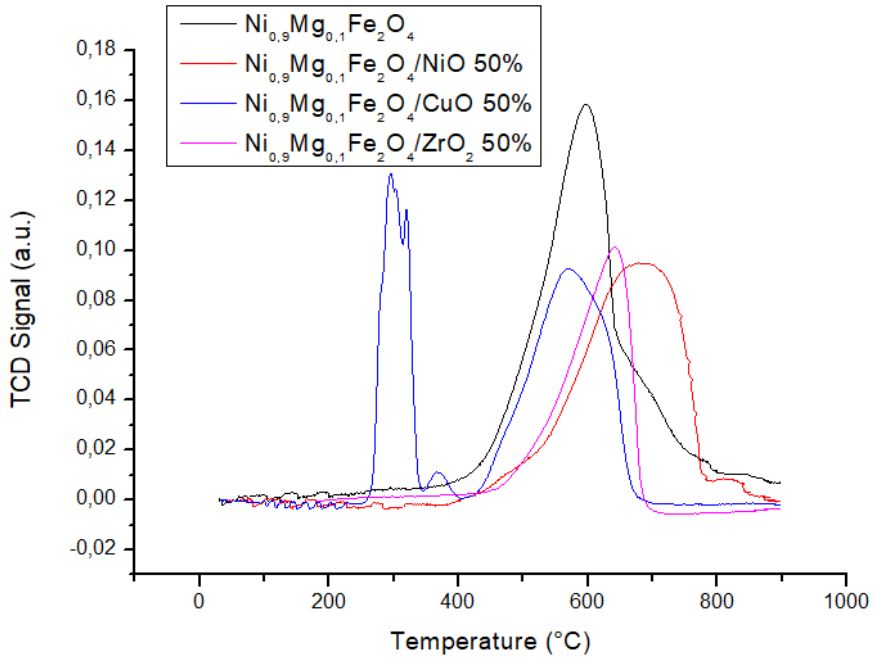

Figure 87. H_2-TPR of the pure $Ni_{0,9}Mg_{0,1}Fe_2O_4$ (black line) and this spinel mixed with different oxides at 50 % in mass by wet ball milling: NiO (red line), CuO (blue line) and ZrO_2 (pink line).

We can see that the best results are obtained mixing the spinel with copper oxide because the reduction starts at lower temperature. The effect of zirconia in the system isn't so good because we can see that the area of the reduction curve is the smaller. In fact this material is an inert one, so it doesn't release oxygen neither at very high temperatures and using this as support, in catalytic terms, is a problem because it only reduces the amount of material active in the splitting. By the way, higher peaks and ending reduction temperatures are achieved using nickel oxide as support.

Table 32, once again, shows the information obtained from these measurements:

System	Total O moles in the material (mol)	Moles reticular O released (mol)	Lost mass (g)	Moles lost O (%)	T start reduction (°C)	Maximum reduction T (°C)	T end reduction (°C)
$Ni_{0,9}Mg_{0,1}Fe_2O_4$	$8{,}66\cdot10^{-4}$	$7{,}72\cdot10^{-4}$	$1{,}24\cdot10^{-2}$	89	330	596,3	820
$Ni_{0,9}Mg_{0,1}Fe_2O_4$/NiO 50% by mass	$7{,}68\cdot10^{-4}$	$6{,}74\cdot10^{-4}$	$1{,}08\cdot10^{-2}$	88	370	678,9	880
$Ni_{0,9}Mg_{0,1}Fe_2O_4$/CuO 50% by mass	$7{,}47\cdot10^{-4}$	$7{,}27\cdot10^{-4}$	$1{,}16\cdot10^{-2}$	97	250	569,6	720
$Ni_{0,9}Mg_{0,1}Fe_2O_4$/ZrO_2 50% by mass	$8{,}39\cdot10^{-4}$	$4{,}25\cdot10^{-4}$	$6{,}80\cdot10^{-3}$	51	410	641,9	730

Table 32. Main information noticeable by H_2-TPR of pure $Ni_{0,9}Mg_{0,1}Fe_2O_4$ and the systems composed by this spinel mixed with functional oxides (as copper oxide and nickel oxide) and an inert oxide (zirconium oxide), all of them mixed with the catalyst at 50 % in mass with wet ball milling.

It can be seen that also in quantitative terms that using zirconia as a support material reduces the oxygen release by the system. Another time it is confirmed that copper oxide is the best support material because all the process temperatures taken into account are lower and also the percentage of oxygen moles lost is higher. The use of zirconia and nickel oxide, by the way, worsens the propriety of the pure $Ni_{0,9}Mg_{0,1}Fe_2O_4$ on reduction measures.

With regard to oxidation, figure 87 shows the various systems:

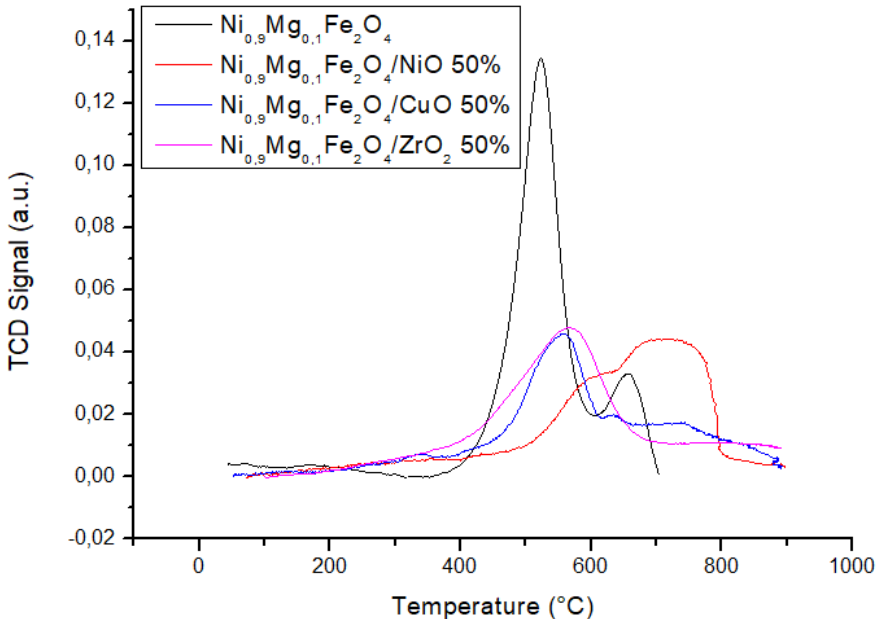

Figure 87. O_2-TPO performed after H_2-TPR of the pure $Ni_{0,9}Mg_{0,1}Fe_2O_4$ (black line) and this spinel mixed with NiO (red line), CuO (blue line) and ZrO_2 (pink line).

It can be seen that all the oxides mixed with the catalyst tend to shrink the oxidation curve and to enlarge it. So the peaks are all smaller than the $Ni_{0,9}Mg_{0,1}Fe_2O_4$ one but, how we can see in table 33, the percentage of oxygen moles reobtained are all similar to the others.

System	Total moles O in the material (mol)	Moles reticular O reobtained (mol)	Recovery mass (g)	Moles O reobtained (%)	T start oxidation (°C)	Maximum oxidation T (°C)	T end oxidation (°C)
$Ni_{0,9}Mg_{0,1}Fe_2O_4$	$8,66 \cdot 10^{-4}$	$7,34 \cdot 10^{-4}$	$1,17 \cdot 10^{-2}$	95	350	523,1	700
$Ni_{0,9}Mg_{0,1}Fe_2O_4$/NiO 50% by mass	$7,68 \cdot 10^{-4}$	$6,79 \cdot 10^{-4}$	$1,09 \cdot 10^{-2}$	100	370	721,7	870
$Ni_{0,9}Mg_{0,1}Fe_2O_4$/CuO 50% by mass	$7,47 \cdot 10^{-4}$	$6,00 \cdot 10^{-4}$	$9,60 \cdot 10^{-3}$	83	230	555,4	900
$Ni_{0,9}Mg_{0,1}Fe_2O_4/ZrO_2$ 50% by mass	$8,39 \cdot 10^{-4}$	$4,16 \cdot 10^{-4}$	$6,65 \cdot 10^{-3}$	98	340	563,9	720

Table 33. Similarly to H_2-TPR, in table are reported the main information obtained by O_2-TPO of the system composed by pure catalyst and these oxide mixed at 50 % in mass with nickel oxide, copper oxide or zirconium oxide by wet ball milling.

We can see that for oxidation measures the best material is the pure spinel because most of the temperatures considered are lower. Mixing this catalyst with copper oxide, by the way, helps by anticipating the oxidation starting temperature, but this reaction lasts up until 900 °C and maybe beyond. We can also notice that the reobtained moles percentage using zirconium oxide as support is very high but instead the oxygen moles reobtained are very low when compared to those of the other systems. This is why the percentage is calculated by dividing the moles of oxygen reabsorbed during O_2-TPO by those released during H_2-TPR.

3.11.4.2. Carbon dioxide splitting:

With regard to carbon dioxide splitting, only the results obtained after pre-treatment were compared, since the materials were not thermally reduced at 1000 °C. The results are shown in table 34:

System	Total moles O in the material (mol)	CO_2 moles splitted I cycle (mol)	Recovery mass (g)	moles O reobtained (%)	CO_2 moles splitted II cycle (mol)	recovery mass (g)	moles O reobtained (%)
$Ni_{0,9}Mg_{0,1}Fe_2O_4$	$8,66 \cdot 10^{-4}$	$4,05 \cdot 10^{-4}$	$6,48 \cdot 10^{-3}$	47	$3,92 \cdot 10^{-4}$	$6,28 \cdot 10^{-3}$	45
$Ni_{0,9}Mg_{0,1}Fe_2O_4$/NiO 50% by mass	$7,68 \cdot 10^{-4}$	$3,42 \cdot 10^{-4}$	$5,47 \cdot 10^{-3}$	45	$3,32 \cdot 10^{-4}$	$5,31 \cdot 10^{-3}$	43
$Ni_{0,9}Mg_{0,1}Fe_2O_4$/CuO 50% by mass	$7,47 \cdot 10^{-4}$	$4,22 \cdot 10^{-4}$	$6,75 \cdot 10^{-3}$	56	$2,59 \cdot 10^{-4}$	$4,14 \cdot 10^{-3}$	35
$Ni_{0,9}Mg_{0,1}Fe_2O_4$/ZrO_2 50% by mass	$8,39 \cdot 10^{-4}$	$3,02 \cdot 10^{-4}$	$4,83 \cdot 10^{-3}$	36	$2,81 \cdot 10^{-4}$	$4,50 \cdot 10^{-3}$	34

Table 34. Information obtained by catalytic activity tests, using a mass spectrometer. These compounds are made of pure $Ni_{0,9}Mg_{0,1}Fe_2O_4$ and this spinel mixed at 50 % in mass by wet ball milling with nickel oxide, copper oxide and zirconium oxide.

We can see that mixing the catalyst with zirconium oxide at 50 % gives the worst performances because, how we saw after with H_2-TPR and O_2-TPO, this support is inert and so it doesn't release (and reobtain) oxygen. Using this type of support, so, leads to reduce the moles of carbon dioxide splitted. Copper oxide, by the way, gives the best performances during the first cycle but it is not cyclable because during the second cycle there is a high lowering in CO_2 moles splitted, caused by high sintering. All of the other compounds instead have more or less the same behaviour during the two cycles, there is a little loss of recovery mass probably due to sintering of the particles, as we saw with SEM images post-cycles.

3.11.5. Influence of the type of support mixed at 20 % with the catalyst:

3.11.5.1. H_2-TPR and O_2-TPO:

For systems with supports mixed at 20 % by mass with the catalyst by wet ball milling, the graph of H_2-TPR is shown in figure 88, below:

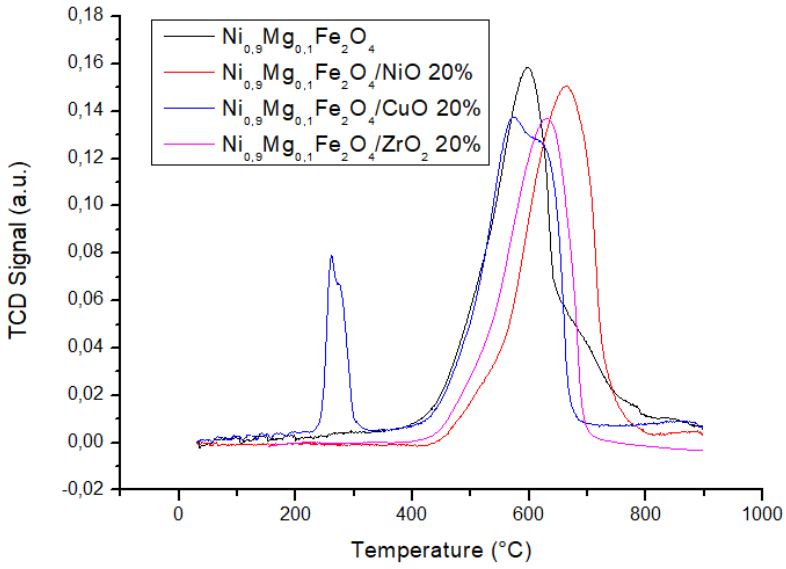

Figure 88. H_2-TPR of the pure $Ni_{0,9}Mg_{0,1}Fe_2O_4$ (black line) and this spinel mixed with different oxides at 20 % in mass by wet ball milling: NiO (red line), CuO (blue line) and ZrO_2 (pink line).

It could be noticed that CuO have a good effect on the material because it anticipates the reduction in terms of temperatures. We can also see that in this case there are two peaks, one derived from copper oxide at

lower temperature and the other from spinel at higher temperature. All of the other supporting material don't change significantly the form of the reduction's curve from the pure one, but they lead to a its shift. There is also the disappear of the shoulder that is formed at higher temperature on the pure spinel's H_2-TPR when it is supported, so the ending temperature is lower in all cases.

Table 35 shows the most important data from these measurements:

System	Total O moles in the material (mol)	Moles reticular O released (mol)	Lost mass (g)	Moles lost O (%)	T start reduction (°C)	Maximum reduction T (°C)	T end reduction (°C)
$Ni_{0,9}Mg_{0,1}Fe_2O_4$	$8{,}66\cdot10^{-4}$	$7{,}72\cdot10^{-4}$	$1{,}24\cdot10^{-2}$	89	330	596,3	820
$Ni_{0,9}Mg_{0,1}Fe_2O_4$/NiO 20% by mass	$8{,}27\cdot10^{-4}$	$7{,}60\cdot10^{-4}$	$1{,}22\cdot10^{-2}$	92	430	669,7	830
$Ni_{0,9}Mg_{0,1}Fe_2O_4$/CuO 20% by mass	$8{,}19\cdot10^{-4}$	$7{,}86\cdot10^{-4}$	$1{,}26\cdot10^{-2}$	96	230	571,9	710
$Ni_{0,9}Mg_{0,1}Fe_2O_4/ZrO_2$ 20% by mass	$8{,}55\cdot10^{-4}$	$6{,}78\cdot10^{-4}$	$1{,}08\cdot10^{-2}$	79	390	629,6	740

Table 35. Main information noticeable by H_2-TPR of pure $Ni_{0,9}Mg_{0,1}Fe_2O_4$ and the systems composed by this spinel mixed with functional oxides (as copper oxide and nickel oxide) and an inert oxide (zirconium oxide), all of them mixed with the catalyst at 20 % in mass with wet ball milling.

Also quantitatively we can see that the material mixed with copper oxide at 20 % in weight is the material that shows the best performances, in all cases, so regarding process temperatures and oxygen released. Zirconium oxide is the worst support in case of moles of oxygen lost, but about temperatures the worst material is the one with nickel oxide as support.

Figure 89 shows the graph containing all the O_2-TPO carried out on the same systems:

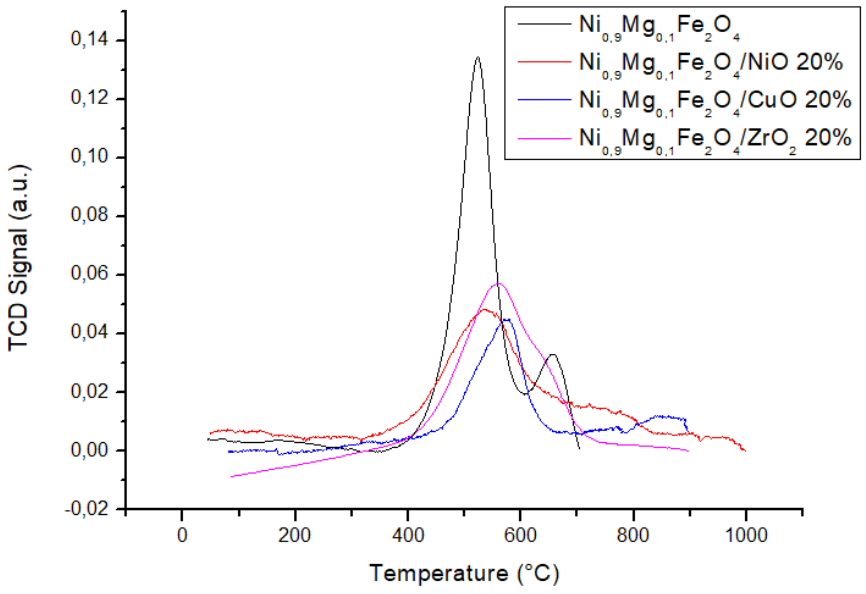

Figure 89. O_2-TPO performed after H_2-TPR of the pure $Ni_{0,9}Mg_{0,1}Fe_2O_4$ (black line) and NiO (red line), CuO (blue line) and ZrO_2 (pink line) mixed with the spinel at 20 % in weight.

It can be noticed that also with 20 % in mass of supporting material, the oxidation curve is smaller in intensity but wider than the one obtained for the pure catalyst.

Finally, in table 36, the information obtained from these oxidations is reported:

System	Total moles O in the material (mol)	Moles reticular O reobtained (mol)	Recovery mass (g)	Moles O reobtained (%)	T start oxidation (°C)	Maximum oxidation T (°C)	T end oxidation (°C)
$Ni_{0,9}Mg_{0,1}Fe_2O_4$	$8,66 \cdot 10^{-4}$	$7,34 \cdot 10^{-4}$	$1,17 \cdot 10^{-2}$	95	350	523,1	700
$Ni_{0,9}Mg_{0,1}Fe_2O_4$/NiO 20% by mass	$8,27 \cdot 10^{-4}$	$6,72 \cdot 10^{-4}$	$1,07 \cdot 10^{-2}$	88	310	535,2	840
$Ni_{0,9}Mg_{0,1}Fe_2O_4$/CuO 20% by mass	$8,19 \cdot 10^{-4}$	$6,23 \cdot 10^{-4}$	$9,97 \cdot 10^{-3}$	79	190	577,8	/
$Ni_{0,9}Mg_{0,1}Fe_2O_4/ZrO_2$ 20% by mass	$8,55 \cdot 10^{-4}$	$6,70 \cdot 10^{-4}$	$1,07 \cdot 10^{-2}$	99	380	559,8	750

Table 36. Information noticeable by O_2-TPO of pure spinel and metal oxides (such as nickel oxide, copper oxide and zirconium oxide) mixed with the catalyst at 20 % by wet ball milling.

About oxygen moles reobtained by O_2-TPO we can notice that the best material seems to be the pure spinel because it regains more oxygen with respect to other materials, but the sample supported with zirconium oxide reobtains almost all of the oxygen moles released before, so it seems to be the system more stable. About temperatures, it can be seen that the oxidation starts at a very low temperature in the sample mixed with 20 % in mass of copper oxide, but the system with the lower peak temperature is the pure spinel one and also it has the lower oxidation ending temperature.

3.11.5.2. Carbon dioxide splitting:

Since none of materials release oxygen at 1000 °C the following table (table 37) has been compiled only with the data obtained thanks to the hydrogen pre-treatment carried out up to 580 °C and consequent splitting of carbon dioxide at 1000 °C.

System	Total moles O in the material (mol)	CO_2 moles splitted I cycle (mol)	Recovery mass (g)	moles O reobtained (%)	CO_2 moles splitted II cycle (mol)	recovery mass (g)	moles O reobtained (%)
$Ni_{0,9}Mg_{0,1}Fe_2O_4$	$8,66 \cdot 10^{-4}$	$4,05 \cdot 10^{-4}$	$6,48 \cdot 10^{-3}$	47	$3,92 \cdot 10^{-4}$	$6,28 \cdot 10^{-3}$	45
$Ni_{0,9}Mg_{0,1}Fe_2O_4$/NiO 20% by mass	$8,27 \cdot 10^{-4}$	$3,70 \cdot 10^{-4}$	$5,92 \cdot 10^{-3}$	45	$3,58 \cdot 10^{-4}$	$5,73 \cdot 10^{-3}$	43
$Ni_{0,9}Mg_{0,1}Fe_2O_4$/CuO 20% by mass	$8,19 \cdot 10^{-4}$	$4,19 \cdot 10^{-4}$	$6,71 \cdot 10^{-3}$	51	$3,62 \cdot 10^{-4}$	$5,78 \cdot 10^{-3}$	44
$Ni_{0,9}Mg_{0,1}Fe_2O_4/ZrO_2$ 20% by mass	$8,55 \cdot 10^{-4}$	$3,75 \cdot 10^{-4}$	$6,00 \cdot 10^{-3}$	44	$3,66 \cdot 10^{-4}$	$5,86 \cdot 10^{-3}$	43

Table 37. Information obtained by catalytic activity tests, using a mass spectrometer. These compounds are made of pure $Ni_{0,9}Mg_{0,1}Fe_2O_4$ and this spinel mixed at 20 % in mass by wet ball milling with nickel oxide, copper oxide and zirconium oxide.

About catalytic activity we can see that during the first cycle copper oxide also at 20 % in mass boosts the spinel performances a lot, but it quickly loses reactivity, so it is the less stable system how we saw thanks to SEM images; the other material that split more CO_2 is the pure $Ni_{0,9}Mg_{0,1}Fe_2O_4$ one. We can notice also that

the lower splitting is achieved using nickel oxide as a support and that the best reversibility is obtained mixing the catalyst with zirconium oxide (in that case there is no sintering how seen with SEM images).

4. CONCLUSIONS

All of XRD diffractograms reveal that spinel doesn't react with supporting powders because all of the catalyst reflexes don't shift. There is only the appearance of the supports' reflexes that add up to those of $Ni_{0,9}Mg_{0,1}Fe_2O_4$.

In all of systems mixed by wet ball milling, the concentration isn't homogeneous as seen in the case of pure catalyst. It changes varying the zone because the spinel didn't react with the supporting powders, but they bonded each other, and so on an area on which was made EDX there can be a particle of supporting material or not, and this changes a lot the percentage of atomic concentration. All of the results reported with system mixed with ball milling, as the one on table 6, are a mean of different areas on which is done EDX. So we can say that wet ball milling is a good way to mix different powders and that the sintering operated after filtration is a successful path in order to bond supports and catalyst, as seen in SEM images.

About H_2-TPR measurement, we can see that the utilization of copper oxide gives a peak related to CuO contribution, but it doesn't have the same starting reduction temperature when supported than that obtained when it is pure, so probably the spinel and the support interact between each other. Also, it is interesting to see that supporting the spinel with nickel oxide leads to an increase of process temperatures, and that using zirconia as support doesn't change the pure $Ni_{0,9}Mg_{0,1}Fe_2O_4$ curve's shape so probably they don't interact. The best results, using all types of supports, are obtained mixing them at 20 % in weight with the catalyst; the best material seems to be $Ni_{0,9}Mg_{0,1}Fe_2O_4$ with CuO at 20 % in weight because it lowers all process temperatures and also release more oxygen than the others.

On the other side, O_2-TPO measurements show that copper oxide isn't as good as for reduction, because it increases the maximum peak temperature and the oxidation doesn't end even at 900 °C. Also in this case, supporting the spinel with 20 % of powders in mass gives best results and incredibly by using zirconia the system regains almost all of oxygen lost during the reduction also if, watching at reticular oxygen moles reobtained, it is lower than that regained by other composites. In all cases, supporting the spinel leads to a decrease of the intensity of the peak during O_2-TPO but it widens a lot.

Unfortunately, none of the systems release oxygen at 1000 °C on inert flowing gas because the O_2 signal that the mass spectrum acquire remains stable all the time. A pre-treatment is necessary to reduce the catalyst in the wustite phase, and this is carried out flowing 5 % of hydrogen in helium from ambient temperature to 580 °C at a rate of 10 °C/min.

None of the sample produced oxygen during the CO_2 splitting, so the materials regain the O_2 released during the pre-treatment catching it from carbon dioxide and producing CO.

About the CO_2 conversion time, all of the compounds work in nearly 20 min instead of the one mixed with copper oxide at 50 % in weight during the first cycle, which employs 24 minutes to split carbon dioxide, probably because there is a sintering as we can see in SEM post-cycles images. This sintering leads to a lower surface area and therefore to a slower conversion.

After all, the best compound during the first cycle is $Ni_{0,9}Mg_{0,1}Fe_2O_4$ mixed at 50 % in mass with copper oxide, but it loses reactivity during the second cycle because of a very high sintering, as we can see with SEM post-cycles images. Mixing these two oxides at 20 % leads to a balance between higher reactivity than that of pure spinel and also less sintering than that of the system previously described.

The most stable material is that with zirconium oxide mixed at 20 % in mass with the spinel, but it is less reactive because of ZrO_2 that is an inert material and so doesn't participate in the carbon dioxide splitting.

The use of nickel oxide as a support provides in all cases, both at 50 % and 20 %, an intermediate trend between stability and reactivity.

In the end, we can see how difficult the carbon dioxide splitting is, because of these very high operation temperatures and because of materials' sintering. Even at 1000 °C there isn't an oxygen release by none of systems but probably the samples mixed with copper oxide reduce at a temperature below 1400 °C as we can notice by H_2-TPR curves. Sintering is a big problem with this type of reaction because, how it can be seen in case of copper oxide mixed at 50 % in weight with the spinel, during the second cycle performance are very lowered. Supporting the catalyst with oxides that reduces at lower temperature, by the way, seems to be the best way to decrease the reduction temperature of all the compound and also to achieve more CO_2 moles splitted. In the future, it could be interesting to see what happens when water vapor and carbon dioxide are fluxed together on the reduced sample, if there is syngas production. Also a CO_2-TPO can be a useful analysis in order to see form what temperature all of these compounds start to split carbon dioxide. The use of copper resulted to be very good for this type of reaction, so it could be interesting to see what happens when it is inserted on the spinel's structure, for example instead of magnesium, and also to try to stabilize his oxide so that it doesn't highly sinter during the splitting tests.

5. APPENDIX

In the XPS analysis you should always look for the carbon peak, which is located on 285 eV. Once you find it, you have to shift the whole graph to the result of the difference between the peak of the carbon found and the theorical peak. This is because the instrument uses a grounding to balance the residual positive charges in the material after the emission of the electrons, charges that obviously attract the electrons that would be released and that therefore shift the graph to higher bond energies. The more conductive the sample is, the less shift you have because the charge is balanced more easily by grounding.

To make the measurements at the mass spectrometer, it was necessary to use two tubes, one empty and one with the sample, in order to eliminate an instrumental artifact. In fact, there is the formation of a peak concentration of carbon dioxide, above 10 %, which is not attributable to the behavior of the material, which would release CO_2 instead of splitting it. The use of an empty tube, as well as to have a profile of concentration of injected gases' trend and, therefore, to refer to the next measurement, also is useful to remove this artifact. As can be seen in figure 90, in fact, there is a peak concentration too high, more than that inserted, of carbon dioxide (instead of 10 % measures a percentage concentration of about 11,3 %):

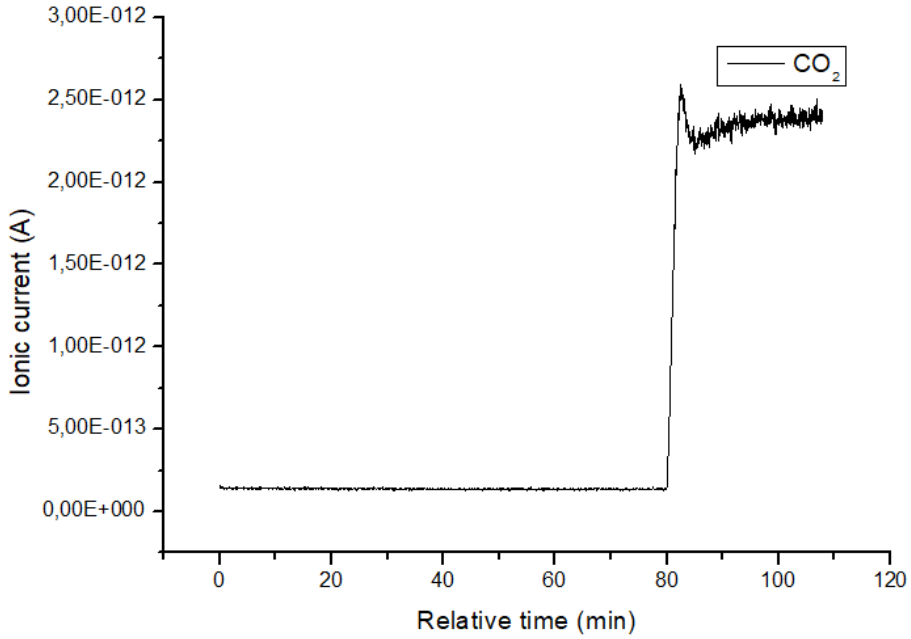

Figure 90. Graph of the trend of carbon dioxide during the splitting phase. It is interesting to observe the initial peak, which is formed during the increase in concentration of CO_2. The use of the graph of the ionic current as a function of time indicates precisely that this peak is an experimental artifact.

The graph of the ionic current detected by the instrument as a function of the time in minutes was inserted to identify the actual artifact. The graph of concentration as a function of time could be deceiving since there may simply be an error in reading another species present in the system, such as helium, which is detected in a lower percentage concentration in the system and therefore increases the concentration of carbon dioxide. With this, however, we highlight the actual formation of the peak concentration, which takes about 3 minutes to become the signal actually sought, without artifact.

The use of a second empty tube, in fact, leads to the formation of this artifact only in the first measurement, therefore on the tube without sample, thus improving the detection of the behavior of the sample when placed to split the carbon dioxide, like in figure 91:

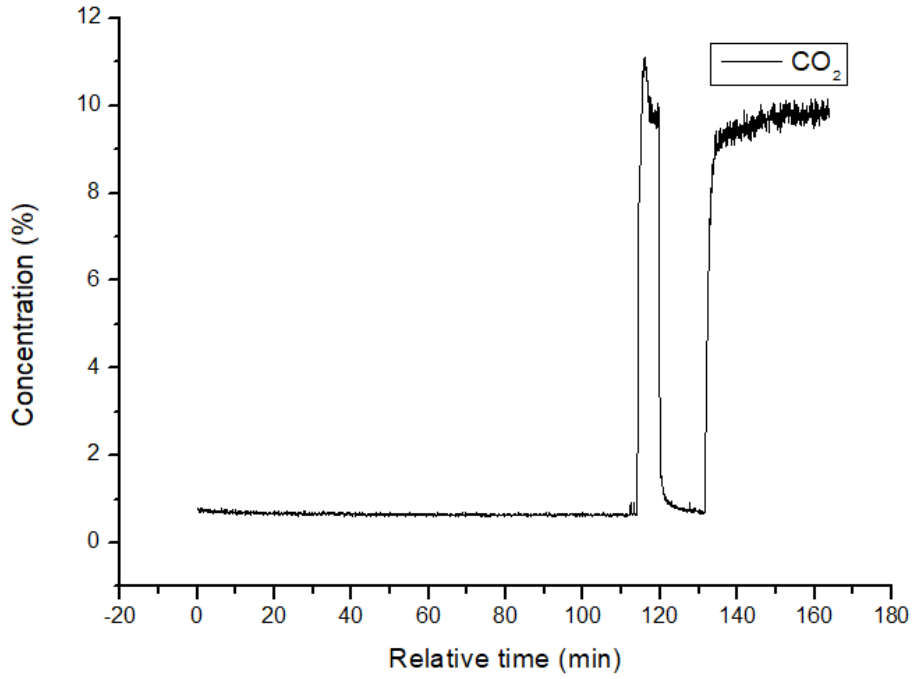

Figure 91. Trend of the percentage concentration of carbon dioxide as a function of time in minutes. As can be seen, in this case the artifact occurs during the passage of gas into the empty tube, while when it passes into the tube with the sample this does not occur.

As you can see, the peak occurs during the time in which the gases go into the empty tube, or the first increase in concentration, leaving the measure of the actual catalytic activity of the sample, or the second increase in concentration of carbon dioxide, without this artifact.

Below is a diagram of the experimental setup to obtain this measurement with two tubes, figure 92:

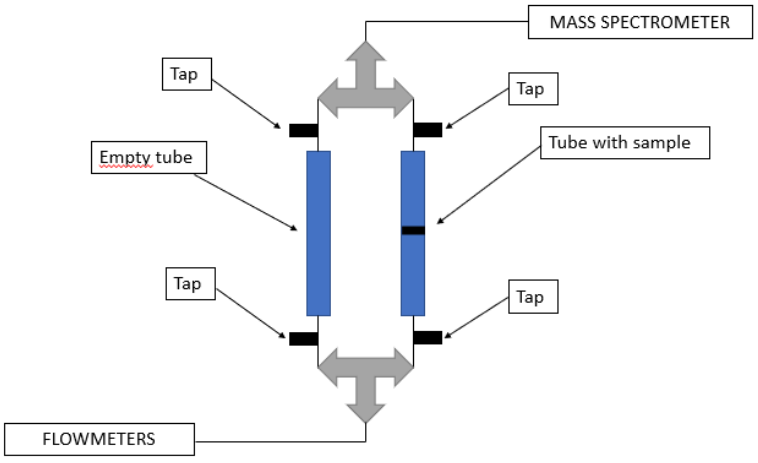

Figure 92. Diagram of the experimental setup used to avoid the formation of the instrumental artifact during the carbon dioxide splitting phase, as well as to have a reference of the concentration of the same in an empty tube.

The reduction takes place only in the tube with the sample, so the two taps of that tube are opened and the others are closed. In this way the gas mixture passes only into the tube on the right. Before the splitting phase, the two taps of the tube with the sample are closed and the other two of the empty tube are opened, the carbon dioxide is passed to 10 % in helium, the signal detected in the mass spectrometer is expected to

become stable and finally the CO_2 concentration is brought back to 0 %. The taps of the empty tube are then closed and the others are opened and the concentration of carbon dioxide coming out of the flow meters is brought back to 10 %.

6. REFERENCES

1. https://www.rainews.it/dl/rainews/articoli/clima-onu-riscaldamento-globale-a8786fca-9d95-4df6-9c64-0e9840fb1897.html.
2. https://en.wikipedia.org/wiki/Atmosphere_of_Earth.
3. 90-Flood Impact Assessment Tool (FLIAT)-An Object-Relational GIS Tool for Flood Impact Assessment in Flanders, Belgium.
4. *FISCHER-TROPSCH PROCESS*.
5. https://it.wikipedia.org/wiki/Anidride_carbonica.
6. Zheng, Y. *et al.* Energy related CO2 conversion and utilization: Advanced materials/nanomaterials, reaction mechanisms and technologies. *Nano Energy* vol. 40 512–539 (2017).
7. Bhosale, R. R. *et al.* A decade of ceria based solar thermochemical H2O/CO2 splitting cycle. *International Journal of Hydrogen Energy* 34–60 (2019) doi:10.1016/j.ijhydene.2018.04.080.
8. Khamhangdatepon, T., Sornchamni, T., Siri-Nguan, N., Laosiripojana, N. & Hartley, U. W. A dual reactor for isothermal thermochemical cycles of h2 o/co2 co-splitting using la0.3 sr0.7 co0.7 fe0.3 o3 as an oxygen carrier. *Processes* **9**, (2021).
9. Levêque, G., Abanades, S., Jumas, J. C. & Olivier-Fourcade, J. Characterization of two-step tin-based redox system for thermochemical fuel production from solar-driven CO2 and H2O splitting cycle. *Industrial and Engineering Chemistry Research* **53**, 5668–5677 (2014).
10. Bhosale, R. R. *et al.* A decade of ceria based solar thermochemical H2O/CO2 splitting cycle. *International Journal of Hydrogen Energy* 34–60 (2019) doi:10.1016/j.ijhydene.2018.04.080.
11. Coker, E. N., Ambrosini, A. & Miller, J. E. Compositional and operational impacts on the thermochemical reduction of CO2to CO by iron oxide/yttria-stabilized zirconia. *RSC Advances* **11**, 1493–1502 (2021).
12. Min, K., Jun, Z., Ning, Z., Wei, W. & Yu-han, S. *CO production via thermochemical CO 2 splitting over Ni ferrite-based catalysts*. *JOURNAL OF FUEL CHEMISTRY AND TECHNOLOGY* vol. 42 (2014).
13. Teknetzi, I., Nessi, P., Zaspalis, V. & Nalbandian, L. Ni-ferrite with structural stability for solar thermochemical H2O/CO2 splitting. *International Journal of Hydrogen Energy* **42**, 26231–26242 (2017).
14. le Gal, A., Abanades, S. & Flamant, G. CO2 and H2O splitting for thermochemical production of solar fuels using nonstoichiometric ceria and ceria/zirconia solid solutions. *Energy and Fuels* **25**, 4836–4845 (2011).
15. Haeussler, A., Abanades, S., Julbe, A., Jouannaux, J. & Cartoixa, B. Solar thermochemical fuel production from H2O and CO2 splitting via two-step redox cycling of reticulated porous ceria structures integrated in a monolithic cavity-type reactor. *Energy* **201**, (2020).
16. Lorentzou, S., Karagiannakis, G., Pagkoura, C., Zygogianni, A. & Konstandopoulos, A. G. Thermochemical CO2 and CO2/H2O splitting over NiFe2O4 for solar fuels synthesis. in *Energy Procedia* vol. 49 1999–2008 (Elsevier Ltd, 2014).

17. Portarapillo, M. *et al.* Syngas production through H2O/CO2 thermochemical splitting. *Chemical Engineering Transactions* **74**, 43–48 (2019).

18. Riaz, A. *et al.* Concentration-Dependent Solar Thermochemical CO 2 /H 2 O Splitting Performance by Vanadia–Ceria Multiphase Metal Oxide Systems . *Research* **2020**, 1–12 (2020).

19. Takalkar, G. & Bhosale, R. R. Thermochemical CO2 splitting using a sol-gel–synthesized Mg-ferrite–based redox system. *International Journal of Energy Research* **43**, 6983–6993 (2019).

20. Takalkar, G., Bhosale, R. R., AlMomani, F. & Khraisheh, M. Thermocatalytic splitting of CO2 using sol-gel synthesized Co-ferrite redox materials. *Fuel* **257**, (2019).

21. Takalkar, G., Bhosale, R. R., AlMomani, F., Rashid, S. & Shakoor, R. A. Ni incorporation in MgFe2O4 for improved CO2-splitting activity during solar fuel production. *Journal of Materials Science* **55**, 11086–11094 (2020).

22. Qiu, Y. *et al.* Efficient CO2 to CO conversion at moderate temperatures enabled by the cobalt and copper co-doped ferrite oxygen carrier. *Journal of Energy Chemistry* **46**, 123–132 (2020).

23. Huang, J. *et al.* Anti-sintering non-stoichiometric nickel ferrite for highly efficient and thermal-stable thermochemical CO2 splitting. *Chemical Engineering Journal* **404**, (2021).

24. Nadoll, P. & Mauk, J. L. Wüstite in a hydrothermal silver-lead-zinc vein, Lucky Friday mine, Coeur d'Alene mining district, U.S.A. *American Mineralogist* **96**, 261–267 (2011).

25. Mora Mendoza, E. Y. *et al.* Iron oxides as efficient sorbents for CO2 capture. *Journal of Materials Research and Technology* **8**, 2944–2956 (2019).

26. Akram, W., Sanjay & Hassan, M. A. Chemical looping combustion with nanosize oxygen carrier: a review. *International Journal of Environmental Science and Technology* vol. 18 787–798 (2021).

27. Shaikh, S. F., Ubaidullah, M., Mane, R. S. & Al-Enizi, A. M. Types, Synthesis methods and applications of ferrites. in *Spinel Ferrite Nanostructures for Energy Storage Devices* 51–82 (Elsevier, 2020). doi:10.1016/b978-0-12-819237-5.00004-3.

28. Zate, M. K., Raut, S. D., Shirsat, S. D., Sangale, S. & Kadam, A. S. Ferrite nanostructures. in *Spinel Ferrite Nanostructures for Energy Storage Devices* 13–34 (Elsevier, 2020). doi:10.1016/b978-0-12-819237-5.00002-x.

29. https://www.sciencedirect.com/topics/chemical-engineering/citric-acid.

30. *Chimica del Ferro*. http://iscamap.chem.polimi.it/citterio/it/education/inorganic-chemistry-introduction/inorganic-chemistry-lessons/.

31. Kappes, M., Iannuzzi, M. & Carranza, R. M. Hydrogen Embrittlement of Magnesium and Magnesium Alloys: A Review. *Journal of The Electrochemical Society* **160**, C168–C178 (2013).

32. Basharat, F., Rana, U. A., Shahid, M. & Serwar, M. Heat treatment of electrodeposited NiO films for improved catalytic water oxidation. *RSC Advances* **5**, 86713–86722 (2015).

33. https://en.wikipedia.org/wiki/Nickel(II)_oxide.

34. https://en.wikipedia.org/wiki/Zirconium_dioxide.

35. https://it.wikipedia.org/wiki/Ossido_ferroso-ferrico.

36. https://en.wikipedia.org/wiki/Copper(II)_oxide.

37. Jafarbegloo, M., Tarlani, A., Mesbah, A. W., Muzart, J. & Sahebdelfar, S. NiO-MgO Solid Solution Prepared by Sol-Gel Method as Precursor for Ni/MgO Methane Dry Reforming Catalyst: Effect of Calcination Temperature on Catalytic Performance. *Catalysis Letters* **146**, 238–248 (2016).

38. Beckers, J. & Rothenberg, G. Redox properties of doped and supported copper-ceria catalysts. *Dalton Transactions* 6573–6578 (2008) doi:10.1039/b809769k.

39. Chen, M., Wang, Y., Liang, T., Yang, J. & Yang, Z. Hydrogen production from steam reforming of ethylene glycol over iron loaded on MgO. in *AIP Conference Proceedings* vol. 1794 (American Institute of Physics Inc., 2017).

40. Chamoumi, M. & Abatzoglou, N. NiFe2O4 production from α-Fe2O3 via improved solid state reaction: Application as catalyst in CH4 dry reforming. *Canadian Journal of Chemical Engineering* **94**, 1801–1808 (2016).

AKNOWLEDGEMENTS

I want to thank Professor Antonella Glisenti for accepting me as a thesis student, for all the help you gave me, for the great willingness to listen to me and give me advice on what to do, not only about the thesis, and for having supported me a lot to convince me that what I was doing was right.

I would like to thank all the guys in the IMPACT group for the advices, for teaching me a lot about the laboratory and not, for following me and for supporting me. Thank you also and above all for creating a beautiful environment where there is serenity and joy. During the time I was at home because of the virus or even during the Christmas holidays, I swear you that I often repeated to my parents that I missed going to the office with you. I want to thank you one by one because you have all made a significant contribution in the writing of my thesis: thanks to Elena, Giovanni, Giacomo, Enrico, Simone, Gabriel, Jonathan, Lorenzo, Andrea, Pietro, Dario, Roberta and Andrea.

I would like to thank my family that is Valter, Mariangela, Nicole, Federica and Matteo for supporting me, cheering up and having fun playing with me when I needed it. Even when I am sad you always know how to rejoice with your liveliness.

I would also like to thank my relatives and all my friends, you too have helped me a lot when needed, rejoicing and helping me on many occasions and in many ways.